Title
Democratized Microdroplet Technologies for the Analysis of Single Immune Cell Secretions

Author
Dimatteo, Robert

Publication Date
2021

Peer reviewed|Thesis/dissertation

UNIVERSITY OF CALIFORNIA

Los Angeles

Democratized Microdroplet Technologies for the Analysis of Single Immune Cell Secretions

A dissertation submitted in partial satisfaction of the requirements for the degree Doctor of Philosophy in Chemical & Biomolecular Engineering

by

Robert Dimatteo

2021

ABSTRACT OF THE DISSERTATION

Democratized Microdroplet Technologies for the

Analysis of Single Immune Cell Secretions

By

Robert Dimatteo

Doctor of Philosophy in Bioengineering

University of California, Los Angeles 2021

Professor Dino Di Carlo, Co-Chair

Professor Harold Monbouquette, Co-Chair

Variations in protein secretions between individual cells directly influences their functional activity in many applications. However, the inherent complexity associated with the accurate detection and quantification of secreted factors leaves these proteins vastly underutilized as phenotypic markers today.

Here we report on the development, optimization, and application of novel, easy-to-use, droplet-based technologies for the detection and isolation of single viable immune cells based on their secreted factors. We first demonstrate that rapid compartmentalization significantly

improves the resolution and accuracy of single-cell secretion studies. Using an ultra-high throughput microfluidic step emulsifier, we encapsulated 1,000 cells/second into uniformly sized 70 μm droplets, providing an environment to rapidly concentrate molecules and prevent intercellular diffusion. When combined with a commercially available cytokine capture reagent, droplet encapsulation reduced >99% of false positive signals generated during a screen of IL-2 production from primary T cells. Cells remained viable throughout analysis and could be sorted using standard fluorescence activated cell sorting, providing an easy method of isolating functionally unique clones for downstream analysis.

Next, we detail the development of a novel lab-on-a-particle platform which enables the assessment of single cell secretions using only standard laboratory equipment and without the need for specialized knowledge of microfluidic device fabrication or operation. In this approach precisely engineered hydrogel nanovials are utilized as a surface to bind cells, partition them into uniform compartments, and capture their secreted products. The utility of this platform is initially highlighted by screening differences in the total antibody production levels of individual cells within a producer cell line (CHO-DP12), revealing that antibody titers can be increased by 50% through a single selection and expansion of high-producers. Subsequently, we highlight the platform versatility through the successful detection of antigen specific antibodies from hybridoma and primary plasma cells, as well as cytokine secretions from primary T cells. Finally, we detail methods to optimize parameters for the sorting of our hydrogel nanovials across commonly utilized commercial flow sorters.

As a whole, this work explores methods to democratize droplet based single cell analysis to develop open-source screening tools which will advance basic immunological science and inform novel cell based biotechnology applications.

The dissertation of Robert Dimatteo is approved.

Aaron S. Meyer

Yvonne Yu-Hsuan Chen

Harold G. Monbouquette, Committee Co-Chair

Dino Di Carlo, Committee Co-Chair

University of California Los Angeles

2021

DEDICATION

This work is dedicated to all the friends and family who have supported me along this long and arduous journey. Most notably, I would like to acknowledge my parents, John E. Dimatteo Jr. and Agnieszka Dimatteo. From a young age you taught me to be curious, to embrace new adventures, and to put my best effort into everything that I do. Your constant love and support helps me to push myself past my comfort zone every day. Without you I would not have been able to finish this work.

I would also like to thank Lauren Schenker for keeping me (relatively) sane over the course of my Ph.D. You are my best friend in the entire world and the tiny family we have grown with Mochi and Pippa means the world to me. The adventures we have had together are some of my fondest memories and I cannot wait to travel the world together with you in the future.

Next, although I moved away from my family for graduate school, I have been fortunate enough to have found adoptive families here in California. I would like to thank both Paige Taylor and Don Fisher for sharing holidays with me, for teaching me about everything from music composition to classic car restoration, and for inviting me over to watch jeopardy, your support along the way has really meant a lot to me. Additionally, thanks to Joseph and Judy Ilvento for giving me a home away from home in Carpinteria. Whenever grad school became too stressful I could always count on a visit to you guys to recharge my batteries.

The countless hours I spent inside the lab these past few years would not have been bearable without all of the close friends I made along the way. Each and every member of the Di Carlo lab family has shaped my graduate school experience in a positive way. Through your friendship, and in some cases mentorship, I have learned to become a better researcher and a better person. Special thanks to Elias Sideris, the first person I met at UCLA and someone who

has been instrumental in helping me navigate my career in graduate school and beyond. I appreciate your life advice and reminders that I should balance work with fun, whether through intramural sports, hikes, or over drinks. Lastly, but perhaps most importantly, thanks to Anh Phong Tran for never sleeping and for sharing countless laughs with me through phone calls at all hours of the day. You are one of the most genuine people I have ever met, and I consider myself lucky for your friendship.

Finally, I must acknowledge the tremendous support of my advisor Dino Di Carlo. Whoever made up the saying the third time's the charm must have been referring to my grad school career, but after passing through two other research groups my only regret in joining your lab was that I did not get here sooner. I have always been impressed by your abilities as an innovator and as a scientific storyteller. Thank you for taking a chance on me and for helping me reach the finish line. You were a great mentor who I hope will turn into a great friend in the future.

TABLE OF CONTENTS

LIST OF FIGURES

ACKNOWLEDGMENTS

Chapter 1 is adapted from parts of Dimatteo R., Miwa H., de Rutte J., Ghosh R., Zhu S, Di Carlo D. "Single-Cell Secretion Sorting for Cell Therapies" (*In Progress).* RD, HM, DD, outlined the scope of the manuscript. RD, JD, RG, created the figures. RD, HM, JD, SZ, identified relevant sources. RD wrote the text with contributions from other authors.

Chapter 3 is adapted from: Dimatteo R.*, de Rutte J.*, Archang M., van Zee M., Koo F., Lee S., Sharrow A., Krohl PJ., Mellody M., Zhu S., Eichenbaum, J., Kizerwetter M., Udani S., Ha K., Bertozzi A., Spangler, J., Damoiseaux R., Di Carlo D. (2021). "Suspendable microcontainers for massively parallel single-cell functional analysis and sorting" (*In Submission*). JD designed the fabrication workflow for the drop-carrier particles. JD, RDi, SL, and SZ fabricated nanovials. RDi, FK, SU optimized suspension cell binding strategies. JD, RDi. and MV developed cell secretion protocols. JD, RDi, MV, RDa and DD designed the flow sorting studies. JD, RDi and RDa performed cell sorting experiments. RDi performed secretion cross-talk experiments. MV performed suspension adapted CHO cell experiments. RDi performed CHO cell ELISA experiments. RDi, FK, SL, performed hybridoma antigen specific secretion assay and sorting experiments. MA vaccinated mice and MA and RDi performed primary B cell experiments. MM, AS, and RDa optimized heavy chain amplification. PK, MK and JS conducted transient expression experiments. KH and AB developed the framework for calculating the volume energy curves and volume splitting curves.

Chapter 4 is adapted from: Dimatteo, R.*, de Rutte, J.*, Zhu, S., Archang, M., & Di Carlo, D. (2021). "Sorting Single-Cell Microcarriers using Commercial Flow Cytometers", (*Accepted,*

SLAS Technology). JD, RD, and DD conceived and planned out the main experiments of this study. RD performed experiments involving the FACSAria and Sony SH800 and scatter enrichment experiments. JD, RD, and DD interpreted these results and RD and JD performed analysis. JD and SZ fabricated particles used in the study and performed On-chip sort experiments and analysis. MA isolated B cells used in this study and performed HRP biotin quantification study. JD, RD, and DD wrote the manuscript. JD prepared final figures with help from other authors.

Chapter 5 is adapted from parts of Dimatteo, R., Miwa H., de Rutte J., Ghosh R., Zhu S, Di Carlo D. Single-Cell Secretion Sorting for Cell Therapies (*In Progress)* as well as unpublished data. RD, HM, DD, outlined the scope of the manuscript. RD, JD, RG, created the figures. RD, HM, JD, SZ, identified relevant sources. RD, FK performed cytokine secretion studies on primary T cells. RD wrote the text.

VITA

EDUCATION

B.S. in Chemical and Biological Engineering (2014), Tufts University, Medford, MA

RESEARCH APPOINTMENTS

Graduate Student Researcher (2017-2021), University of California, Los Angeles

Professor Dino Di Carlo, Department of Bioengineering

Graduate Student Researcher (2016-17), University of California, Los Angeles

Professor Tatiana Segura, Department of Chemical and Biomolecular Engineering

Graduate Student Researcher (2015-2016), University of California, Los Angeles

Professor Philip Romero, Department of Chemical and Biomolecular Engineering

PUBLICATIONS

- *(In Preparation)* Dimatteo, R., Miwa H., de Rutte J., Ghosh R., Zhu S, Di Carlo D. *Single-Cell Secretion Sorting for Cell Therapies*. 2021
- *(In Submission)* Dimatteo, R.*, de Rutte, J.*, Archang M., van Zee M., Koo D., Lee S., Sharrow A., Krohl P., Melody M., Zhu S., Eichenbaum J., Kizerwetter M., Udani S., Ha K., Bertozzi A., Spangler, J., Damoiseaux R., Di Carlo D. *Suspendable microcontainers for massively parallel single-cell functional analysis and sorting*. 2021
- *(Accepted)* Dimatteo R*, de Rutte J*, Zhu S, Archang M, Di Carlo D. *Sorting Single-Cell Microcarriers using Commercial Flow Cytometers*, SLAS Technology, 2021
- *(In Review)* Lee S, de Rutte J, Dimatteo R, Koo D, Di Carlo D. *Scalable Fabrication of 3D Structured Microparticles Using Induced Phase Separation*, ACS Nano, 2021
- Dimatteo R, Darling NJ, Segura T. *In situ forming injectable hydrogels for drug delivery and wound repair*. Advanced Drug Delivery Reviews, 2018

- Escuin-Ordinas H, Liu Y, Sun L, Hugo W, Dimatteo R, Huang R, Krystofinski P, Azhdam A, Lee J, Comin-Anduix B, Cochran A, Lo R, Segura T, Scumpia P, Ribas A. *Wound healing with topical BRAF inhibitor therapy in a diabetic model suggests tissue regenerative effects*. PLOS ONE, 2021
- Zhu S, Li S, Escuin-Ordinas H, Dimatteo R, Xi W, Ribas A, Segura T. *Accelerated wound healing by injectable star poly (ethylene glycol)-b-poly (propylene sulfide) scaffolds loaded with poorly water-soluble drugs.* Journal of Controlled Release, 2018
- Li S, Nih LR, Bachman H, Fei P, Li Y, Nam E, Dimatteo R, Carmichael ST, Barker T, Segura T. *Hydrogels with precisely controlled integrin activation dictate vascular patterning and permeability*. Nature Materials, 2017

PRESENTATIONS

- Dimatteo R, Lo D, Di Carlo D. *Droplet-Enhanced On-Cell Encoding of Single Cell Secretory Function.* MicroTAS. 2019 October 27-31; Basel, Switzerland

HONORS AND AWARDS

- Sensors (MDPI) - Outstanding Sensors and Actuators, Detection Technologies Poster Award – MicroTAS 2019; Basel, Switzerland
- Top Presentation – UCLA Chemical and Biomolecular Engineering 4th Year Symposium, Spring 2019
- UCLA Biotechnology Training Grant Fellowship, 2016-2018
- UCLA Graduate Dean's Scholar, 2015-2017

Chapter 1. Introduction: Understanding Protein Production from Single Cells

Decades of advancement in genetic engineering, bioprocessing, and basic medical science, have fostered the emergence of cellular therapeutics as a novel pillar of medicine[1]. These approaches transform populations of cells into armies of living drugs which can expand within a patient and provide long term treatments against otherwise intractable chronic and systemic illness. However, as the field continues to progress, it is becoming clear that we are still fundamentally limited in our understanding of the phenotypic traits that endow cells with therapeutically beneficial properties[2-5]. The intricacies of cellular biology enable the execution of complex tasks which cannot be achieved with small molecule drugs or biologics. In optimal scenarios, populations of therapeutic cells can home to sites of infection, integrate environmental cues to modulate the intensity of their response, and survive and proliferate to prevent disease relapse. Unfortunately, the complexity of these behaviors also renders design and characterization of such drugs immensely more difficult[6-8]. Unlike small molecules or proteins, functional potency of cells cannot be ascertained from simple metrics like primary structure or affinity. Mutations at both the genetic[9] and epigenetic[10] levels may confer functional advantages on select cell clones which translate to variations in biological potency in vivo. Similarly, differences in expansion protocols may result in exhaustion or selective proliferation of subsets of cells. Further advancements, through rational design and standardization of cellular therapies will rely on foundational technologies which can, (1) rapidly and reliably probe cellular phenotype to identify the quality metrics critical for therapeutic design and, (2) and enrich for cells with desirable properties to standardize optimal drug formulation.

Perhaps the most direct metric of functional potency, can be found by measuring the propensity of cells to secrete bioactive proteins. Indeed, the vastness of the secretome underscores its importance in a wide array of biological processes. Of the ~20,000 protein coding genes, ~3,000 proteins are predicted to be secreted, compared to ~5,000 membrane bound proteins[11]. These secreted factors lead to outsized biological effects compared to membrane bound molecules because of their ability to diffuse and rapidly remodel signaling between many nearby cells and tissues (Figure 1-1). Local increases in growth factor concentrations can aid the regeneration and maturation of vasculature, enabling tissue regrowth after traumatic injury. Cytokines and chemokines work in concert to coordinate the activity of immune cells as they respond to pathogens. Proteolytic enzymes catalyze reactions in the cellular microenvironment, proving critical in functions such as extracellular matrix (ECM) remodeling. Unfortunately, functional profiling and selection of cellular therapeutics is not standard in drug development pipelines[12]. Furthermore, in the small fraction of cases where profiling approaches are carried out, researchers focus on selection via differentially expressed surface molecules, factors which allude to cellular role, but are not fully descriptive of inherent bioactivity[13]. There is still a critical need for techniques which can augment current selection approaches with this complimentary set of secretory data. Recently, numerous proof of principle approaches have been reported in the literature, but are not yet broadly available. The continued design and optimization of such phenotyping technologies, particularly platforms that profile individual cell clones massively in parallel, will become invaluable design tools for the engineering of more complex next-generation cell therapies.

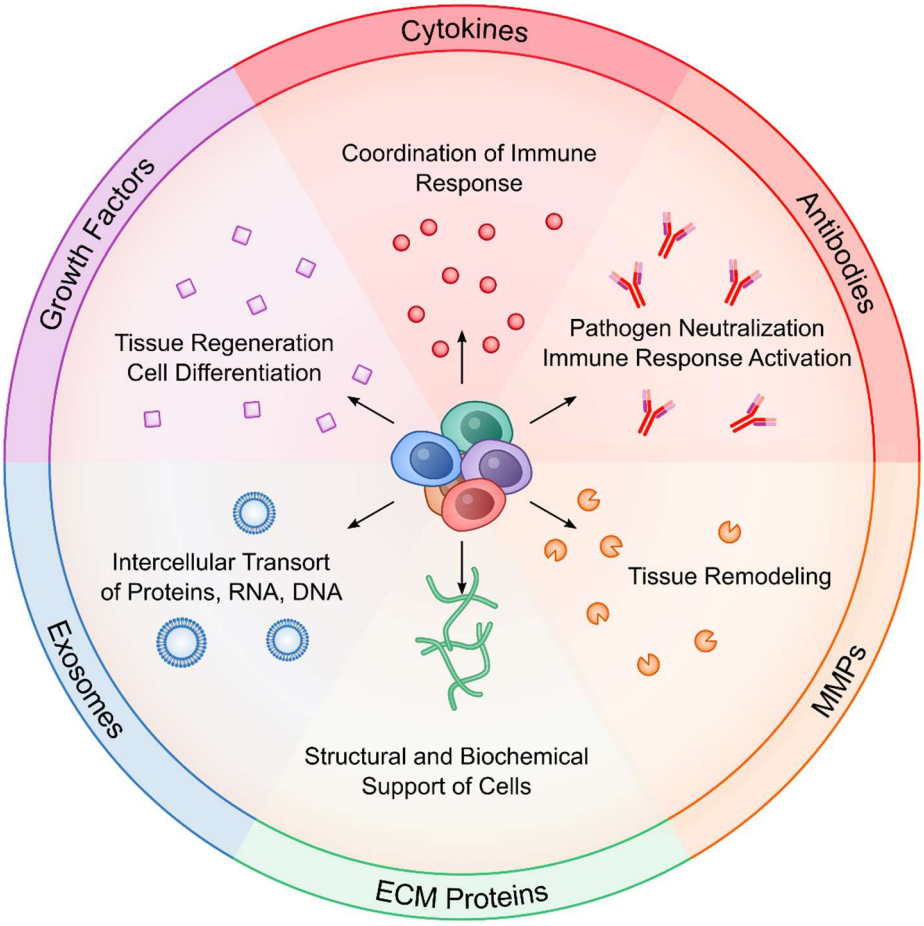

Figure 1-1 Overview of cellular secretions.

Cells secrete numerous factors, including proteins and extracellular vesicles into their surroundings to shape their local microenvironment. Small families of proteins such as growth factors and cytokines signal to other types of cells to coordinate tissue regeneration and differentiation, or coordinate immunological responses to infection. Specialized molecules known as antibodies are produced by B cells and serve to inhibit pathogen function while simultaneously alerting the immune system to their presence. Matrix metalloproteinases (MMPs) degrade extracellular matrix (ECM) proteins to break down tissues, and new ECM proteins can also be secreted to reform them after injury. Exosomes are small vesicles which deliver intracellular proteins, RNAs and DNAs directly to the cytoplasm of receiving cells, altering their behavior. The development of novel systems to study the types and relative amounts of products secreted by individual cells will yield tremendous benefits for advancing basic biological understanding and novel cellular therapeutic applications.

1.1. Single-Cell Profiling Concepts and Design

Single cell secretion assays rely on three critical processes: (1) partitioning of single cells into individual compartments, (2) detection of secreted proteins via biochemical reporter molecules and, (3) measurement of the detection signals and isolation of cells based on these Readouts (Figure 1-2). In this section we will provide a background behind the fundamental concepts and design considerations used to achieve each of these functions.

1.1.1. Compartmentalization

The partitioning of cells into uniform compartments serves several fundamental purposes in the design of single cell secretion profiling systems. First, physical segregation of cells eliminates crosstalk between neighboring cell clones ensuring that readouts generated in each compartment represent only the physical properties of the cells contained within. Second, localization of cells within small volume (often nano- or picoliter scale) containers allows rapid concentration of secreted products, shortening the incubation time required to generate detectable levels of molecules. Lastly, maintaining uniformity in both the size and shape of formed compartments normalizes assay conditions between cells, enabling direct comparison of generated signals across populations. Although there is no ideal compartmentalization strategy for all scenarios, factors such as the desired number of cells to be screened, the average protein production rate, and whether cell recovery is needed, can help dictate the type and size of compartments used.

The two most prevalent compartmentalization strategies are physical confinement, using microfabricated wells and channels[14], or through the formation of aqueous droplets within an immiscible oil solution[15].

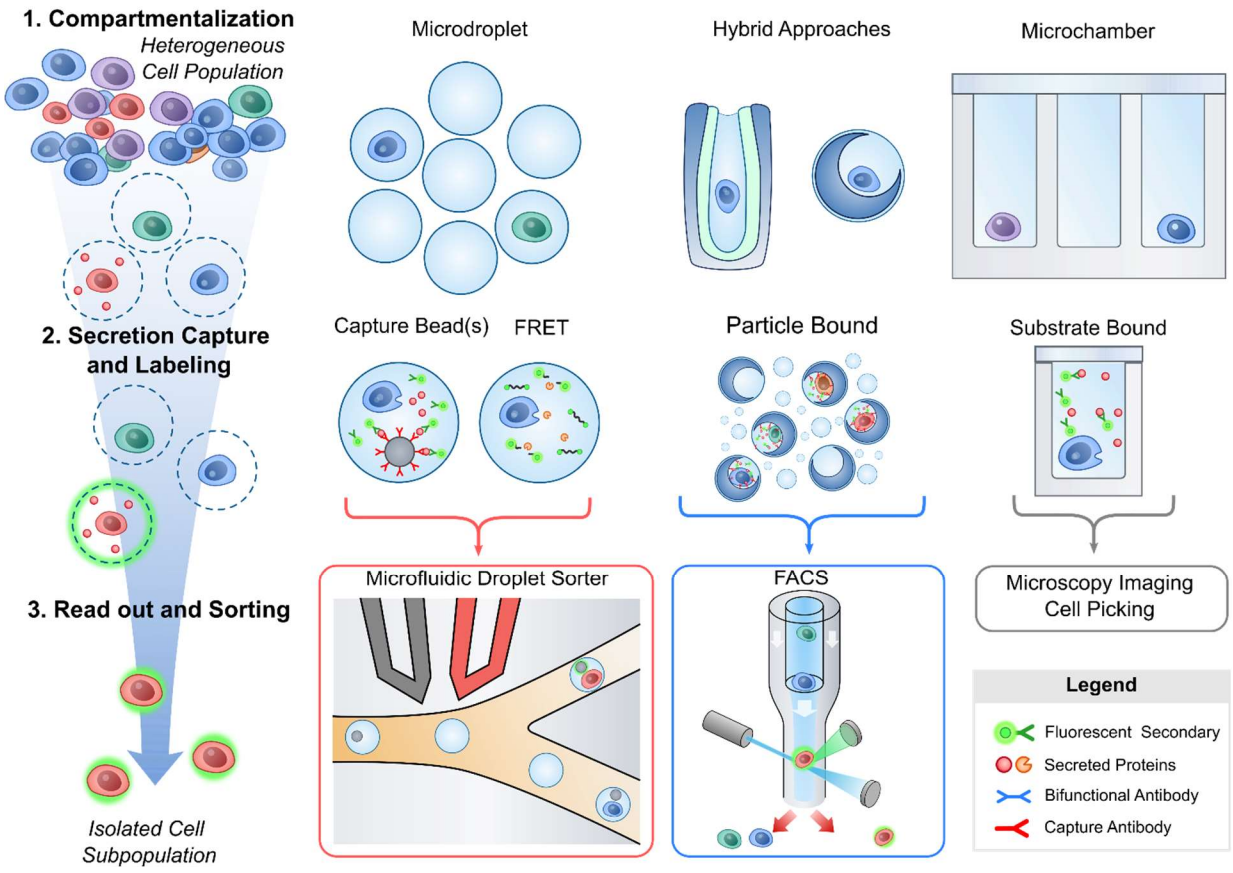

Figure 1-2 Fundamental Principles of Single Cell Secretion Screening

Analysis of secreted products from individual cells relies on three fundamental principles. **1.** Cells must be compartmentalized into individual containers so that their secreted products are rapidly concentrated and cannot intermix with secretions from neighboring cells. This can be accomplished using microfabricated compartments, aqueous emuslions, or hybrid particle templated approaches. **2.** The presence of secreted molecules must be converted into detectable signals. One common method to label secreted proteins is by using a fluorescent ELISA, where antibodies concentrate secretions onto a solid phase where they can be detected with secondary fluorescently labeled detection antibodies. For bioactive molecules like enzymes, substrates that fluoresce upon cleavage can also be used. **3.** Finally to recover cells of interest, each compartment must be assessed and sorted based on the intensity of the accumulated secretion signal. To recover cells from microwells low throughput liquid handlers are needed. Droplets are typically sorted directly on microfluidic chips using techniques such as dielectrophoresis. Hybrid technologies compatible with commercially available high throughput flow sorters are starting to emerge as alternative options.

Microfabricated geometries are beneficial in that each compartment is coupled with a solid phase, such as a well plate bottom, rendering them compatible with both adherent and suspension cell types. Additionally, microfabricated compartments can be made with removable lids[16], or coupled with pumps and valves[17-19] to perform washing steps and deliver reagents to cells after compartmentalization[20]. In contrast, addition of reagents into stably formed water-in-oil emulsions is non-trivial, limiting most reactions carried out in aqueous droplets to a one-pot format where all necessary reagents are pre-mixed and encapsulated simultaneously. Even so, a major advantage of microdroplets is that they can be formed rapidly and continuously, with the final number of compartments limited only by the precursor liquid volume, instead of the footprint of a physical mold which is not easily scaled. Droplets are also easily stored and can be precisely manipulated using microfluidic systems.

Recently, several groups have developed novel hybrid compartmentalization systems in which shaped polymeric microparticles can be used to template the formation of uniform aqueous droplets within a surrounding oil phase through simple mechanical agitation[21-25]. These techniques preserve many of the best facets of both microfabricated and droplet-based approaches, by enabling washing steps and reagent exchange while retaining the ability to manipulate and in some cases even sort the formed compartments. A particularly interesting study by Destgeer and colleagues demonstrated that pooled populations of particles with slightly varied geometries can be used to multiplex droplet screens[23]. For example, the morphology of a particle cavity can be altered to serve as a visual barcode denoting the analyte a droplet is measuring, and the cavity size can be tuned to manipulate the assay dynamic range and limit of detection. These types of physical barcodes may one day be used to perform functional assays against distinct protein targets from a single population of cells simultaneously.

1.1.2. Detection

Once cells are confined, the accumulation of secreted products must be transduced into a detectable signal to enable the qualitative or quantitative assessment of protein production. The most common approach to carry this out is through the use of sandwich immunoassays. Here, solid surfaces functionalized with antigen specific antibodies are utilized to concentrate target proteins from the surrounding solution, enabling localized detection of the analytes with fluorescent or enzymatically labeled reporter antibodies. In both microfabricated and hybrid particle-based compartmentalization schemes capture antibodies can be conjugated directly to the surface of the chamber or particle, enabling signal generation from any sub-volume containing a cell[26, 27]. In contrast, droplet-based technologies require secondary solid capture phases, often in the form of antibody coated polymeric microparticles, to be co-encapsulated alongside individual cells[28, 29]. Notably, in order to preserve the fidelity of single cell assays it is often desired to restrict the number of compartments containing more than one cell. This is typically done by diluting the input cell population such that most generated droplets are empty and a small subset of droplets (~10-30%) contain a cell. Such loading inefficiencies grow exponentially in detection schemes relying on co-encapsulation of both a single cell and a single capture phase, and can significantly reduce the fraction of an analyzed cell population which can be assayed[30]. While in principle it is feasible to circumvent some of these issues by loading capture particles in extreme excess such that each droplet will contain a multitude of particles, in practice the resolution of multi-particle platforms typically suffers as signals are diffusely scattered throughout each compartment and can be masked by background fluorescence. An interesting workflow reported by Chokkalingam et al. was able to circumvent these limitations by forming droplets in an agarose rich aqueous phase. This enabled gelation of droplets after

formation, allowing the researchers to wash away background signal from the sample while retaining the secreting cell and capture beads within the gel mesh[31].

Alternatives to fluorescent sandwich immunoassays have also been reported and may be preferred depending on the type of analyte being studied and the limit of detection required. For example, targets with proteolytic activity such as matrix metalloproteinases can often be measured using fluorescence energy resonance transfer (FRET) approaches, where initially quenched fluorescent peptide substrates are cleaved by secreted enzymes to generate signal[32-34]. FRET analysis typically offers lower limits of detection compared to fluorescent ELISA as individual enzymes can cleave multiple substrate molecules before losing activity, amplifying generated signals. However, this phenonmenon can also easily lead to increases in the assay false positive rate as even a few molecules encapsulated in a compartment away from the secreting cell can generate detectable levels of fluorescence signal. Carefully designed microfluidic systems can be used to wash samples, either passively[35] or actively[36]. Additional approaches which have also recently gained traction in the literature include plasmonic sensor based immunoassays[37] which function by measuring the shift in resonance frequency of nanoparticles conjugated to antibodies and do not require washing steps, and active particle clustering strategies which leverage surface functionalization[38] or externally applied magnetic forces[39] to create large localized particle clusters in the presence of antigen that are subsequently optically or fluorescently detected.

Finally, it should be mentioned that while variations to the aforementioned detection approaches exist, the use of antibodies to detect secreted proteins is a conserved feature across the majority of assays reported to date. Selection of the proper antibody or pairs of antibodies is imperative to proper assay performance. Low affinity (high dissociation constant, K_D) antibodies

can result in false negatives or low signal[40]. Polyclonal antibody mixtures can improve signals by binding to multiple epitopes on the target antigen but also display higher rates of off target binding. When designing a secretion assay against a new target protein it is recommended to initially test several antibodies both for sensitivity and specificity towards the target antigen.

1.1.3. Analysis and Sorting

The ability to quantify secreted molecules and to sort cells of interest in real time based on these measurements is the final feature which must be considered during the design of single-cell screening technologies. Here the performance of static microfabricated compartmentalization schemes deviates greatly from droplet-based technologies. Microfabricated wells and compartments are nearly always analyzed via fluorescence microscopy where the presence of antibodies or other biomolecular sensors can be detected through excitation of the compartment surface. The static nature of microwells combined with the high spatial resolution afforded by fluorescence microscopy enhances the multiplexing capabilities of microwell assays, as analytes can be detected based on combinations of emitted light wavelengths and localization, with some reports demonstrating detection of over 40 analytes simultaneously in a single assay[41]. However, to date isolation strategies are highly inefficient and typically rely on automated liquid handlers which are limited to throughput on the order of 1 cell per minute[42]. Recently technologies have come to market which enable parallelized retrieval of cells from compartments using optical tweezers [43, 44] but these novel tools are still prohibitively expensive and not widely available.

In contrast the inherent mobility of microdroplets renders them compatible with high-throughput continuous sorting modalities. Fluorescence activated droplet sorting (FADS) is perhaps the most commonly utilized approach for microdroplet isolation[29, 45, 46]. In this

strategy an interrogating laser irradiates droplets as they pass through a microfluidic channel and the resulting fluorescence intensity is recorded. If the intensity of the analyzed droplet is sufficiently above a pre-selected threshold an electric field is applied as the droplet passes a downstream junction and droplets containing cells of interest are captured in collection reservoirs. While FADS offers significant improvements in both analysis and detection throughputs over microwell array-based sorting, it should be noted that FADS throughputs are typically reported in units of events/second, where an event is any analyzed droplet. While state of the art FADS sorters typically operate at throughput around 10^3 events/second most analyzed droplets will be empty to prevent multi-cell loading. The actual rate of cellular events analyzed is typically an order of magnitude less.

Fluorescence activated cell sorting is still widely considered to be the gold standard technology for cell sorting, with typical sort throughputs on the order of 10^4 events/second. Unfortunately, standard flow sorters are incapable of processing water-in-oil emulsions, rendering translation of microdroplet based secretion assays difficult. Brower et al. demonstrated preliminary feasibility of sorting single-cell containing microdroplets using flow cytometry by forming water-oil-water double emulsions where an outer surfactant stabilized oil layer preserves droplet stability within the aqueous flow of the cytometer[47, 48], but the generation of such double emulsions is significantly more complex than their single-phase counterparts. Alternative approaches, such as gelation of aqueous droplets can also be utilized, but subsequent recovery of cells from within the microgel is non-trivial[31]. Hybrid, technologies utilizing micro-particles as cell carriers and templates for droplet formation are ideal candidates for enabling analysis of single cell secretions using flow cytometry, however the microparticle size is often a limiting factor in terms of the compatibility with flow cytometry. To date the dropicle platform described

below is the only hybrid secretion assay format with broad compatibility across commercial flow sorters.

1.2. Commercial Technologies for Single Cell Secretion Profiling

Historically, the use of single cell functional screening technologies has been mostly an academic pursuit, where scientists and engineers developed prototype systems to probe, identify, and enrich subsets of cells based on their production of model antigens. However, in recent years, several technologies have emerged to the forefront of the field, demonstrating broad utility in clinical and industrial scale applications, successfully transitioning from prototype systems into commercial products. Below we highlight a subset of the state of the art in commercialized and emerging commercial technologies for single cell functional screening.

1.2.1. Single-Cell Barcode Chips

Single-cell barcode chips (SCBCs) are concentrated arrangements of microfabricated compartments used for highly multiplexed single cell screening (Figure 1-3A). The defining feature of each SCBCs compartments stems from the unique patterning technology used to spatially localize capture antibodies along the compartment surface[27]. Prior to running an assay each distinct capture antibody used in a multiplexed assay is localized into a single vertical bar along the floor of each chamber in the array. This spatially distinct collection of parallel antibody bars yields an extra layer of barcoding for the system, allowing identification of secreted proteins based on both the fluorescence emission spectra and physical location of the reporter antibody targeting a specific antigen. First generation microchamber arrays were reported in the work of Ma et al.[13], whereby each array was manufactured from PDMS bound to antibody coated glass substrates and pneumatic valves were used to seal off each compartment after cell loading.

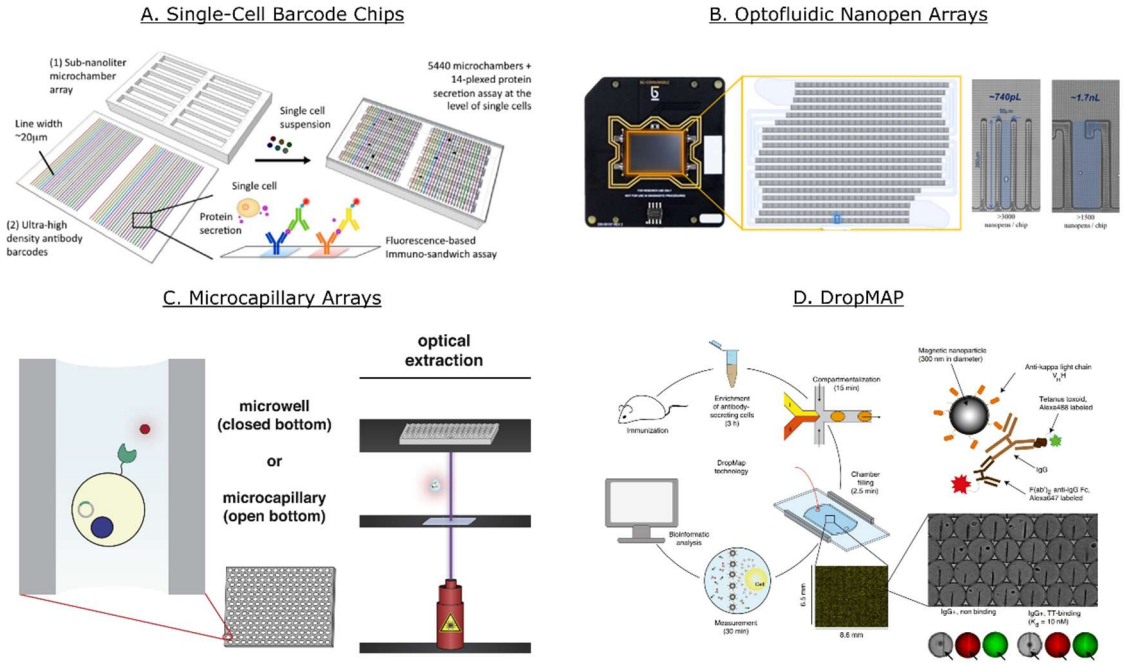

Figure 1-3 Commercialized Platforms for Single Cell Secretion Profiling

Several single cell functional profiling platforms have emerged past the prototype stage to full fledged commercial products. (A) Single-cell barcode chips (commercialized by Isoplexis) are arrays of microfabricated compartments which are useful for highly multiplexed analysis of secreted products. Compartments are decorated with highly ordered arrays of antibodies against target proteins, this allows multiplexing based on both the fluorescent signal of reporter molecules and their binding location. (B) Optofluidic nanopen arrays are fabricated on special substrates which are densely loaded with phototransistors that generate dielectrophoretic forces after excitation with high intensity light. This enables precise manipulation of cells on particles throughout the chip using optoelectronic positioning. The automation and precise control offered by this system enable complex bioassays to be carried out, such as assays that require co-loading of two cells or monitoring of cell growth. (C) Microcapillary arrays can also be used to capture single cells. Here surface tension holds each sub-volume in place while samples are analyzed microscopically. If cells of interest are identified, a laser is used to recover the sample into microwells for further analysis. (D) In DropMAP cells are encapsulated into uniformly sized microdroplets alongside capture antibody functionalized paramagnetic nanoparticles and parked in an incubation chamber. When samples are held in the presence of a magnetic field the nanoparticles form a visible beadline which yields fluorescent signal in the presence of secreted target proteins. Panel A adapted with permission from [49]. Copyright 2013 American Chemical Society. Panel B adapted with permission from [43]. Copyright 2019 Wiley. Panel C adapted with permission from [50]. Copyright 2017 Elsevier. Panel D adapted with permission from [39]. Copyright 2017 Nature Publishing Group.

Since this initial prototype, newer SCBC designs have been reported which increase the number of cells (103 cells/chip)[49] and number of analytes per cell (40+ simultaneous targets)[51] which can be screened in a single assay.

Since its emergence the SCBC has been commercialized into an all-in-one cellular analysis platform (Isolight) developed by Isoplexis. The platform has been used to screen a wide array of cell types including T cells[52], macrophages[53], NK cells[54], and tumor cells[55, 56] for a multitude of clinical applications. One area in which the technology truly excels is in the analysis of T cell quality for CAR-T cell therapies. Isoplexis has developed a unique metric referred to as the polyfunctional strength index (PSI) which consolidates information on the number of different secreted proteins and the relative amount of each secreted protein into a single value representing the functional activity of an individual screened cell[57]. For CAR-T applications the PSI metric correlates well with clinical activity. In one analysis Rossi et al. showed that enrichment of highly polyfunctional cells in pre-infusion anti-CD19 CAR-T cell products was predictive of complete response for the treatment of patients suffering from aggressive refractory non-Hodgkin lymphoma[58]. Continued validation of such results across large patient populations will prove significant for identifying subsets of patients likely to respond to treatment, or who may experience significant side effects from therapy, guiding clinical decision making.

In another study, researchers successfully utilized 32-plex isoplexis cytokine secretion data to identify variations in potency for different CAR constructs, aiding in the fundamental understanding of the mechanisms behind disease relapse in a phase 1 clinical trial of B cell acute lymphoblastic leukemia[59]. While limited in scope to the comparison of only two unique CAR constructs, this work alludes to the potential of single cell functional screening in providing more

thorough assessments of CAR function from early-stage in vitro screens. Taken together, the unparalleled depth of screening offered by SCBC technologies enables researchers to describe variations in cellular phenotypes at resolutions unattainable with most technologies. Similar chip designs have also been utilized for the multiplexed detection of exosome products[60], and future design iterations may offer the capability to simultaneously detect additional biomarkers alongside cytokines. However, it should be noted that the limitations in cellular loading and batch nature of the SCBC assay limit the utility for analysis of truly rare cellular phenotypes.

1.2.2. Optofluidic Nanopen Arrays

Similar to the aforementioned technologies, optofluidic nanopen arrays are highly ordered arrangements of microfabricated compartments (Figure 1-3B) which can be loaded with individual cells. The geometry of nanopens generally varies based on design, but each structure consists of deep chambers ranging from a few hundred picoliters to nanoliters in volume, featuring a small opening on one end to facilitate cell loading and nutrient exchange. Uniquely however, the microfabricated features are patterned onto specialized substrates containing numerous phototransistors which generate dielectrophoretic forces upon excitation with high intensity light[61]. When utilized for single cell studies populations of cells are placed onto each array and single clones are guided in parallel into individual nanopens through these optically generated forces using a technique called optoelectronic positioning. Any remaining unloaded cells are then washed away. A major benefit of this workflow is that the directed nature of loading is not governed by typical Poisson statistics, permitting higher proportions of chambers on each chip to be loaded with cells.

The continued optimization of optofluidic nanopen arrays has led to the creation of an industrial scale platform, Beacon®, developed by Berkeley Lights[43]. While this technology is

still limited in its cellular analysis throughput due to the footprint constraints on the microfabricated chips (~3500 pens/chip), the increased precision and automation afforded by the built-in image processing and optical manipulation yield tremendous benefit in many industrial workflows. Cells, multiple cells, or cells and capture beads can all be simultaneously localized within nanopens, permitting the assessment of increasingly complex biological phenomena such as interactions between immune cells and cells expressing target antigens. Additionally, the expansion of individual cells into clonal populations is permitted on-chip[62], and subsets of expanded populations can be collected into individual wells simultaneously for concurrent downstream assessment of genotype and phenotype[44, 63].

The precise control over cell culture parameters offered by the Beacon® system also renders assays compatible with hard to maintain primary cell types such as lymphocytes. For example, work by Winters and colleagues highlighted the ability to assay antigen specific antibody production directly from primary murine antibody secreting B cells (ASCs)[64]. Using the beacon platform researchers were able to recover a set of 44 antigen specific ASCs, from an initial population of 952 primary cells within a single day. This work yielded 13 distinct sets of paired heavy and light chain antibody sequences with unprecedented speed, potentially providing a more streamlined route to the development of high-quality antibody drugs over traditional approaches such as hybridoma analysis or phage display. Notably however, the authors mentioned that without significant optimization the use of optoelectronic positioning significantly affected the viability of fragile primary ASCs and loading via gravity was preferred. Even so, the complete range of applications enabled by the Beacon platform is only starting to be explored. It is not difficult to envision how extensions of preliminary studies reported in the

literature can be used to identify beneficial genetic variations in therapeutic cells based on the results of multiplexed cytokine secretion or killing assays.

1.2.3. Microcapillary Arrays

In another variation on traditional microfabricated chambers, cells can also be captured into highly ordered arrays of microcapillaries (Figure 1-3C) for subsequent analysis and sorting[50]. Microcapillary arrays are easily loaded through capillary action when the open ends of each chamber come into contact with pre-diluted cell mixtures. Although one end of each capillary is unsealed, liquid volumes in chambers are maintained through surface tension, this allows suspension of microcapillary arrays over standard microscope setups and direct imaging of settled cells with minimal focusing adjustments. Microcapillary arrays can contain over 1 million individual chambers, but cell loading is dictated by poisson statistics, meaning that in order to limit the number of capillaries containing multiple cells most capillaries will be empty. An innovative technique first reported by the Cochran lab demonstrated that laser induced cavitation can be used to disrupt the volumes help in each chamber, allowing directed recovery of capillary volumes on demand[65]. In a workflow the authors refer to as μSCALE (microcapillary single-cell analysis and laser extraction) this automated imaging strategy and laser assisted recovery was utilized to screen for improved antibody, enzyme, and fluorescent protein variants produced by mutated libraries of yeast and E. coli[66]. Since then, the technology has been commercialized by xCella biosciences where it was marketed as the xPloration^{TM} screening platform and utilized mostly for antibody engineering strategies. Recently xCella was acquired by Ligand pharmaceuticals and is now part of their OmniAb® technology suite for the production of humanized antibody products.

1.2.4. DropMAP

DropMAP (Figure 1-3D) is a microfluidic droplet based platform which was first reported in 2017 when Eyer et al. sought to develop a more quantitative and high-throughput technology to screen antibody production from B cells[67]. The DropMAP platform has two components. First, a microfluidic droplet generator is used to encapsulate single cells into uniformly sized microdroplets alongside fluorescently labeled detection antibodies and paramagnetic nanoparticles functionalized with capture antibodies. Subsequently, the formed droplets are held in a monolayer within a secondary collection reservoir and incubated to allow accumulation of secretions from the captured cells. The detection of secreted molecules proceeds in an analogous manner to most other bead-based secretion assays (see detection concept section above) with the notable exception that the paramagnetic capture nanoparticles used in this assay form micron scale aggregates, termed beadlines, after application of a magnetic field. This is a critical feature, as the aggregation of capture beads will localize the fluorescence signal over time in the presence of antigen, rendering the presence of target proteins visible over background without washing steps.

During assays the collection reservoir is analyzed over time via standard fluorescence microscopy and the change in fluorescence intensity of each beadline is tracked to monitor the secretion rate of individual cells. Although in principle arrays of droplets temporarily parked within a collection reservoir function identically to on-chip fabricated microcompartments the droplets used in this approach take up much more of the device footprint, raising the number of cells that can be assayed in a single chamber to ~20,000[68]. Detection of secreted molecules occurs rapidly, with some studies reporting the identification of actively secreting cells in less than 30 minutes, however viable cells can also be maintained within compartments for up to 12

hours allowing easy observation of changes in secretion kinetics rather than simply assessing total protein production as in traditional endpoint assays.

While initial applications of the DropMAP technology focused on developing novel insights into the humoral immune response of B cells to vaccine or infection[69-71], the platform and its reported use cases have expanded significantly in recent years[68]. Shortly after commercialization by HIFIBio in 2019, reports of a novel variation of DropMAP compatible with on-chip dielectrophoretic sorting and next generation sequencing (CelliGO) emerged, raising analysis throughputs even further to 2.5 million cells/experiment[72]. Additionally, the platform has been successfully utilized to screen cytokine secretions from T cells following chemical stimulation as well as from primary monocytes isolated from both healthy and septic patients. DropMAP certainly has promise as a broadscale analytical tool for immunological monitoring through quantitative kinetic secreting screening. However, it should be noted that true quantitative analysis using the platform may require significant optimization by the end user as factors such as the number of particles in each droplet, the concentration and affinity of the antibodies used, and the secretion rate of the cells can all effect the assay's sensitivity, limit of detection, and dynamic range[68].

1.2.5. Particle Templated Droplets (Dropicles)

As demonstrated in the sections above, the vast majority of the single-cell functional screening technologies which have been commercialized to date have taken the form of ordered arrays of static microcompartments. These types of systems are appealing products because they are easily fabricated and distributed to consumers, who can then use them as single-use disposable cartridges in specialized instruments that automate analysis and data collection. However, the batch nature of these types of workflows significantly limits the number of cells

that can be analyzed in each run. In biological applications rare cell subsets such as antigen specific antibody secreting cells, or polyfunctional T cells, often comprise exceedlingly low fractions of a given population[58, 64]. Thus, screening these cell types with currently available technologies often requires pre-enrichment with either fluorescence or magnetically activated cell sorting (FACS and MACS), laborious processes in their own right.

Our lab has recently developed a completely novel platform for single-cell analysis centered around the use of precisely fabricated polymeric microparticles (drop-carrier particles) which can capture single cells, partition them into aqueous compartments (dropicles), report the presence of secreted signals, and finally isolate desirable cell clones through standard flow cytometry, which we report on in depth in chapter 3 and 4 of this work. Notably, while particle fabrication requires microfluidic technology, the fully formed particle samples are stable and can be distributed for use as a consumable reagent that is compatible with all standard labware. Particles are formed based on user need in sizes ranging from 35 μm to 105 μm in diameter, and contain a single uniformly sized cavity (20-60 μm in diameter) which can be loaded with cells. Cells are attached to particles via either antibodies targeting cell surface markers (suspension cell binding) or through integrin binding peptides (adherent cell binding). After adhesion, emulsions can be formed through simple pipetting induced mechanical shear on aqueous particle suspensions in the presence of fluorinated oil. Once partitioned, cell loaded particles are incubated and any secreted products are captured back on the particle surface. Finally, emulsions are destabilized, and particles can be recovered, stained with fluorescently labeled reporter antibodies or antigens, and sorted with standard flow cytometry.

The dropicle workflow is highly generalizable and has been used successfully with a wide variety of adherent (chinese hamster ovary cells (CHO), human embryonic kidney cells

(HEK), mesenchymal stem cell (MSC)), and suspension (B cells, T cells, hybridomas, macrophages) cell types for single cell protein production assays, across numerous commercially available flow sorters (BD FACSAriaTM II, BDFACSAriaTM III, Sony SH800, On-Chip Sort). (see chapters 3 and 4). Initial studies demonstrated the ability to screen and sort highly productive antibody secreting CHO cell clones as well as antigen specific antibody secreting hybridomas and murine B cells for antibody discovery applications at rates around 1,000 events/second. Uniquely in this workflow, cells are only encapsulated for the time duration necessary to attain a detectable amount of secretion signal, several minutes to hours depending on the cell type. For the remainder of the assay, cells are maintained in fresh media with free exchange of nutrient and waste products. One downside of the platform is that it requires significantly more hands-on time from the end user, as assays are not automated in a complex instrument, however, this factor also yields an extreme amount of assay customizability depending on user need. Furthermore, there is no need to pre-enrich cell populations of rare cells as functional readouts can be sorted directly using standard FACS. While the dropicle platform is still in its infancy, and numerous applications are still untapped, it was recently commercialized by Partillion Bioscience. Initial work has highlighted the feasibility of working directly with primary antibody secreting cells, but a natural extension is evaluation of cytokine production from T cells for cell therapies and we present some preliminary data on T cell compatibility with dropicles in chapter 5. Additionally, this platform is the first reported droplet-based screening technology fully compatible with adherent cell types and may provide a unique tool to screen understudied cell types such as mesenchymal stem cells at the single cell level for regenerative therapy applications.

1.3. References

[1] M.A. Fischbach, J.A. Bluestone, W.A. Lim, Cell-Based Therapeutics: The Next Pillar of Medicine, Sci Transl Med, 5 (2013).

[2] D.H. Busch, S.P. Frassle, D. Sommermeyer, V.R. Buchholz, S.R. Riddell, Role of memory T cell subsets for adoptive immunotherapy, Semin Immunol, 28 (2016) 28-34.

[3] H.M. Knochelmann, A.S. Smith, C.J. Dwyer, M.M. Wyatt, S. Mehrotra, C.M. Paulos, CAR T Cells in Solid Tumors: Blueprints for Building effective Therapies, Front Immunol, 9 (2018).

[4] W.M. Kong, S.F. Lacey, J.J. Melenhorst, J.A. Fraietta, Biomarkers in chimeric antigen receptor T-cell therapy, Biomark Med, 12 (2018) 415-418.

[5] C. Nombela-Arrieta, J. Ritz, L.E. Silberstein, The elusive nature and function of mesenchymal stem cells, Nat Rev Mol Cell Bio, 12 (2011) 126-131.

[6] J.Q. Yin, J. Zhu, J.A. Ankrum, Manufacturing of primed mesenchymal stromal cells for therapy, Nat Biomed Eng, 3 (2019) 90-104.

[7] S. Lin-Gibson, S. Sarkar, Y. Ito, Defining quality attributes to enable measurement assurance for cell therapy products, Cytotherapy, 18 (2016) 1241-1244.

[8] R. Haddock, S. Lin-Gibson, N. Lumelsky, R. McFarland, K. Roy, K. Saha, J. Zhang, C. Zylberberg, Manufacturing cell therapies: the paradigm shift in health care of this century, NAM Perspectives, (2017).

[9] J.A. Fraietta, C.L. Nobles, M.A. Sammons, S. Lundh, S.A. Carty, T.J. Reich, A.P. Cogdill, J.J.D. Morrissette, J.E. DeNizio, S. Reddy, Y. Hwang, M. Gohil, I. Kulikovskaya, F. Nazimuddin, M. Gupta, F. Chen, J.K. Everett, K.A. Alexander, E. Lin-Shiao, M.H. Gee, X.J. Liu, R.M. Young, D. Ambrose, Y. Wang, J. Xu, M.S. Jordan, K.T. Marcucci, B.L. Levine, K.C. Garcia, Y.B. Zhao, M. Kalos, D.L. Porter, R.M. Kohli, S.F. Lacey, S.L. Berger, F.D. Bushman, C.H. June, J.J. Melenhorst, Disruption of TET2 promotes the therapeutic efficacy of CD19-targeted T cells, Nature, 558 (2018) 307-+.

[10] H.A. Abdelsamed, C.C. Zebley, H. Nguyen, R.L. Rutishauser, Y.P. Fan, H.E. Ghoneim, J.C. Crawford, F. Alfei, S. Alli, S.P. Ribeiro, A.H. Castellaw, M.A. McGargill, H.J. Jin, S.K. Boi, C. Speake, E. Serti, L.A. Turka, M.E. Busch, M. Stone, S.G. Deeks, R.P. Sekaly, D. Zehn, E.A.

James, G.T. Nepom, B. Youngblood, Beta cell-specific CD8(+) T cells maintain stem cell memory-associated epigenetic programs during type 1 diabetes, Nat Immunol, 21 (2020) 578-+.

[11] M. Uhlen, L. Fagerberg, B.M. Hallstrom, C. Lindskog, P. Oksvold, A. Mardinoglu, A. Sivertsson, C. Kampf, E. Sjostedt, A. Asplund, I. Olsson, K. Edlund, E. Lundberg, S. Navani, C.A. Szigyarto, J. Odeberg, D. Djureinovic, J.O. Takanen, S. Hober, T. Alm, P.H. Edqvist, H. Berling, H. Tegel, J. Mulder, J. Rockberg, P. Nilsson, J.M. Schwenk, M. Hamsten, K. von Feilitzen, M. Forsberg, L. Persson, F. Johansson, M. Zwahlen, G. von Heijne, J. Nielsen, F. Ponten, Tissue-based map of the human proteome, Science, 347 (2015).

[12] S.R. Riddell, D. Sommermeyer, C. Berger, L.F. Liu, A. Balakrishnan, A. Salter, M. Hudecek, D.G. Maloney, C.J. Turtle, Adoptive Therapy With Chimeric Antigen Receptor-Modified T Cells of Defined Subset Composition, Cancer J, 20 (2014) 141-144.

[13] C. Ma, R. Fan, H. Ahmad, Q.H. Shi, B. Comin-Anduix, T. Chodon, R.C. Koya, C.C. Liu, G.A. Kwong, C.G. Radu, A. Ribas, J.R. Heath, A clinical microchip for evaluation of single immune cells reveals high functional heterogeneity in phenotypically similar T cells, Nat Med, 17 (2011) 738-U133.

[14] H. Park, H. Kim, J. Doh, Multifunctional Microwell Arrays for Single Cell Level Functional Analysis of Lymphocytes, Bioconjugate Chem, 29 (2018) 672-679.

[15] A.B. Theberge, F. Courtois, Y. Schaerli, M. Fischlechner, C. Abell, F. Hollfelder, W.T.S. Huck, Microdroplets in Microfluidics: An Evolving Platform for Discoveries in Chemistry and Biology, Angew Chem Int Edit, 49 (2010) 5846-5868.

[16] Q. Han, N. Bagheri, E.M. Bradshaw, D.A. Hafler, D.A. Lauffenburger, J.C. Love, Polyfunctional responses by human T cells result from sequential release of cytokines, P Natl Acad Sci USA, 109 (2012) 1607-1612.

[17] M.A. Unger, H.P. Chou, T. Thorsen, A. Scherer, S.R. Quake, Monolithic microfabricated valves and pumps by multilayer soft lithography, Science, 288 (2000) 113-116.

[18] M. Junkin, A.J. Kaestli, Z. Cheng, C. Jordi, C. Albayrak, A. Hoffmann, S. Tay, High-Content Quantification of Single-Cell Immune Dynamics, Cell Rep, 15 (2016) 411-422.

[19] J.W. Hong, V. Studer, G. Hang, W.F. Anderson, S.R. Quake, A nanoliter-scale nucleic acid processor with parallel architecture, Nature Biotechnology, 22 (2004) 435-439.

[20] L. Armbrecht, R.S. Muller, J. Nikoloff, P.S. Dittrich, Single-cell protein profiling in microchambers with barcoded beads, Microsyst Nanoeng, 5 (2019).

[21] M.N. Hatori, S.C. Kim, A.R. Abate, Particle-Templated Emulsification for Microfluidics-Free Digital Biology, Anal Chem, 90 (2018) 9813-9820.

[22] C.Y. Wu, M.X. Ouyang, B. Wang, J. de Rutte, A. Joo, M. Jacobs, K. Ha, A.L. Bertozzi, D. Di Carlo, Monodisperse drops templated by 3D-structured microparticles, Sci Adv, 6 (2020).

[23] G. Destgeer, M.X. Ouyang, C.Y. Wu, D. Di Carlo, Fabrication of 3D concentric amphiphilic microparticles to form uniform nanoliter reaction volumes for amplified affinity assays, Lab on a Chip, 20 (2020) 3503-3514.

[24] J.d. Rutte, R. Dimatteo, M.v. Zee, R. Damoiseaux, D.D. Carlo, Massively parallel encapsulation of single cells with structured microparticles and secretion-based flow sorting, bioRxiv, (2020) 2020.2003.2009.984245-982020.984203.984209.984245.

[25] R. Novak, Y. Zeng, J. Shuga, G. Venugopalan, D.A. Fletcher, M.T. Smith, R.A. Mathies, Single-Cell Multiplex Gene Detection and Sequencing with Microfluidically Generated Agarose Emulsions, Angew Chem Int Edit, 50 (2011) 390-395.

[26] A.O. Ogunniyi, C.M. Story, E. Papa, E. Guillen, J.C. Love, Screening individual hybridomas by microengraving to discover monoclonal antibodies, Nat Protoc, 4 (2009) 767-782.

[27] Y.S. Shin, H. Ahmad, Q. Shi, H. Kim, T.A. Pascal, R. Fan, W.A. Goddard, 3rd, J.R. Heath, Chemistries for patterning robust DNA microbarcodes enable multiplex assays of cytoplasm proteins from single cancer cells, Chemphyschem, 11 (2010) 3063-3069.

[28] T. Konry, M. Dominguez-Villar, C. Baecher-Allan, D.A. Hafler, M.L. Yarmush, Droplet-based microfluidic platforms for single T cell secretion analysis of IL-10 cytokine, Biosensors and Bioelectronics, 26 (2011) 2707-2710.

[29] L. Mazutis, J. Gilbert, W.L. Ung, D.A. Weitz, A.D. Griffiths, J.A. Heyman, Single-cell analysis and sorting using droplet-based microfluidics, Nat Protoc, 8 (2013) 870-891.

[30] P. Kumaresan, C.J. Yang, S.A. Cronier, R.G. Blazej, R.A. Mathies, High-throughput single copy DNA amplification and cell analysis in engineered nanoliter droplets, Anal Chem, 80 (2008) 3522-3529.

[31] V. Chokkalingam, J. Tel, F. Wimmers, X. Liu, S. Semenov, J. Thiele, C.G. Figdor, W.T.S. Huck, Probing cellular heterogeneity in cytokine-secreting immune cells using droplet-based microfluidics, Lab on a Chip, 13 (2013) 4740-4740.

[32] M. Wang, M.H. Nai, R.Y.J. Huang, H.L. Leo, C.T. Lim, C.H. Chen, High-throughput functional profiling of single adherent cells via hydrogel drop-screen, Lab on a Chip, 21 (2021) 764-774.

[33] Y.C. Chen, Y.H. Cheng, P. Ingram, E. Yoon, Single Cell Proteolytic Assays to Investigate Cancer Clonal Heterogeneity and Cell Dynamics Using an Efficient Cell Loading Scheme, Sci Rep-Uk, 6 (2016).

[34] K.K. Zeming, R. Lu, K.L. Woo, G.Y. Sun, K.Y. Quek, L.F. Cheow, C.H. Chen, J. Han, S.L. Lim, Multiplexed Single-Cell Leukocyte Enzymatic Secretion Profiling from Whole Blood Reveals Patient-Specific Immune Signature, Anal Chem, 93 (2021) 4374-4382.

[35] T.Y. Jing, Z.X. Lai, L.D. Wu, J.Y. Han, C.T. Lim, C.H. Chen, Single Cell Analysis of Leukocyte Protease Activity Using Integrated Continuous-Flow Microfluidics, Anal Chem, 88 (2016) 11750-11757.

[36] M. Dhar, J.N. Lam, T. Walser, S.M. Dubinett, M.B. Rettig, D. Di Carlo, Functional profiling of circulating tumor cells with an integrated vortex capture and single-cell protease activity assay, P Natl Acad Sci USA, 115 (2018) 9986-9991.

[37] S.C. Wei, M.N. Hsu, C.H. Chen, Plasmonic droplet screen for single-cell secretion analysis, Biosens Bioelectron, 144 (2019).

[38] T. Yu, A. Bhat, A. Henderson, J. Hull, A.S. Basu, A Novel Computer Vision System for Integrated Biomolecule and Cell Assays, Ieee Sensor, (2019).

[39] K. Eyer, R.C. Doineau, C.E. Castrillon, L. Briseño-Roa, V. Menrath, G. Mottet, P. England, A. Godina, E. Brient-Litzler, C. Nizak, Single-cell deep phenotyping of IgG-secreting cells for high-resolution immune monitoring, Nature biotechnology, 35 (2017) 977.

[40] A.J. Torres, A.S. Hill, J.C. Love, Nanowell-Based Immunoassays for Measuring Single-Cell Secretion: Characterization of Transport and Surface Binding, Anal Chem, 86 (2014) 11562-11569.

[41] Y. Lu, Q. Xue, M.R. Eisele, E.S. Sulistijo, K. Brower, L. Han, E.A.D. Amir, D. Pe'er, K. Miller-Jensen, R. Fan, Highly multiplexed profiling of single-cell effector functions reveals deep functional heterogeneity in response to pathogenic ligands, P Natl Acad Sci USA, 112 (2015) E607-E615.

[42] J.H. Choi, A.O. Ogunniyi, M.D. Du, M.N. Du, M. Kretschmann, J. Eberhardt, J.C. Love, Development and Optimization of a Process for Automated Recovery of Single Cells Identified by Microengraving, Biotechnology Progress, 26 (2010) 888-895.

[43] M. Jorgolli, T. Nevill, A. Winters, I. Chen, S. Chong, F.F. Lin, M. Mock, C. Chen, K. Le, C. Tan, P. Jess, H. Xu, A. Hamburger, J. Stevens, T. Munro, M. Wu, P. Tagari, L.P. Miranda, Nanoscale integration of single cell biologics discovery processes using optofluidic manipulation and monitoring, Biotechnol Bioeng, 116 (2019) 2393-2411.

[44] A. Mocciaro, T.L. Roth, H.M. Bennett, M. Soumillon, A. Shah, J. Hiatt, K. Chapman, A. Marson, G. Lavieu, Light-activated cell identification and sorting (LACIS) for selection of edited clones on a nanofluidic device, Commun Biol, 1 (2018).

[45] J.C. Baret, O.J. Miller, V. Taly, M. Ryckelynck, A. El-Harrak, L. Frenz, C. Rick, M.L. Samuels, J.B. Hutchison, J.J. Agresti, D.R. Link, D.A. Weitz, A.D. Griffiths, Fluorescence-activated droplet sorting (FADS): Efficient microfluidic cell sorting based on enzymatic activity, Lab on a Chip, 9 (2009) 1850-1858.

[46] D. Vallejo, A. Nikoomanzar, B.M. Paegel, J.C. Chaput, Fluorescence-Activated Droplet Sorting for Single-Cell Directed Evolution, Acs Synth Biol, 8 (2019) 1430-1440.

[47] K.K. Brower, C. Carswell-Crumpton, S. Klemm, B. Cruz, G. Kim, S.G.K. Calhoun, L. Nichols, P.M. Fordyce, Double emulsion flow cytometry with high-throughput single droplet isolation and nucleic acid recovery, Lab on a Chip, 20 (2020) 2062-2074.

[48] K.K. Brower, M. Khariton, P.H. Suzuki, C. Still, G. Kim, S.G.K. Calhoun, L.S. Qi, B. Wang, P.M. Fordyce, Double Emulsion Picoreactors for High-Throughput Single-Cell Encapsulation and Phenotyping via FACS, Anal Chem, 92 (2020) 13262-13270.

[49] Y. Lu, J.J. Chen, L.Y. Mu, Q. Xue, Y. Wu, P.H. Wu, J. Li, A.O. Vortmeyer, K. Miller-Jensen, D. Wirtz, R. Fan, High-Throughput Secretomic Analysis of Single Cells to Assess Functional Cellular Heterogeneity, Anal Chem, 85 (2013) 2548-2556.

[50] C.K. Longwell, L. Labanieh, J.R. Cochran, High-throughput screening technologies for enzyme engineering, Curr Opin Biotech, 48 (2017) 196-202.

[51] Y. Lu, Q. Xue, M.R. Eisele, E.S. Sulistijo, K. Brower, L. Han, E.D. Amir, D. Pe'er, K. Miller-Jensen, R. Fan, Highly multiplexed profiling of single-cell effector functions reveals deep functional heterogeneity in response to pathogenic ligands, P Natl Acad Sci USA, 112 (2015) E607-E615.

[52] Q. Xue, E. Bettini, P. Paczkowski, C. Ng, A. Kaiser, T. McConnell, O. Kodrasi, M.F. Quigley, J. Heath, R. Fan, S. Mackay, M.E. Dudley, S.H. Kassim, J. Zhou, Single-cell multiplexed cytokine profiling of CD19 CAR-T cells reveals a diverse landscape of polyfunctional antigen-specific response, J Immunother Cancer, 5 (2017).

[53] Y.P. Chen, H.J. Kim, H.Y. Wu, T. Price-Troska, J.C. Villasboas, S. Jalali, A.L. Feldman, A.J. Novak, Z.Z. Yang, S.M. Ansell, SIRP alpha expression delineates subsets of intratumoral monocyte/macrophages with different functional and prognostic impact in follicular lymphoma, Blood Cancer J, 9 (2019).

[54] H. Zhu, R.H. Blum, D. Bernareggi, E.H. Ask, Z.M. Wu, H.J. Hoel, Z.P. Meng, C.S. Wu, K.L. Guan, K.J. Malmberg, D.S. Kaufman, Metabolic Reprograming via Deletion of CISH in Human iPSC-Derived NK Cells Promotes In Vivo Persistence and Enhances Anti-tumor Activity, Cell Stem Cell, 27 (2020) 224-+.

[55] Q.H. Shi, L.D. Qin, W. Wei, F. Geng, R. Fan, Y.S. Shin, D.L. Guo, L. Hood, P.S. Mischel, J.R. Heath, Single-cell proteomic chip for profiling intracellular signaling pathways in single tumor cells, P Natl Acad Sci USA, 109 (2012) 419-424.

[56] M. Elitas, K. Brower, Y. Lu, J.J. Chen, R. Fan, A microchip platform for interrogating tumor-macrophage paracrine signaling at the single-cell level, Lab on a Chip, 14 (2014) 3582-3588.

[57] C. Ma, A.F. Cheung, T. Chodon, R.C. Koya, Z.Q. Wu, C. Ng, E. Avramis, A.J. Cochran, O.N. Witte, D. Baltimore, B. Chmielowski, J.S. Economou, B. Comin-Anduix, A. Ribas, J.R. Heath, Multifunctional T-cell Analyses to Study Response and Progression in Adoptive Cell Transfer Immunotherapy, Cancer Discov, 3 (2013) 418-429.

[58] J. Rossi, P. Paczkowski, Y.W. Shen, K. Morse, B. Flynn, A. Kaiser, C. Ng, K. Gallatin, T. Cain, R. Fan, S. Mackay, J.R. Heath, S.A. Rosenberg, J.N. Kochenderfer, J. Zhou, A. Bot, Preinfusion polyfunctional anti-CD19 chimeric antigen receptor T cells are associated with clinical outcomes in NHL, Blood, 132 (2018) 804-814.

[59] J.Y. Spiegel, S. Patel, L. Muffly, N.M. Hossain, J. Oak, J.H. Baird, M.J. Frank, P. Shiraz, B. Sahaf, J. Craig, M. Iglesias, S. Younes, Y. Natkunam, M.G. Ozawa, E. Yang, J. Tamaresis, H. Chinnasamy, Z. Ehlinger, W. Reynolds, R. Lynn, M.C. Rotiroti, N. Gkitsas, S. Arai, L. Johnston, R. Lowsky, R.G. Majzner, E. Meyer, R.S. Negrin, A.R. Rezvani, S. Sidana, J. Shizuru, W.K. Weng, C. Mullins, A. Jacob, I. Kirsch, M. Bazzano, J. Zhou, S. Mackay, S.J. Bornheimer, L. Schultz, S. Ramakrishna, K.L. Davis, K.A. Kong, N.N. Shah, H.Y. Qin, T. Fry, S. Feldman, C.L. Mackall, D.B. Miklos, CAR T cells with dual targeting of CD19 and CD22 in adult patients with recurrent or refractory B cell malignancies: a phase 1 trial, Nat Med, 27 (2021) 1419-+.

[60] Y.H. Ji, D.Y. Qi, L.M. Li, H.R. Su, X.J. Li, Y. Luo, B. Sun, F.Y. Zhang, B.C. Lin, T.J. Liu, Y. Lu, Multiplexed profiling of single-cell extracellular vesicles secretion, P Natl Acad Sci USA, 116 (2019) 5979-5984.

[61] H.Y. Hsu, A.T. Ohta, P.Y. Chiou, A. Jamshidi, S.L. Neale, M.C. Wu, Phototransistor-based optoelectronic tweezers for dynamic cell manipulation in cell culture media, Lab on a Chip, 10 (2010) 165-172.

[62] K. Le, C. Tan, H. Le, J. Tat, E. Zasadzinska, J. Diep, R. Zastrow, C. Chen, J. Stevens, Assuring Clonality on the Beacon Digital Cell Line Development Platform, Biotechnol J, 15 (2020).

[63] K.G. Beaumont, W. Hamou, N. Bozinovic, T.R. Silvers, H. Shah, A. Dave, K. Allette, M. Strahl, Y.-c. Wang, H. Arib, A. Antoine, E. Ellis, M. Smith, B. Bruhn, P. Dottino, J.A. Martignetti, E. Schadt, M. White, R. Sebra, Multiparameter cell characterization using nanofluidic technology facilitates real-time phenotypic and genotypic elucidation of intratumor heterogeneity, bioRxiv, (2018) 457010.

[64] A. Winters, K. McFadden, J. Bergen, J. Landas, K.A. Berry, A. Gonzalez, H. Salimi-Moosavi, C.M. Murawsky, P. Tagari, C.T. King, Rapid single B cell antibody discovery using nanopens and structured light, mAbs, 11 (2019) 1025-1035.

[65] S. Lim, B. Chen, M.S. Kariolis, I.K. Dimov, T.M. Baer, J.R. Cochran, Engineering High Affinity Protein-Protein Interactions Using a High-Throughput Microcapillary Array Platform, Acs Chem Biol, 12 (2017) 336-341.

[66] B. Chen, S.W. Lim, A. Kannan, S.C. Alford, F. Sunden, D. Herschlag, I.K. Dimov, T.M. Baer, J.R. Cochran, High-throughput analysis and protein engineering using microcapillary arrays, Nat Chem Biol, 12 (2016) 76-+.

[67] K. Eyer, R.C.L. Doineau, C.E. Castrillon, L. Briseño-Roa, V. Menrath, G. Mottet, P. England, A. Godina, E. Brient-Litzler, C. Nizak, A. Jensen, A.D. Griffiths, J. Bibette, P. Bruhns, J. Baudry, Single-cell deep phenotyping of IgG-secreting cells for high-resolution immune monitoring, Nat. Biotechnol., 35 (2017) 977-982.

[68] Y. Bounab, K. Eyer, S. Dixneuf, M. Rybczynska, C. Chauvel, M. Mistretta, T. Tran, N. Aymerich, G. Chenon, J.F. Llitjos, F. Venet, G. Monneret, I.A. Gillespie, P. Cortez, V. Moucadel, A. Pachot, A. Troesch, P. Leissner, J. Textoris, J. Bibette, C. Guyard, J. Baudry, A.D. Griffiths, C. Vedrine, Dynamic single-cell phenotyping of immune cells using the microfluidic platform DropMap, Nat Protoc, 15 (2020) 2920-2955.

[69] M. Heo, G. Chenon, C. Castrillon, J.M. Bibette, P. Bruhns, A.D. Griffiths, J. Baudry, K. Eyer, Deep phenotypic characterization of immunization-induced antibacterial IgG repertoires in mice using a single-antibody bioassay, Commun Biol, 3 (2020).

[70] K. Eyer, C. Castrillon, G. Chenon, J. Bibette, P. Bruhns, A.D. Griffiths, J. Baudry, The Quantitative Assessment of the Secreted IgG Repertoire after Recall to Evaluate the Quality of Immunizations, J Immunol, 205 (2020) 1176-1184.

[71] K. Eyer, One by One - Insights into Complex Immune Responses through Functional Single-cell Analysis, Chimia, 74 (2020) 716-723.

[72] A. Gérard, A. Woolfe, G. Mottet, M. Reichen, C. Castrillon, V. Menrath, S. Ellouze, A. Poitou, R. Doineau, L. Briseno-Roa, High-throughput single-cell activity-based screening and sequencing of antibodies using droplet microfluidics, Nature Biotechnology, (2020) 1-7.

Chapter 2. Compartmentalization aided On-cell cytokine Capture for Single Poisson T cell Secretion Assays

2.1. Introduction

Direct modulation of T lymphocyte biology, either genetically through the expression of chimeric receptors, or physically via the addition of antibodies against inhibitory checkpoint proteins, has demonstrated profound efficacy towards the treatment of systemic hematological malignancies[1]. These novel treatments, termed immunotherapies, refine the immune system's ability to differentiate between self and non-self, enabling natural biological defense mechanisms to identify and eradicate otherwise intractable tumors. Unfortunately, broad translation of such approaches is currently limited, resulting in tremendous variation in clinical outcomes both between patients and amongst sub-types of cancers treated[2-7]. One barrier to the design of more effective personalized immunotherapies, stems from an incomplete characterization of the phenotypic traits which enable T-cells to excel at policing the body, including factors that affect proliferative potential, cell stemness, and aggressiveness upon stimulation by their cognate antigen[8-11].

Currently immunophenotyping approaches primarily focus on analyzing cells through labeled surface antigens. While these methods yield insights into the primary role of cells (e.g. Helper-T cells, Cytotoxic T-cells etc.) they reveal little about their metabolic activity or propensity to respond to immunogenic challenges[12, 13]. A complimentary set of phenotypic information can be found by examining the diverse array of proteins secreted by T-cells. These cytokines and chemokines directly coordinate the complex set of behaviors necessary for proper immune responses, including recruiting cells to the area of interest, stimulating them to induce

clearance of pathogens, and restricting activity once the targets have been cleared. Cytokine production is also directly translatable to a variety of immunotherapeutic approaches. High concentrations of interferon-α and interleukin-2 (IL-2) have been administered directly to patients to respectively suppress tumor proliferation or induce T-cell expansion[14, 15]. Armored CAR T-Cells have been designed which constitutively express pro-inflammatory cytokines that can counteract immunosuppressive microenvironments typically associated with solid tumors[16, 17]. Even more recently, engineered synthetic-notch receptors have enabled construction of user defined custom T-cell secretion programs, facilitating targeted production of therapeutic molecules which may be too toxic to apply systemically[18]. While these synthetic biology approaches to cytokine control are beneficial, they add significant complexity to the manufacture of therapeutic T-cell products, which is not ideal.

Interestingly, single cell studies have alluded to the presence of a small fraction of otherwise indistinguishable polyfunctional T-cells which secrete many cytokines simultaneously and in excess, and whose presence in pre-infusion products correlates well with clinical outcomes[12, 13, 19]. Therefore, the development of profiling technologies which can screen and sort T-cells based on functional behavior directly, by quantifying protein production from individual clones, could aid therapeutic strategies by enabling downstream analysis of the genetic or epigenetic mutations which improve clonal fitness[20], and subsequently enriching pre-infusion cell populations with desirable phenotypes.

Several approaches to measure secreted proteins from individual cells have been introduced over the past few years. The most widely used of these, intracellular cytokine staining, is rapid and compatible with standard flow cytometry, but requires fixation and permeabilization, leaving cells non-viable[21]. Well based micro-confinement approaches have

also been developed and used to detect up to 42 different cytokines simultaneously using a combination of fluorescent and spatial barcoding experiment and recovery of interesting clones is not straightforward[22, 23]. Microfluidic workflows leveraging water-in-oil emulsions partially circumvent these limitations by enabling cell recovery through emulsion destabilization[24, 25]. However, most of these approaches rely on co-encapsulation of cells with cytokine capture beads, an inefficient process which necessitates the use of custom sorting tools that can process intact emulsions, to preserve the linkage between cells and their associated bead readout. Finally, new highly automated advanced analysis systems are being introduced to the market, but adoption of these technologies is limited in most research settings due to exceedingly large capital costs[26, 27].

One particularly intriguing secretion profiling methodology makes use of bispecific antibodies to capture cytokines directly onto the surface of secreting cells, rendering them compatible with traditional immunostaining and flow cytometry workflows[28]. Unfortunately, these tools are standardly used to interrogate cells in bulk solution, leaving them highly susceptible to crosstalk between neighboring cells and loss of signal from cytokines that diffuse away from the local microenvironment[29].

In this work we expand on the use of cell-surface based capture assays by combining bispecific antibody technology with high-throughput microfluidic droplet generation using step-emulsification (Fig 2-1). Single-cell cytokine production in partitioned aqueous volumes yields detectable secretion signals in as little as 3 hours, while simultaneously increasing assay accuracy, and improving signal intensity on actively secreting cell clones over bulk.

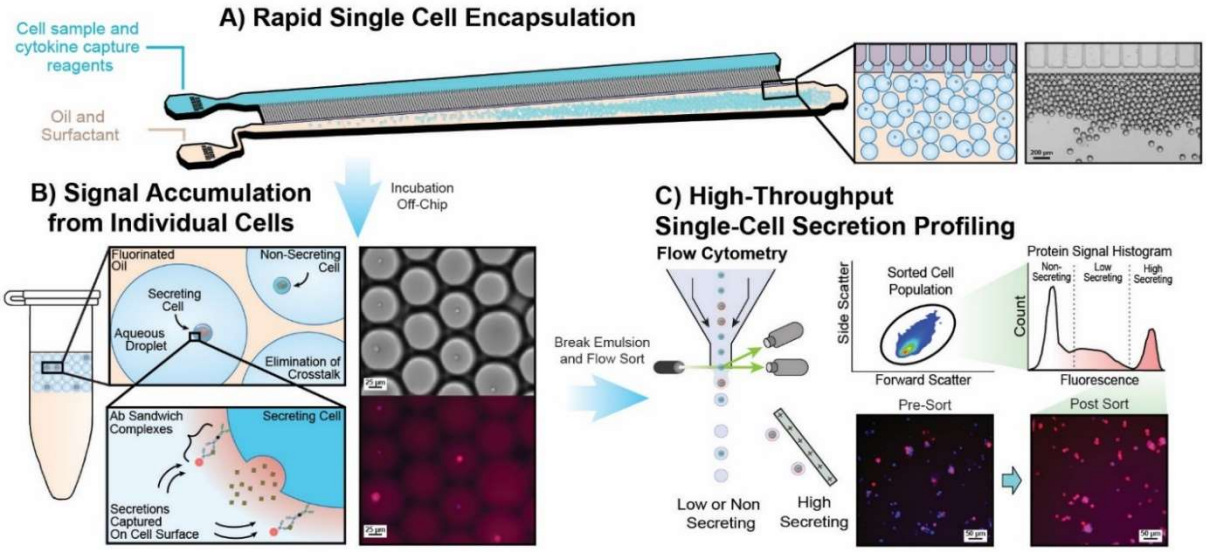

Figure 2-1 . Illustration of the droplet enhanced on-cell cytokine encoding workflow.

A) Cells are co-encapsulated with anti-cytokine capture and detection probes within uniformly sized microdroplets using a highly parallelized step emulsification device. **B)** Droplets are incubated off chip, enabling accumulation of secreted proteins without cross-talk to neighboring cells. The presence of secreted cytokines in each droplet is encoded back onto the secreting cell's surface as a fluorescent sandwich immunocomplex. **C)** The emulsion is then broken and recovered cells can be analyzed using standard flow cytometry. Analyzed cells remain viable throughout the entire process and can be subsequently expanded in culture.

Moreover, the highly parallelized droplet generation scheme we employ, increases cell encapsulation throughputs by over an order of magnitude compared to previously reported microfluidic secretion screens[24, 25, 29, 30], preventing bulk background accumulation of secreted proteins during longer encapsulation workflows, and enabling screening of larger cell populations. The continued development of such easy-to-use functional profiling tools will remove fundamental limitations to immune cell screening and can directly yield large populations of phenotypically enriched, viable T-cells for subsequent molecular analysis and therapeutic use.

2.2. Materials and Methods

2.2.1. Culture of Primary T cells

Trima filters were purchased from the UCLA virology core and eluted to recover concentrated volumes of whole blood. T cells were isolated from the trima filter eluent using the RosetteSep^{TM} Human T Cell Enrichment Cocktail (STEMCELL Technologies) according to manufacturer instructions and immediately frozen at a concentration of $1x10^7$ cells/mL of freezing media. Before analysis, each aliquot of T cells was rapidly thawed and transferred into pre-warmed ImmunoCult^{TM}-XF T Cell Expansion Media supplemented with 25 uL/mL ImmunoCult^{TM} Human CD3/CD28 T cell activatior, and 50 IU/mL IL-2 at a final concentration of $1x10^6$ cells/mL. Cells were passaged twice a week. Culture media was replenished with 50 IU/mL of IL-2 every 2 days. Cells were cultured in a sterile incubator at 37^{o}C and 5% CO_2 for up to 3 weeks before thawing a fresh vial of cells.

2.2.2. Device Fabrication

Step emulsification devices were fabricated using master molds previously utilized for high-throughput production of microgels. Detailed description of wafer fabrication can be found

in de Rutte et al.[31]. Devices were formed from molds using PDMS Sylgard 184 kit (Dow Corning). The polymer base and crosslinker were combined at a 10:1 ratio, poured into the mold, degassed, and cured in a 70ºC oven overnight. The following morning devices were cut from the mold and entry/exit ports were formed by biopsy punching through the polymer at either end of the device. Cut PDMS slabs were then activated alongside glass microscope slides (VWR) in an air-based plasma cleaner (Harrick Plasma) and subsequently bound together. Each formed device was incubated for another 30 mins in a 70ºC oven to strengthen the bond between device and glass substrate. Finally, the device was filled with Aquapel, set aside for 1 minute, and flushed with Novec-7500 fluorinated oil to render the channels hydrophobic.

2.2.3. Droplet Based On-Cell Cytokine Capture Assay

T cells were taken from bulk culture, washed into fresh media and added into a single well of a 12-well plate at a concentration of $5x10^6$ cells/mL. Wells were supplemented with 100 ng/mL phorbol 12-myristate 13-acetate (PMA) and 2.5 µM ionomycin, and cells were incubated in this activating mixture for a period of six hours. During the final hour of incubation CellTracker™ Blue CMAC dye was added into the activated cell mixture at a final concentration of 20 µM to label the cells. After incubation, cells were washed thoroughly a total of 3 times to remove any secreted IL-2 background that had accumulated within the solution over the course of the incubation. $1x10^6$ cells were removed from the activated cell population and rapidly reconstituted into fresh media containing 50 uL/mL miltenyi IL-2 capture reagent and 50 µL/mL miltenyi phycoerythrin (PE) conjugated anti-IL-2 detection antibody within a 1 mL syringe. Simultaneous 2 mL of a 2% mixture of Pico-Surf™ fluorinated surfactant (3M) diluted into Novec-7500 engineered fluid (3M) was prepared and placed in a separate syringe. The two solutions were injected into our prefabricated step-emulsification droplet generator at flow rates

of 125 μL/min and 250 μL/min for the aqueous cell mixture and fluorinated oil phases respectively. The tubing used to couple the feed syringes to the droplet generator were mechanically agitated every few minutes to prevent cells from settling before reaching the device, aiding the uniform distribution of cells between the 200 parallel droplet generating channels. Formed droplets were collected in 15 mL conical tubes, covered with 500 μL of light mineral oil (Sigma-Aldrich) to prevent evaporation and incubated at 37°C and 5% CO_2 for 1-6 hours depending on experimental need.

After sufficient incubation time cell samples were recovered from droplets according to the protocol reported in Mazutis et al.[30]. Briefly, the bottom fraction of clear, unemulsified Novec oil was first removed from the conical tube. Next, 5 mL of fresh media was added to the emulsified samples to serve as a diluent for uncaptured IL-2 secretions immediately after disruption of the droplets. Subsequently 500 μL of 1H,1H,2H,2H-Perfluoro-1-octanol (PFO) was added to the tube and samples were stored at room temperature for ~5 minutes while the emulsion destabilized and the cells were released. The top phase of the sample was then removed, leaving the bottom PFO phase behind. The recovered cell solution was spun down at 300g for 5 mins and reconstituted in fresh media a total of 3 times to wash cells. Cell samples were then analyzed via flow cytometry.

2.2.4. Secretion Cross Talk Assay

T cells were split into two populations, one population was activated with PMA and ionomycin as described above but remained unlabeled, the other was non-activated (maintained in fresh media at the same concentration and time duration as the activated sample) and labeled with 20 μM of a CellTracker™ DeepRed dye. The activated and non-activated cell populations

were then analyzed either independently or in a 1:1 mixture in bulk culture or droplet assay formats.

Bulk Assay Format: Cells were divided into three samples (non-activated, activated, and 1:1 mixture) and were washed 3X in cold media before analysis. Four million cells from each condition were obtained and resuspended in 80 μL of cold media. 20 μL of IL-2 capture reagent were then added to each sample and the cell/antibody mixture was incubated on ice for 5 minutes. Follow this incubation, cells were quickly resuspended into 10 mL of warm media and incubated with vigorous agitation at 37ºC. At each tested time point, 2.5 mL of sample was removed from the bulk solution, washed 3X in old media, and finally resuspended in 80 μL of cold media. Samples were then labeled with 20 μL of PE labeled anti-IL-2 reported antibodies on ice over a period of 10 minutes. Samples were washed 3X once more and analyzed via flow cytometry.

Droplet Assay Format: Cells were analyzed as described in the droplet-based on-cell cytokine analysis section above with the notable exception that three samples (non-activated, activated, and 1:1 mixture) were analyzed at each timepoint spanning 0-4 hours. Non-activated cells were labeled with 20 μM of a CellTracker™ DeepRed dye to differentiate from activated cells.

2.2.5. Flow Cytometry

For non-sorting experiments all data was collected on a 2-laser BD FACS Canto II. PE flurophores were excited using a 488 nm laser and filtered using 556LP and 585/42 filters. Cell tracker labeled were excited using a 633 nm laser and filtered through a 686/20 filter.

All cell sorting experiments were conducted by the UCLA flow cytometry core facility using a 4-laser BD FACS Aria II. PE flurophores were excited using a 561 nm laser and filtered

using a 585/15 filter. Blue cell tracker labels were excited using a 355 nm laser and filtered through a 450/50 filter.

2.3. Results

2.3.1. Highly Parallelized Single Cell Encapsulation

Analysis of secreted products from individual cells is inherently difficult due to diffusion of proteins away from their production source. Droplet microfluidic technology has emerged as a method of choice in single-cell secretion screening, because of its ability to partition cells into micron scale droplets which both trap and concentrate biomolecules. Unfortunately, most microfluidic designs generate droplets in a serial manner, rapidly reaching an upper processing limit (typically ~1-2 μL/min of aqueous sample). This restricts the number of cells that can be assayed before upstream accumulation of secreted products reduces assay integrity. Such throughput limitations serve as a fundamental barrier to adoption of functional cellular profiling approaches in pre-clinical research, where large amounts of cells often must be screened simultaneously to identify rare phenotypes.

To overcome these challenges, we adapted a highly parallelized step-emulsification device for our functional screening workflow (Fig. 2-2A, B)[32, 33]. Step-emulsification exploits rapid pressure drops experienced by fluids emerging from confined channels into taller collection reservoirs to induce droplet pinch off[34]. The primary advantage of this technique is that droplet generation is highly flow invariant, with channel geometric features dictating droplet size rather than individual fluid flow rates. In our design a single aqueous inlet flow is evenly distributed between 200, parallel nozzles, each of which can generate droplets at a rate of ~4000 droplets/minute.

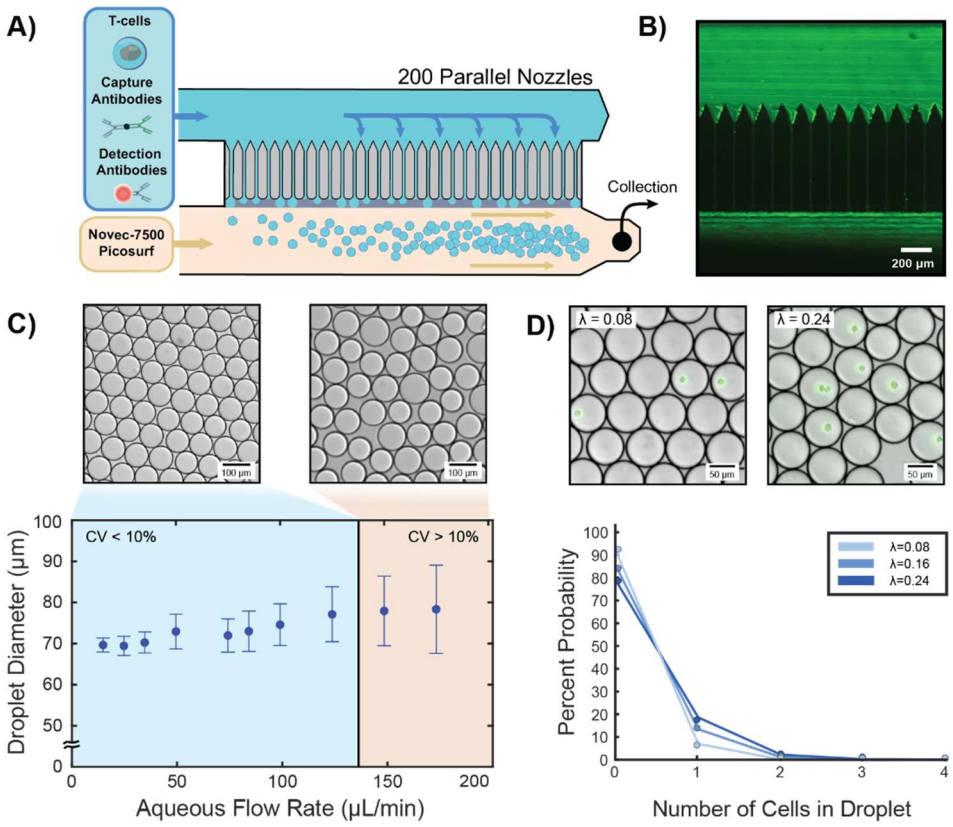

Figure 2-2. Microfluidic droplet generator characterization.

A) Our microfluidic droplet generator uses step emulsification to generate monodisperse droplets from 200 channels in parallel. In a typical secretion assay cells are loaded into the aqueous inlet along with capture and detection antibodies, pass uniformly between all channels, and are encapsulated into ~70 µm diameter droplets as the aqueous phase passes into a surfactant stabilized fluorinated oil. **B)** High exposure time fluorescent images show that cells travel through the device uniformly, ensuring that loading is not biased to a specific region of the device (top). **C)** Droplet size and uniformity is minimally affected by flow rates. As we increase aqueous flow rates from 15 to 175 µL/min the average droplet diameter varied from 70 to 78 µm. When droplets are generated too rapidly, they begin to crowd around the outlet of downstream nozzles, allowing more fluid to enter each droplet before pinch off and increasing sample CV. At our chosen flow rate of 125 µL/min our device generates roughly 10,000 droplets per second. **D)** Known concentrations of primary human T-cells were encapsulated using our microfluidic step emulsifier and imaged to determine the number of cells in each droplet. The experimental cell distribution (dots) followed the expected Poisson distribution (lines) demonstrating that parallelized encapsulation followed predictable loading trends.

We determined the optimal operating conditions for our device by simultaneously assessing cell viability, and droplet uniformity as a function of flow rate, with the goal of maximizing viable cell throughput without sacrificing assay consistency. Primary human T cells flowing through our device remained viable at all tested flow rates, indicating that shear stresses encountered during passage through the narrow (35 μm) channel nozzles were not a significant assay limitation, and implying that cells would remain active for subsequent functional screens. The average droplet diameter also remained relatively stable over a large range of flow rates, ranging from 70-78 μm across all tested conditions (Fig 2-2C). Interestingly, we found that the major limitation in device operation stemmed from accumulation of previously generated droplets around downstream nozzles at high flow rates, physically precluding the expansion of newer droplets over the channel step, and resulting in the production of larger (>100 μm) diameter droplets from several nozzles towards the end of the device. Thus, we restricted device operation to 125 μL/min which was the highest tested flow rate preserving stringent droplet monodispersity (CV <10%). Importantly, at this throughput we are already capable of producing ~10,000 droplets/second, resulting in cell processing rates an order, to multiple orders of magnitude faster than previously reported secretion screens using standard flow focusing device geometries[30].

Due to the parallelized nature of our device, we also verified that cell loading proceeded uniformly rather than biasing towards specific channel regions (Figure 2-2B). To test this, we labeled T cells with CellTrackerTM Green CMFDA dye and reconstituted them at known cell concentrations ranging from 400k-1.4 million cells/mL. The resulting samples were then encapsulated and imaged using fluorescence microscopy to identify the number of cells within each droplet. The average cell occupancy for each condition closely followed expected Poisson

distributions for all three tested conditions ($\lambda = 0.08, 0.16, 0.24$) (Fig 2-2D), indicating that single cell partitioning could be stringently enforced through control of initial cell concentrations. Thus, our step emulsification platform can be utilized as an efficient, high-throughput alternative to traditional serial encapsulation approaches, enabling compartmentalization of over 10^3 viable cells/second with less than 0.5% of droplets containing multiple cells.

2.3.2. Droplet Mediated On-Cell Cytokine Screening

Solid phase substrates are critical components of all secretion capture workflows due to their ability to concentrate diffuse biomolecules and translate their presence into detectable signals. However, assay schemes necessitating the co-delivery of both cells and substrates into a single droplet lead to subsequent non-idealities in both screening and sorting, as not all cells will have capture substrates present in their droplets, and traditional flow cytometers are generally incapable of screening intact oil droplets.

Our assay design relies on the use of commercially available capture and detection probes (Miltenyi Biotec) which instead transduce the presence of cytokines from the cellular microenvironment into a membrane localized fluorescence signal, allowing each secreting cell to function as its own solid phase capture substrate (Fig 2-3A). Typically, these assays are performed on bulk cell populations where cytokines can diffuse from secreting cells onto their neighbors yielding false positive signals. We hypothesized that translation of these on-cell molecular biosensing workflows into a droplet-based assay format would improve reliability by locally concentrating secreted molecules around producer cells, increasing signal, while simultaneously eliminating interaction between screened cells to reduce background.

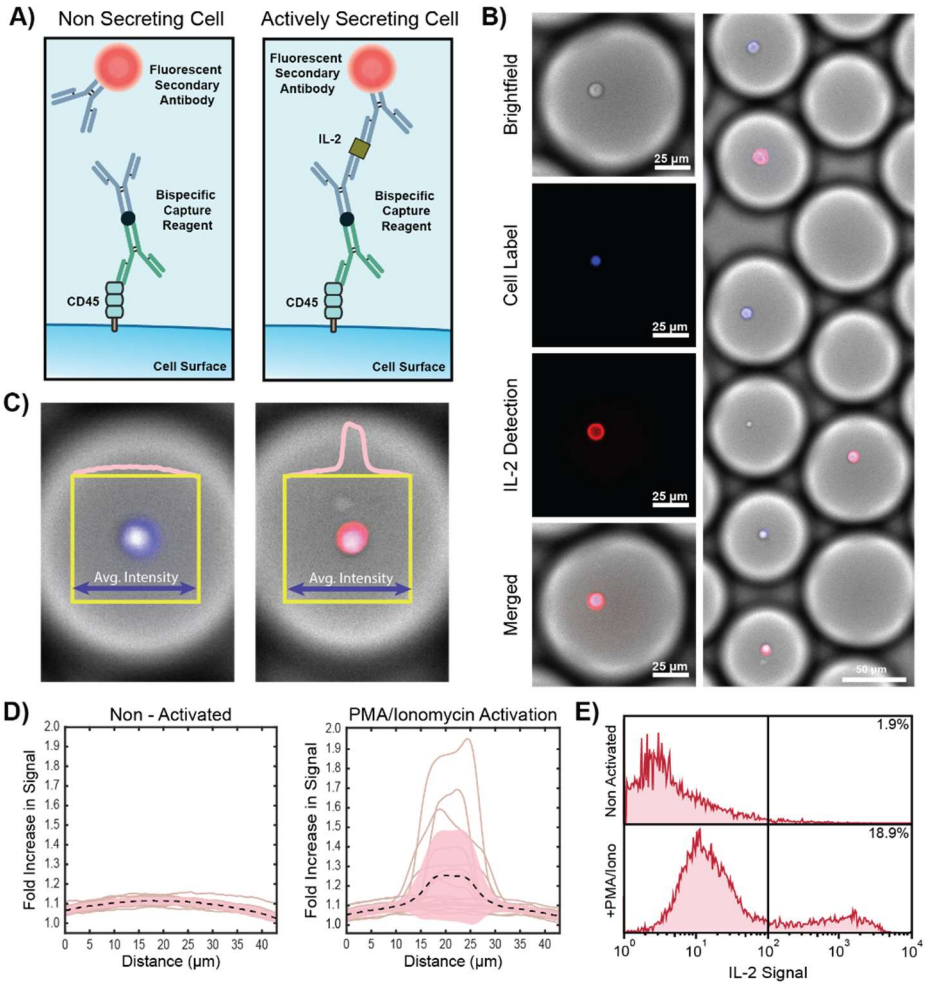

Figure 2-3. Characterization of droplet mediated on-cell cytokine encoding.

A) Cells are co-encapsualted into droplets alongside bispecific capture antibodies and fluorescently labelled secondary antibodies. The capture antibodies bind to surface expressed CD45 molecules and have a second free end to capture secreted IL-2. As IL-2 is secreted and bound to the cell surface free floating secondary antibodies begin to localize to the cell membrane. **B)** Brightfield and fluorescence images of T cells secreting IL-2 in droplets. T cells labeled with cell tracker dye (blue) generate a fluorescent ring around their periphery (red) after accumulation of secretion. **C)** The fluorescence intensity of cell containing droplets was integrated across each droplet cross section. **D)** When cells are in their basal state, fluorescence intensity was roughly uniform across droplets. When cells were chemically stimulated using PMA and ionomycin fluorescence signal aggregated on the cell surface rendering the cells visible over background. **E)** After 6 hours of incubation in droplets 1.9% of non-activated cells yielded IL-2^+ signal while 18.9% of activated cells yielded IL-2^+ signal over the same time period.

To test our screening approach, we compared the secretion signal obtained from T cells stimulated by the small molecule activators phorbol 12-myristate 13-acetate (PMA) and ionomycin versus control cells incubated in media without activation. We selected the T cell growth cytokine IL-2 as our analyte of interest because of its broad utility as a functional quality marker in cell therapy development pipelines, and due to its strong upregulation upon T cell activation.

Because addition of reagents into formed droplets is non-trivial, we chose to pre-mix both anti-IL2 capture and PE conjugated anti-IL2 detection probes with cells prior to encapsulation. Although this type of one pot assay may be prone to high background due to cell-cell and cell-reagent interactions in the feed syringe, care was taken to ensure that cells were thoroughly washed and encapsulated in under ten minutes after mixing with the capture and detection probes. Preliminary fluorescence visualization of newly formed droplets revealed a homogeneous fluorescence signal across each droplet volume. This indicated that although capture reagents were free to coat cell surfaces there was no detectable IL-2 within any droplet, leaving fluorescent secondary antibodies free floating. After emulsification, samples were incubated at 37ºC for 6 hours to provide sufficient time for IL-2 accumulation in each cell loaded droplet. Upon subsequent re-visualization notable differences were observed between the activated and non-activated cell populations, with a subset of activated T cells possessing a clear fluorescent signal localized along their periphery, while none of the control population was discernable over the fluorescent droplet background (Figure 2-3B, C). This was indicative of sequestration of IL-2 by both capture and detection reagents encoding individual cell secretion histories back onto the cell surface through the formation of fluorescent sandwich immunocomplexes.

Finally, after confirmation that our one pot droplet assay successfully translated IL-2 production into a detectable signal we destabilized the formed emulsions, recovered cells into an excess of fresh media, and analyzed the full population using flow cytometry. As expected, activation significantly increased IL-2 production, with 18.9% of cells staining positive for IL-2 versus just 1.9% of non-activated cells yielding IL-2^+ signal after the 6 hour incubation period. Interestingly however, although activation increased the fraction of IL-2^+ cells 10-fold over control only about 20% of T cells produced detectable levels of IL-2, alluding to an underlying phenotypic heterogeneity in the T cell population.

2.3.3. Encapsulation reduces secretion secretion crosstalk

Because of the heterogeneity in phenotype of the analyzed cell population it is critical to ensure that crosstalk between cells is minimized and that measurements of single cell protein secretions are not confounded by protein production from neighboring cells. In light of this we compared the resolution of IL-2 production afford by our high throughput droplet based on-cell cytokine capture assay compared to the standard unencapsulated approach. CellTracker™ DeepRed labeled non-activated T cells and unlabeled PMA/ionomycin activated T cells were prepared and analyzed alone and in 1:1 mixed ratios both in bulk and droplet based secretion assays (Fig 2-4).

When non-activated cells were analyzed alone, no IL-2 production was detected in either the bulk or emulsion assays at any timepoint (Fig 2-4A, C). However, once the two samples were mixed, both activated and non-activated T cell populations rapidly acquired fluorescent signal, rendering the two indiscernible after only an hour in bulk solution (Fig 2-4B).

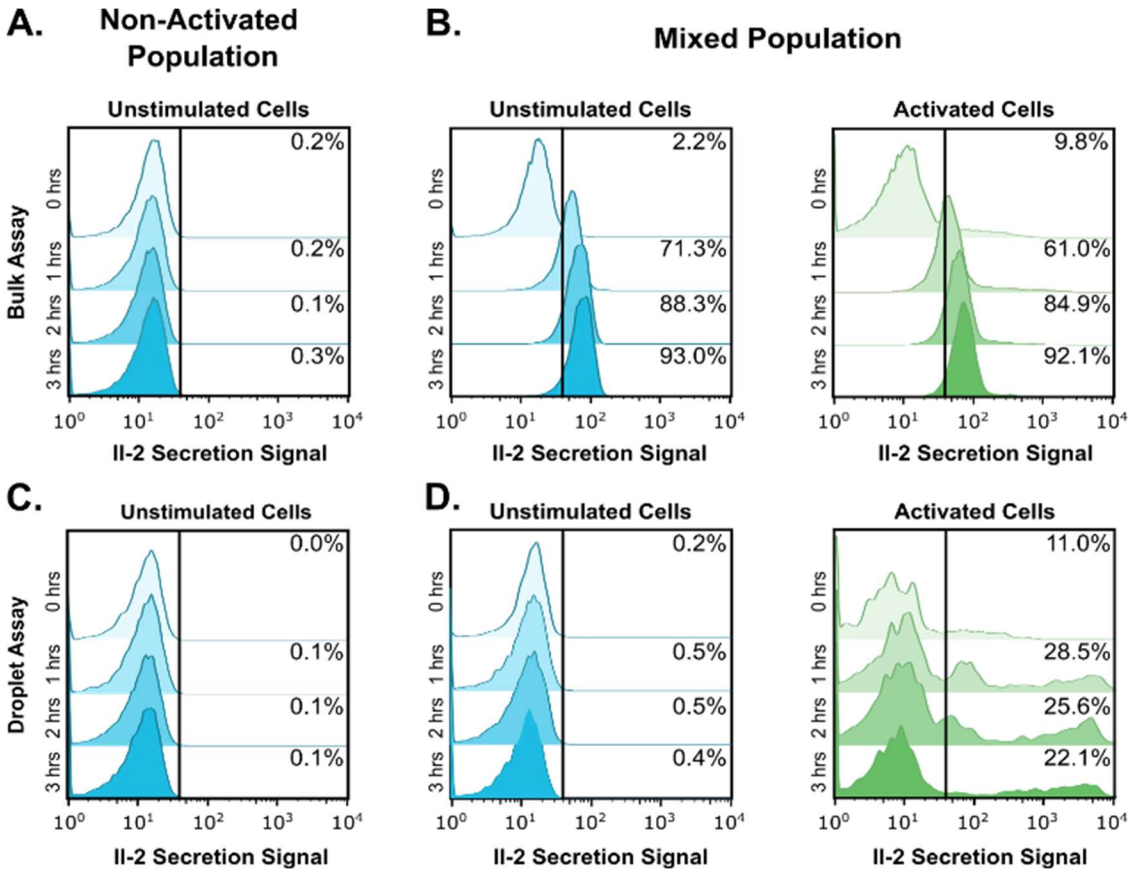

Figure 2-4. Comparison of on-cell cytokine capture in bulk solution and in droplet formats. IL-2 production was analyzed from CellTracker™ DeepRed labaled non-activated T cells and unlabeled, PMA/ionomycin activated T cells individually and in 1:1 cell mixtures using both bulk solution and droplet based assay formats. Non-activated T cells generated no detectable signal at any time point in both **A)** bulk and **C)** droplet based assay formats. **B)** When mixed together in bulk solution both activated and non-activated T cells rapidly accumulated fluorescent signal, becoming indiscernible from one another in as little as 1 hour. **D)** After encapsulation secretions from mixed cell populations were easily discernible with less than 0.5% of non-activated T cells, and >20% of activated T cells yielding IL-2^+ signal after 3 hours of incubation.

In contrast, partitioning through microfluidic step emulsification preserved clear variations in signal between the two populations, with less than 0.5% of non-activated T cells, and 22-29% of PMA/ionomycin activated T cells appearing as IL-2 positive after flow cytometric analysis (Fig 2-4D). Additionally, in the droplet mediated assay samples, IL-2 fluorescent secretion signals spanned more than two orders of magnitude, with the highest secretors appearing over ten times brighter than the highest recorded signals in bulk phase analysis. Thus, we concluded that incubation of cells in droplets during on-cell secretion assay workflows significantly aided in the reduction of false positive signals stemming from proteins diffusing away from their producing cells, while simultaneously enhancing the concentration of secreted products around the cellular microenvironment leading to improved resolution between low and high secreting cell clones.

2.3.4. Enrichment of functionally active T cell clones using FACS

A unique feature of the miltenyi capture and detection probes used in this assay is the association of secreted signals with the cell surface which enables assessment of functional protein production using standard fluorescence activated cell sorting (FACS). To highlight this, we repeated our droplet mediated on-cell secretion assay one more time using CellTracker™ Blue labeled PMA/ionomycin activated T cells. As previously described cells were encapsulated within droplets, incubated to accumulate signal, and subsequently release (Figure 2-5). Upon recovery from the cells were sorted using FACS. Analysis by the flow cytometer revealed three distinct populations, with 63.9% of the total events staining positively with CellTracker™ Blue dye but negative for IL-2 production indicating live non-producing T cells, 17.7% double positive active IL-2 producer cells, and roughly 18% staining negative for both stains presumably indicating cell death. Analyzed cells were sorted by targeting the double positive fluorescent population in our fluorescent scatter plot.

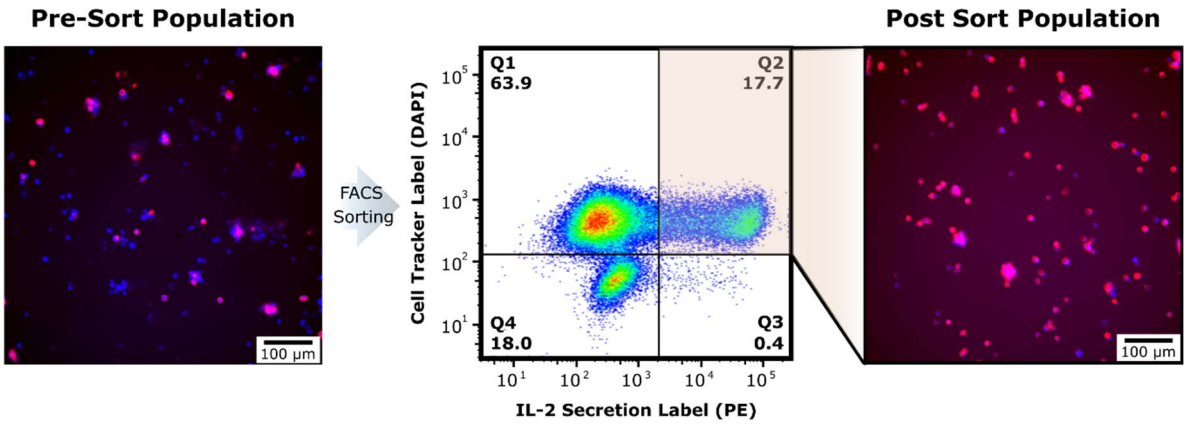

Figure 2-5. Example of post assay FACS sorting based on T cell IL-2 production.

Individual T cells were assayed using our droplet-based cytokine encoding assay. After incubation and recovery roughly 20% of T cells were stained positively for IL-2 production. Samples were sorting using standard FACS by targeting the double positive fluorescent populations (CTB^{+}/PE^{+}) and subsequently analyzed using fluorescence microscopy, revealing a pure sample of positively labeled cytokine secreting cells.

Recovered samples were analyzed using fluorescence microscopy revealing a pure population of IL-2^+ labeled T cells. Recovered samples remained viable and could be expanded over subsequent days (data not shown).

2.4. Discussion

In this work we demonstrated that encapsulation of cells into individual microcompartments can enhance the utility of on-cell cytokine capture by preventing crosstalk between neighboring cells. Commercially available reagents that encode secreted molecules back onto the surface of the secreting cell, such as the cytokine capture assay from Miltenyi Biotec are incredible useful tools for single cell phenotyping because 1) the anchoring of secretions directly to the cell surface enables analysis of functional markers using standard flow cytometry, and 2) cells do not have to be permeabilized and remain viable during the process allowing them to be sorted and analyzed further in downstream assays. However, we and others[29] have noted that analysis of heterogeneous cell populations in bulk solution is non-ideal as secretions from producer cells can accumulate in solution and bind to neighboring non-producing cells, confounding signals.

Microfluidic droplets have been used extensively to compartmentalize individual cells for single-cell screening, but analysis of secreted products in microdroplets is still difficult due to the lack of a built-in solid surface to capture them and report their presence. Typically to analyze secreted proteins cells and solid capture beads are co-encapsulated into droplets, but due to the random nature of droplet loading very few droplets will contain both a single cell and a single particle, leaving most of the starting cell population unusable. The combination of microdroplet based partitioning with the Miltenyi cytokine capture assay is mutual beneficial and solves both of these issues. Compartmentalized cells rapidly accumulate secreted products onto their own

surface without generating false positive signal through protein diffusion, and the cell membrane of each cell is transformed into its own solid capture phase, eliminating the need for co-loading of secondary particles. When analyzing the production of IL-2 from strongly stimulated T cells background accumulation of protein prevented distinction of secreting and non-secreting cells in as little as one hour, whereas in a droplet assay format the same population could be incubated for as long as 3 hours without obscuring individual cell function.

Future efforts to analyze single T cells may leverage this droplet encapsulation feature even further still. For example, multiplexed cytokine detection is of great interest to researchers seeking to understand phenotypes that function optimally in clinical settings[19], however the secretion kinetics of different cytokine targets can vary drastically[35]. Therefore, single timepoint measurements similar to those taken in bulk solution analyses of secreted proteins may inadvertently misclassify cells as non-secreting if production of the target molecules has already concluded or not yet begun. In contrast, incubation of cells within microdroplets yields integrated signals over the entire period of the assay, providing a method to encode the secretion histories of multiple temporally distinct products simultaneously.

Finally, we conclude by mentioning that the major bottleneck in throughput for our assay stems from the rate of microfluidic droplet generation. For all assays in this work, we made use of an ultrahigh throughput step emulsification droplet generator which improved droplet generation rates by over an order of magnitude over traditional microfluidic flow focusing geometries. Even so, our system is limited to an encapsulation rate of roughly 10^3 cells/second, meaning that studies on larger populations of cells quickly become impractical. While in theory throughput can be increased further through parallelization of individual step-emulsification devices further increases in design complexity will translate to technologies that are less

accessible to most researchers. Newer easy to use strategies to enhance the droplet generation and cellular analysis throughput would be welcome additions to the single-cell analysis toolkit.

2.5. References

[1] S. Lim, B. Chen, M.S. Kariolis, I.K. Dimov, T.M. Baer, J.R. Cochran, Engineering High Affinity Protein-Protein Interactions Using a High-Throughput Microcapillary Array Platform, Acs Chem Biol, 12 (2017) 336-341.

[2] S.M. Vareki, C. Garrigos, I. Duran, Biomarkers of response to PD-1/PD-L1 inhibition, Crit Rev Oncol Hemat, 116 (2017) 116-124.

[3] D. Chowell, L.G.T. Morris, C.M. Grigg, J.K. Weber, R.M. Samstein, V. Makarov, F.S. Kuo, S.M. Kendall, D. Requena, N. Riaz, B. Greenbaum, J. Carroll, E. Garon, D.M. Hyman, A. Zehir, D. Solit, M. Berger, R.H. Zhou, N.A. Rizvi, T.A. Chan, Patient HLA class I genotype influences cancer response to checkpoint blockade immunotherapy, Science, 359 (2018) 582-+.

[4] J.A. Fraietta, S.F. Lacey, E.J. Orlando, I. Pruteanu-Malinici, M. Gohil, S. Lundh, A.C. Boesteanu, Y. Wang, R.S. O'Connor, W.T. Hwang, E. Pequignot, D.E. Ambrose, C.F. Zhang, N. Wilcox, F. Bedoya, C. Dorfmeier, F. Chen, L.F. Tian, H. Parakandi, M. Gupta, R.M. Young, F.B. Johnson, I. Kulikovskaya, L. Liu, J. Xu, S.H. Kassim, M.M. Davis, B.L. Levine, N.V. Frey, D.L. Siegel, A.C. Huang, E.J. Wherry, H. Bitter, J.L. Brogdon, D.L. Porter, C.H. June, J.J. Melenhorst, Determinants of response and resistance to CD19 chimeric antigen receptor (CAR) T cell therapy of chronic lymphocytic leukemia, Nat Med, 24 (2018) 563-+.

[5] A.L. Garfall, E.K. Dancy, A.D. Cohen, W.T. Hwang, J.A. Fraietta, M.M. Davis, B.L. Levine, D.L. Siegel, E.A. Stadtmauer, D.T. Vogl, A. Waxman, A.P. Rapoport, M.C. Milone, C.H. June, J.J. Melenhorst, T-cell phenotypes associated with effective CAR T-cell therapy in postinduction vs relapsed multiple myeloma, Blood Adv, 3 (2019) 2812-2815.

[6] R.G. Majzner, C.L. Mackall, Clinical lessons learned from the first leg of the CAR T cell journey, Nat Med, 25 (2019) 1341-1355.

[7] P. Sharma, S. Hu-Lieskovan, J.A. Wargo, A. Ribas, Primary, Adaptive, and Acquired Resistance to Cancer Immunotherapy, Cell, 168 (2017) 707-723.

[8] Y. Xu, M. Zhang, C.A. Ramos, A. Durett, E. Liu, O. Dakhova, H. Liu, C.J. Creighton, A.P. Gee, H.E. Heslop, C.M. Rooney, B. Savoldo, G. Dotti, Closely related T-memory stem cells correlate with in vivo expansion of CAR.CD19-T cells and are preserved by IL-7 and IL-15, Blood, 123 (2014) 3750-3759.

[9] D. Sommermeyer, M. Hudecek, P.L. Kosasih, T. Gogishvili, D.G. Maloney, C.J. Turtle, S.R. Riddell, Chimeric antigen receptor-modified T cells derived from defined CD8(+) and CD4(+) subsets confer superior antitumor reactivity in vivo, Leukemia, 30 (2016) 492-500.

[10] S. Krishna, F.J. Lowery, A.R. Copeland, E. Bahadiroglu, R. Mukherjee, L. Jia, J.T. Anibal, A. Sachs, S.O. Adebola, D. Gurusamy, Z.Y. Yu, V. Hill, J.J. Gartner, Y.F. Li, M. Parkhurst, B. Paria, P. Kvistborg, M.C. Kelly, S.L. Goff, G. Altan-Bonnet, P.F. Robbins, S.A. Rosenberg, Stem-like CD8 T cells mediate response of adoptive cell immunotherapy against human cancer, Science, 370 (2020) 1328-+.

[11] L. Liu, E. Bi, X. Ma, W. Xiong, J. Qian, L. Ye, P. Su, Q. Wang, L. Xiao, M. Yang, Y. Lu, Q. Yi, Enhanced CAR-T activity against established tumors by polarizing human T cells to secrete interleukin-9, Nature Communications, 11 (2020).

[12] C. Ma, A.F. Cheung, T. Chodon, R.C. Koya, Z.Q. Wu, C. Ng, E. Avramis, A.J. Cochran, O.N. Witte, D. Baltimore, B. Chmielowski, J.S. Economou, B. Comin-Anduix, A. Ribas, J.R. Heath, Multifunctional T-cell Analyses to Study Response and Progression in Adoptive Cell Transfer Immunotherapy, Cancer Discov, 3 (2013) 418-429.

[13] C. Ma, R. Fan, H. Ahmad, Q.H. Shi, B. Comin-Anduix, T. Chodon, R.C. Koya, C.C. Liu, G.A. Kwong, C.G. Radu, A. Ribas, J.R. Heath, A clinical microchip for evaluation of single immune cells reveals high functional heterogeneity in phenotypically similar T cells, Nat Med, 17 (2011) 738-U133.

[14] F. Belardelli, M. Ferrantini, E. Proietti, J.M. Kirkwood, Interferon-alpha in tumor immunity and immunotherapy, Cytokine Growth F R, 13 (2002) 119-134.

[15] S.A. Rosenberg, IL-2: The First Effective Immunotherapy for Human Cancer, J Immunol, 192 (2014) 5451-5458.

[16] O.O. Yeku, T.J. Purdon, M. Koneru, D. Spriggs, R.J. Brentjens, Armored CAR T cells enhance antitumor efficacy and overcome the tumor microenvironment, Sci Rep-Uk, 7 (2017).

[17] M.P. Avanzi, O. Yeku, X.H. Li, D.P. Wijewarnasuriya, D.G. van Leeuwen, K. Cheung, H. Park, T.J. Purdon, A.F. Daniyan, M.H. Spitzer, R.J. Brentjens, Engineered Tumor-Targeted T Cells Mediate Enhanced Anti-Tumor Efficacy Both Directly and through Activation of the Endogenous Immune System, Cell Rep, 23 (2018) 2130-2141.

[18] K.T. Roybal, J.Z. Williams, L. Morsut, L.J. Rupp, I. Kolinko, J.H. Choe, W.J. Walker, K.A. McNally, W.A. Lim, Engineering T Cells with Customized Therapeutic Response Programs Using Synthetic Notch Receptors, Cell, 167 (2016) 419-+.

[19] J. Rossi, P. Paczkowski, Y.W. Shen, K. Morse, B. Flynn, A. Kaiser, C. Ng, K. Gallatin, T. Cain, R. Fan, S. Mackay, J.R. Heath, S.A. Rosenberg, J.N. Kochenderfer, J. Zhou, A. Bot, Preinfusion polyfunctional anti-CD19 chimeric antigen receptor T cells are associated with clinical outcomes in NHL, Blood, 132 (2018) 804-814.

[20] D. Di Carlo, Technologies for the Directed Evolution of Cell Therapies, Slas Technol, 24 (2019) 359-372.

[21] B. Sander, J. Andersson, U. Andersson, Assessment of Cytokines by Immunofluorescence and the Paraformaldehyde-Saponin Procedure, Immunol Rev, 119 (1991) 65-93.

[22] E.M. Bradshaw, S.C. Kent, V. Tripuraneni, T. Orban, H.L. Ploegh, D.A. Hafler, J.C. Love, Concurrent detection of secreted products from human lymphocytes by microengraving: Cytokines and antigen-reactive antibodies, Clin Immunol, 129 (2008) 10-18.

[23] Y. Lu, Q. Xue, M.R. Eisele, E.S. Sulistijo, K. Brower, L. Han, E.A.D. Amir, D. Pe'er, K. Miller-Jensen, R. Fan, Highly multiplexed profiling of single-cell effector functions reveals deep functional heterogeneity in response to pathogenic ligands, P Natl Acad Sci USA, 112 (2015) E607-E615.

[24] T. Konry, M. Dominguez-Villar, C. Baecher-Allan, D.A. Hafler, M.L. Yarmush, Droplet-based microfluidic platforms for single T cell secretion analysis of IL-10 cytokine, Biosensors and Bioelectronics, 26 (2011) 2707-2710.

[25] V. Chokkalingam, J. Tel, F. Wimmers, X. Liu, S. Semenov, J. Thiele, C.G. Figdor, W.T.S. Huck, Probing cellular heterogeneity in cytokine-secreting immune cells using droplet-based microfluidics, Lab on a Chip, 13 (2013) 4740-4740.

[26] K. Le, C. Tan, S. Gupta, T. Guhan, H. Barkhordarian, J. Lull, J. Stevens, T. Munro, A novel mammalian cell line development platform utilizing nanofluidics and optoelectro positioning technology, Biotechnology Progress, 34 (2018) 1438-1446.

[27] B. Chen, S.W. Lim, A. Kannan, S.C. Alford, F. Sunden, D. Herschlag, I.K. Dimov, T.M. Baer, J.R. Cochran, High-throughput analysis and protein engineering using microcapillary arrays, Nat Chem Biol, 12 (2016) 76-+.

[28] J.D.M. Campbell, A. Foerster, V. Lasmanowicz, M. Niemoller, A. Scheffold, M. Fahrendorff, G. Rauser, M. Assenmacher, A. Richter, Rapid detection, enrichment and propagation of specific T cell subsets based on cytokine secretion, Clin Exp Immunol, 163 (2011) 1-10.

[29] Y. Yuan, J. Brouchon, J.M. Calvo-Calle, J. Xia, L. Sun, X. Zhang, K.L. Clayton, F.F. Ye, D.A. Weitz, J.A. Heyman, Droplet encapsulation improves accuracy of immune cell cytokine capture assays, Lab on a Chip, 20 (2020) 1513-1520.

[30] L. Mazutis, J. Gilbert, W.L. Ung, D.A. Weitz, A.D. Griffiths, J.A. Heyman, Single-cell analysis and sorting using droplet-based microfluidics, Nat Protoc, 8 (2013) 870-891.

[31] J.M. de Rutte, J. Koh, D. Di Carlo, Scalable High-Throughput Production of Modular Microgels for In Situ Assembly of Microporous Tissue Scaffolds, Adv Funct Mater, 29 (2019).

[32] M. Dhar, J.N. Lam, T. Walser, S.M. Dubinett, M.B. Rettig, D. Di Carlo, Functional profiling of circulating tumor cells with an integrated vortex capture and single-cell protease activity assay, P Natl Acad Sci USA, 115 (2018) 9986-9991.

[33] J. de Rutte, R. Dimatteo, M. van Zee, R. Damoiseaux, D. Di Carlo, Massively parallel encapsulation of single cells with structured microparticles and secretion-based flow sorting, bioRxiv, (2020) 2020.2003.2009.984245.

[34] A. Montessori, M. Lauricella, S. Succi, E. Stolovicki, D. Weitz, Elucidating the mechanism of step emulsification, Phys Rev Fluids, 3 (2018).

[35] Q. Han, N. Bagheri, E.M. Bradshaw, D.A. Hafler, D.A. Lauffenburger, J.C. Love, Polyfunctional responses by human T cells result from sequential release of cytokines, P Natl Acad Sci USA, 109 (2012) 1607-1612.

Chapter 3. Dropicles: A novel tool for single-cell functional screening

3.1. Introduction

The microwell plate has become a foundational component of biological assays because of the ability to scale experiments and integrate with lab automation infrastructure. This simple piece of plasticware allows scientists to add or exchange reagents while preventing cross-talk between samples. The bottom surface of each well can be functionalized to adhere cells, promote cell growth, and perform biomolecular reactions that allow for colorimetric and fluorescent readouts. Biological samples of interest can then be isolated by pipetting fluid from a well. Despite its simplicity and utility, even the smallest format, 1536-well plates, hold volumes that are hundreds of thousands of times larger than cells in each well, limiting the ability to study the functional properties, such as secreted products, from single cells.

The ability to perform functional biological assays at the resolution of the individual cells promises to deepen our understanding of biology and accelerate the development of new biological products. For example, sorting of rare B cells or plasma cells directly based on activity of high affinity secreted antibodies allows for the acquisition of gene sequences that can be used to make new antibody drugs or diagnostic affinity reagents[1-6]. Selection of stable production-grade cells such as Chinese hamster ovary (CHO) cells based on their production rate of humanized IgG protein would allow for the selection of specific clones useful for monoclonal antibody production.[7]

Although technologies have emerged to enable to the probing of single cells, there are significant tradeoffs that either limit functionality or inhibit widespread adoption. Fluorescence activated cell sorting is one of the first single-cell technologies to gain widespread adoption,

enabling users to probe and sort individual cells based on light scatter properties and fluorescently stained molecules at throughputs over 10,000 events per second. Screening of viable cells is typically limited to non-functional parameters such as exterior cell surface proteins (i.e. the clusters of differentiation markers, or CDs) while intracellular markers can be analyzed but require membrane permeabilization and fixation.[8, 9] Approaches have been developed to capture secreted products directly to the cell surface, but these techniques suffer from significant crosstalk between cells.[10-12] Microfluidic technologies have emerged that enable the creation of volumes approaching the size of cells and high-throughput analysis of single cells based on additional properties such as secreted molecules.[13] Devices with microscale chambers as well as water-in-oil droplets generated using microfluidic devices have been employed to isolate cells, accumulate secreted product, and even sort.[14-19] Despite the utility of these existing platforms, the ability to add reagents and perform washing steps during reactions is limited, and microfluidically-generated droplets lack the solid surface of a microwell plate which is critical for standard assay formats like sandwich immunoassays or ELISA. Approaches to overcome these shortcomings have been developed, but each requires specialized assay formats, and often extremely expensive equipment to perform the assays, which hinders widespread adoption.[20-22]

We introduce a new approach to perform functional assays on individual cells at high-throughput using structured microparticles, which act as suspendable and sortable microwells (Figure 3-1). These microparticles or “nanovials” hold single cells in sub-nanoliter volumes of fluid, 100,000 times less volume then 1536-format microwells yet require no new instrumentation.

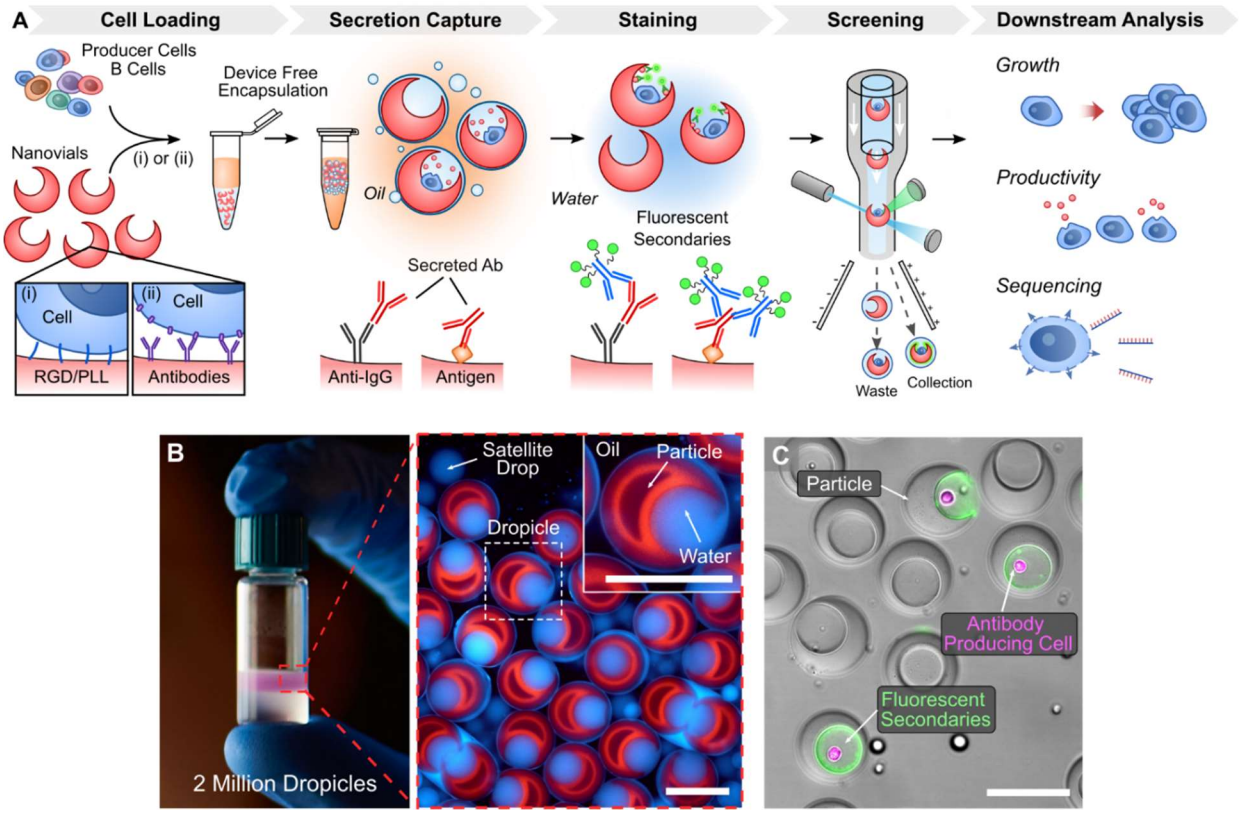

Figure 3-1 . Microparticle platform for high-throughput single cells secretion screening.

(A) Individual cells are loaded into prefabricated microparticles containers (nanovials) and bound using a variety of binding schemes. Particles and associated cells are agitated by pipetting with biocompatible oil and surfactant to generate monodisperse compartments dictated by the particle size (dropicles) preventing crosstalk between microcontainers. Cells are incubated to accumulate secretions on associated particles and transferred back to a water phase for fluorescent labeling. Particles, cells, and associated secretions are then analyzed and sorted using high-throughput commercial flow sorters. Isolated populations can then be analyzed downstream for different phenotypic (growth, productivity) and genotypic properties (RNA expression). **(B)** Photograph of a tube with 2 million dropicles formed using simple pipetting steps in less than 1 minute (left). Fluorescent microscopy image of uniform dropicles formed with fluorescently stained nanovials and water-soluble dye (right) show distinctly sealed sub-nanoliter volumes. **(C)**Microscopy image of nanovials with cells and associated secretions after unsealing the nanovials and staining with fluorescent labels.

Fluids are easily exchanged by centrifugation and pipetting, and each compartment can be sealed and unsealed using biocompatible oils to prevent cross-talk between samples. The surfaces can be modified to bind cells or capture biomolecules for molecular readout. Nanovials can be analyzed and isolated using commonly available FACS instruments enabling screening at rates >1000 events per second. While other particle systems have been utilized to hold sub-nanoliter volumes,[23-27] ours is the first approach that allows attaching and protection of cells in cavities within particles and unlocks new capabilities to expand scale of analysis by integration with flow cytometry that was not previously achieved. Using this new nanovial format we conduct a screen of >500,000 events in less than an hour using commercial FACS instruments, demonstrating single-cell antibody discovery and cell line development workflows that can identify rare antibody secreting cells from an order of magnitude more cells than previous approaches all within one day. A similar experiment would require >1300 384-well plates and at least a week of additional culture to grow up a sufficiently large clonal population of cells to detect secretions in the larger volumes.

3.2. Materials and Methods

3.2.1. Fabrication of nanovials

Particles were fabricated using a standard PDMS microfluidic flow focusing droplet generator. A PEG phase comprised of 28.9% w/w 4-arm PEG-norbornene (Sigma), 3% w/w LAP (Lithium phenyl-2,4,6-trimethylbenzoylphosphinate, Sigma), and 1 mg/mL Biotin-PEG-thiol (5000 MW, Nanocs) in phosphate buffered saline (PBS, pH 7.2) was co-injected with a dextran phase comprised of 11% w/w 40 kDa dextran (Sigma), 1.3% w/w DTT (dithiothreitol, Sigma), and 5 mM RGD pepride (Ac-RGDSPGERCG-NH2, Genscript) in PBS at rates ranging from 0.5-5 μL/min, depending on nanovial size, using syringe pumps (Harvard Apparatus PHD

2000). An oil phase comprised of Novec 7500 (3M) and 0.25% w/w PicoSurf (Sphere Fluidics) was injected at a rate of 10-42 µL/min to partition the aqueous phases into monodisperse water in oil droplets. PEG and dextran polymers phase separated on chip after approximately 5 seconds. The PEG phase was crosslinked with focused UV light through a DAPI filter set and microscope objective (Nikon, Eclipse Ti-S) near the outlet region of the microfluidic device. Crosslinked particles were collected, and oil and dextran were removed using a series of washing steps. Briefly, excess oil was removed by pipetting and a layer of PBS was added on top of the remaining emulsions. A solution of 20% v/v perfluoro-octanol (PFO, Sigma) in Novec 7500 was then added to destabilize the emulsions and transfer particles to the PBS phase. Excess oil was removed, and samples were washed 2X with Novec 7500 to remove the remaining surfactant. Novec 7500 was removed by pipetting and residual oil was removed by washing 2-3X with hexane (Sigma). Samples were then washed 3X with PBS to remove dextran from the system. For cell experiments particles were sterilized by incubating in 70% Ethanol overnight. Particles were then washed 5X with a storage solution comprised of PBS + 0.1% Pluronic F-127 (Sigma) + 1% penicillin/streptomycin (Invitrogen) and stored in a conical tube at 4ºC.

3.2.2. Cell Culture

CHO-K1 and CHO DP-12 Cells: All cells were cultured in incubators at 37°C and 5% CO_2. CHO K1 cells (ATCC CCL61) were cultured in F12 base media (Invitrogen) supplemented with 10% fetal bovine serum (FBS, Invitrogen) and 1% penicillin/streptomycin (Invitrogen). CHO DP-12 cells (ATCC CRL-12445) were maintained according to manufacturer's specifications. Cell culture media was comprised of DMEM (Invitrogen) supplemented with 10% FBS, 1% penicillin/streptomycin, 0.002 mg/mL recombinant human insulin (Sigma), 0.1% Trace Elements

A (Fisher Scientific), 0.1% Trace Elements B (Fisher Scientific), and 200 nM Methotrexate (MTX, SIGMA).

ExpiCHO Cells: ExpiCHO cells (Fisher Scientific A29127) were cultured in ExpiCHO™ Expression Medium (Fisher Scientific) on an orbital shaker in a 37°C incubator with ≥80% relative humidity and 8% CO_2. The shake speed was set to 120 rpm with 25 mm shaking diameter. Cells were seeded at 0.2 x 10^6 viable cells/mL and subcultured when the cell density reached 4 x 10^6 – 6 x 10^6 viable cells/mL.

HEK293 cells: HEK293 cells (ATCC CRL-1573™) were cultured in incubators at 37°C and 5% CO_2 and the media consisted of DMEM, high glucose, pyruvate media (Invitrogen) supplemented with 10% FBS (Invitrogen). Cells were seeded at 2 x 10^4 viable cells/cm^2 and subcultured when concentration reached 6 x 10^4 cells/cm^2.

Hybridoma Cells (HyHel-5 & 9E10): Hybridoma cells were cultured in incubators at 37°C and 5% CO_2 according to manufacturer instructions. HyHel-5 cells were maintained in IMDM media (Invitrogen) supplemented with 10% FBS (Invitrogen) and 1% penicillin/streptomycin (Invitrogen). 9E10 cells were maintained in RPMI media (Invitrogen) supplemented with 10% FBS (Invitrogen) and 1% penicillin/streptomycin (Invitrogen). Cells were passaged down to a final concentration of 4x10^5 cells/mL every two days.

3.2.3. Particle seeding and cell seeding characterization

Stock drop-carrier particles were first concentrated in a conical tube by centrifugation and supernatant was aspirated. Particles were then fluorescently labeled by diluting at a 1:1 ratio with PBS containing 10 μg/mL of Alexa Fluor 568 streptavidin (Fisher Scientific) and incubating for 10 min. Particles were washed 3X with PBS and then dispersed in a well plate at a concentration

of 7.5 µL of concentrated particles per cm of well surface area. Particles were then allowed to settle for 10 min. CHO cells pre-stained with Hoechst were then seeded at a range of concentrations (31-190 cells/mm^2) into the well by carefully pipetting evenly across the well area. Cells were allowed to settle for 15 min and then imaged using a fluorescent microscope. Loading statistics was calculated using custom image analysis algorithms in MATLAB. Particles were first identified using the particle fluorescence channel and cell number was calculated by counting nuclei number within each particle cavity.

3.2.4. ExpiCHO Cell Binding

In order to modify the particle surface with poly-L-Lysine, 100 uL of 55um particles were suspended in 1 mL PBS solution consisting of 1 mg/mL PLL (Thiol-Poly-L-Lysine-Thiol, 32 kDa, Nanosoft Polymers) and 0.2 % w/w LAP (Lithium phenyl-2,4,6-trimethylbenzoylphosphinate, Sigma). The particle suspension was transferred to a glass vial pre-coated with Sigmacote (Sigma SL2-25ML) and the vial was placed on top of a mini stir plate (IKA Lab Disc IKAMAG Magnetic Stirrer) with a micro stir bar in it. With continuous mixing, the particle suspension was exposed to UV for 60 seconds at the power of 2.9 mW/cm^2. The particle suspension was retrieved into a 1.5 mL Eppendorf tube and washed with 0.05% Pluronic buffer three times.

To futher modify particles with fibronectin, 25 ul of PLL conjugated particles were added to 500 uL of either 10 ug/mL or 500 ug/mL fibronectin solution for one hour at room temperature and washed with 0.05% Pluronic buffer three times.

ExpiCHO cell loading was screened through the addition of 1 mL of ExpiCHO expression media with 7.84 uL of PLL or PLL+Fibronectin modified particles and 79,000 ExpiCHO cells were added. Particle and cell suspension was mixed 10 times using a 1 mL

pipette. The plate was incubated on a rocker in 37 °C incubator for 30 minutes, and then incubated for another 2.5 hours on a steady state in the incubator. Particle and cell suspension in each well was strained using 37 um strainer (Stemcell Technologies) and particles were recovered in fresh and pre-warmed ExpiCHO expression media. Recovered particles were imaged using fluorescent microscopy.

3.2.5. HEK293 Cell Binding

PLL and PLL+Fibronectin particles were prepared by the same method mentioned in the ExpiCHO cell binding section above. In each well of a 24 well-plate, 1 mL of DMEM base media (without FBS) with 7.84 uL of PLL or PLL+Fibronectin modified particles and 79,000 HEK293 cells were added. Particle and cell suspension was mixed 10 times using a 1 mL pipette. The plate was incubated on a rocker in 37 °C incubator for 30 minutes, and then incubated for another 2.5 hours on a steady state in the incubator. Particle and cell suspension in each well was strained using 37 um strainer (Stemcell Technologies) and particles were recovered in fresh and pre-warmed DMEM media with 10% FBS. Recovered particles were imaged using fluorescent microscope.

3.2.6. B Cell Binding

PLL+Fibronectin particles were prepared as mentioned in the ExpiCHO cell binding section above. To test capture with anti-surface marker antibodies, particles were first incubated for 10 min in a 130 ug/mL streptavidin solution. Particles were then washed 3X and incubated with a solution containing 2ng aCD45, aCD19, or 1:1 mix of aCD45+aCD19 per uL particle solution at 60ug total antibody concentration. Particles were then washed 3X. 8uL of particles were added to each well of a 24 well plate in 2mL washing buffer, followed by addition of 100,000 cells. The cells were allowed to settle into particle cavities and adhere for 2 hours. The

particles were then strained with a 20um cell strainer to remove unattached cells, and sorted with a BD FACS Aria II or Sony SH800 FACS system.

3.2.7. Dropicle Formation and Characterization

85 μm nanovials were suspended in DMEM base media (Invitrogen) and then concentrated by centrifuging at 300 g for 2-3 minutes and aspirating supernatant. An oil phase comprised of Novec 7500 and 2% w/w PicoSurf was added to the particle suspension at approximately 2X the remaining volume. The sample was then vigorously pipetted for 30 - 60 s (~100 pipettes) using a 200 μL micropipette (Eppendorf). The resulting water-in-oil emulsion was then carefully transferred into a PDMS reservoir by pipetting and imaged. Size distribution characterization was then performed using custom image analysis algorithms in MATLAB. For the fluorescent images shown in Figure 3-1B, particles were first labeled with Alexa Fluor 568 streptavidin and the DMEM was replaced with PBS containing 2 mg/ml fluorescein isothiocyanate-dextran (500k MW, Sigma). For 35 μm nanovials the same procedure was used except the nanovials were first diluted 10 – 15X to reduce fraction of aggregates formed.

3.2.8. Cell Viability Characterization

30 μL of concentrated particles and 48k CHO DP-12 cells were suspended in media and sequentially seeded into individual wells of a 12-well plate. A separate well plate control sample containing no particles was prepared in parallel. Cells were allowed to adhere for 4 hours. Samples containing both the cells and particles were transferred into a 15 ml conical tube, exchanged with fresh media and then concentrated via centrifugation. 100 μL of Novec + 2% w/w PicoSurf was added to the concentrated sample and pipetted for 30 s to encapsulate the particles and associated cells into dropicles. 150 μL of light mineral oil was added on top of the samples to mitigate evaporation during incubation. Samples were then incubated for 2, 12, and

24 hours in an incubator at 37°C and 5% CO_2. To recover cells back into an aqueous phase excess oil was first removed via pipetting and several mL of media was added on top of the emulsions. To destabilize the droplets 50 µL of 20% v/v PFO in Novec 7500 was then pipetted on top of the emulsion layer and the sample was gently agitated. After 5 min most of the droplets were merged and particles and associated cells transferred into the bulk media phase. Optionally, samples can be centrifuged for 15-30 s at 200g to coalesce remaining droplets. The suspension of particles and cells were then transferred by pipetting into a separate conical tube. Samples were washed with PBS and then sequentially stained with calcein AM and propidium iodide. Particle samples were transferred back into a well plate, imaged, and then analyzed in MATLAB to determine cell viability statistics.

3.2.9. CHO Cell Secretion Assay

To identify cells during downstream analysis CHO DP-12 cells were first stained with CellTracker™ Blue CMAC Dye (Thermo Fisher). RGD coated nanovials and cells were seeded into a 12-well plate as described above and then incubated at 37°C for 2 hours to allow cells to adhere to the particles. Particles were then recovered by tilting the well plate and transferring by pipetting. In order to remove unattached cells from the background, samples were strained using a 37 µm reversible cell strainer (STEMCELL Technologies) and then particles were recovered by flipping the cell strainer and washing with a washing buffer comprised of PBS (Ca^{2+},Mg^{2+}), 0.5% BSA (GeminiBio), 1% penicillin/streptomycin and 0.05% Pluronic F-127. To reduce sample loss all conical tubes and pipette tips were first precoated with washing buffer prior to handling particle containing solutions. After recovering from the well plate, samples were washed 2X by centrifuging particles and associated cells at 300 rpm for 3 min, aspirating, and then resuspending in washing buffer. Particles were then labeled with streptavidin (Thermo

Fisher, 434302) by adding 0.415 ng per µL of concentrated particle solution and incubating for 10 min. Samples were then washed 3X with washing buffer and resuspended. Particles were then labeled with Biotin Anti-FC (Thermo Fisher, A18821) by adding 75 pg of the antibodies per µL of concentrated particle solution and incubating for 10 min. After incubation, samples were washed and resuspended in CHO DP-12 media. After re-concentrating, samples were compartmentalized by pipetting with oil and surfactant as described above to create dropicles. Samples were then incubated for a range of times 0, 1, 2, 4, and 8 hours to allow cells to secrete and to facilitate capture of secreted antibodies onto the associated particle matrix via Anti-FC sites. After the incubation period, particles and associated cells were transferred back into media by breaking the emulsions (see live dead section). Samples were then washed and captured secretions were stained with Goat anti-human IgG H&L (Dylight® 488, Abcam ab96911) at a final concentration of 30 pg per µL of initial concentrated particle solution. After 30 min of staining, samples were then washed 5X with a solution of PBS (Ca^{2+}, Mg^{2+}), 2% FBS, 1% penicillin/streptomycin and 0.05% Pluronic F-127 and optionally stained with propidium iodide. Samples were then imaged in both brightfield and fluorescence channels in a well plate. To characterize secretion amount per particle a custom MATLAB algorithm was used to identify particles in brightfield and then count the number of cells, check for the presence of dead stain, and integrate the total secretion label fluorescence intensity for each particle.

3.2.10. Hybridoma Secretion Assay

To better accommodate the smaller sized hybridoma cells, 55 µm diameter nanovials were used for screening antigen-specific antibody production. Nanovial samples were first coated with streptavidin as described in the CHO cell secretion assay above, thoroughly washed, and subsequently labeled with a pre-mixed solution containing both biotin anti-CD45 and biotin

anti-H+L chain antibodies both at concentrations of 20 µg/mL. After 30 minutes of incubation with biotinylated antibodies, nanovials were washed 3x once more, reconstituted into washing buffer and refrigerated. Concurrently 9E10 hybridoma cells were labeled with CellTracker™ Blue dye (Thermo Fisher) and premixed with unlabeled HyHel-5 hybridoma cells at desired concentrations. Importantly the CellTracker™ Blue dye (Thermo Fisher) stain was not used for sorting or enrichment purposes, but served to differentiate the two cell types in pre and post sort analysis to benchmark assay performance. The pre-mixed hybridoma cell populations were next loaded into the chilled antibody coated hydrogel nanovials. Nanovials and cells were maintained at 4°C for 1 hour to lower their metabolic activity and prevent accumulation of secretion onto neighboring unloaded nanovials during the binding process. Following adhesion, unbound cells were removed from the sample by filtering through a 20 µm cell-strainer, and the recovered cell loaded particles were incubated in IMDM media at 37°C for another hour. We found that for rare populations of antigen-specific hybridomas encapsulation could be omitted without appreciable loss of experimental accuracy because target antibody signal was relatively infrequent and cross-talk was minimal, therefore it was omitted for this experiment. Finally, after allowing accumulation of sufficient antibody signal, samples were washed a final time and labeled with 0.75 µg/mL HEL-647. All samples were sorted on a Sony SH800 flow cytometer using the 488 nm and 638 nm lasers in single-cell mode with minor adjustments to the drop delay to account for the larger size of the particle nanovials.

3.2.11. Secretion cross-talk analysis experiment

To analyze potential cross-talk in our single cell secretion system, samples were prepared as described in the cell secretion assay section with several modifications to the protocol. Two sets of samples were prepared, a control sample that was incubated in bulk solution and one

incubated after dropicle formation. Prior to the incubation step a separate suspension of particles containing no cells and tagged with Alexa Fluor 647 streptavidin were mixed into the samples. This was done in order to ensure signal on empty particles that was measured did not arise from cells that may have detached from the particles during various steps of the assay. Samples were washed and capture sites were then added. The bulk samples were then left to incubate in media while the dropicle samples was emulsified in oil via pipetting. After incubating for 15 hours samples were recovered and washed with washing buffer, stained, and imaged as described in the cell secretion assay section. The amount of cross talk was determined by comparing secretion staining intensity on particles with cells with the intensity on the control particles.

3.2.12. Secretion based sorting control experiments

Samples were prepared as described in the cell secretion assay with the following modifications. CHO DP-12 cells and CHO K1 cells were pre-labeled with CellTracker™ Deep Red and CellTracker™ Blue (Thermo Fisher). After labelling, cells were mixed together at various ratios (1:5, 1:100, 1:1000) and loaded into particles (Seeding density ~84/mm^2, lambda ~0.1. All remaining secretion assay steps were as previously described. After labelling secretions on samples with fluorescent secondary antibodies, samples were sorted using a FACS machine (BioSorter, Unionbio). Samples were excited using both 488 nm and 561 nm lasers. Events were triggered based on particle absorbance from the 561 nm laser. Single particle events were gated based on time of flight. Particles with secretion signal were then sorted by thresholding the peak intensity height collected through a 543/22 nm filter. Samples were sorted directly into a 96-well plate and imaged with a fluorescence microscope.

3.2.13. Enrichment of high producing CHO cells

Samples were prepared as described in the cell secretion assay section. After labelling secretions, a fraction of each sample was kept and imaged using fluorescence microscopy. Remaining samples were then sorted using a FACS instrument (On-Chip Sort, On Chip Biotechnologies). Samples were excited with both a 488 nm and 637 nm laser. Particle events were screened based on the forward and side scatter. Particles positive for both cells and secretion signal were gated based on peak fluorescence height collected through a 543/22 nm emission filter and a 676/37 nm emission filter respectively. Two sub-populations were sorted for each sample: (1) particles with cells and positive secretion signal, (2) particles with cells and the top 20% of positive secretion signal. Collected samples were plated and expanded for >10 days. To quantify antibody production of the isolated sub-populations, 30k cells from the expanded sub-populations as well as un-sorted control samples were plated into a 48-well plate. After cells attached the samples were washed, replaced with 400 μL of fresh media, and incubated for 6 hours. Supernatant was then collected, and total human IgG amount was measured using ELISA (IgG (Total) Human ELISA Kit, Invitrogen, BMS2091). Production rate was calculated based off the measured IgG concentration, incubation time, and initial number of cells seeded.

3.2.14. Mouse immunization and B lymphocyte isolation and culture

All experiments involving animals, animal cells, or tissues were performed in accordance with the Chancellor's Animal Research Committee ethical guidelines at the University of California Los Angeles under protocol no ARC-2015-125. Ten week old C56BL/6J mice (Jackson Laboratory) were immunized for a total of 7 times in 28 days with recombinant ovalbumin (Biosearch Technologies) as a model antigen. Immunizations were made by mixing ovalbumin at 1 ug/uL in PBS with equal volume of Inject alum adjuvant (ThermoFisher

Scientific). 250 ug and 25 ug doses of ovalbumin were used initial immunization, and subsequent 7 boosters, respectively. 4 days after final immunization, mice were euthanized with isoflurane overdose followed by cervical dislocation and sterilized by spraying with 70% ethanol. The skin was removed from the lower limbs by making an incision along from the palms to the abdomen, and tibia and femur of both legs were cut from hip and palms. Muscle tissue was then removed, and the four bones were placed in ice cold PBS while processing other mice. The bone ends were cut and the bone marrow was removed by flushing 10 mL of cold PBS through one end using a syringe connected to a 25-gauge needle. The tissue clumps were dissociated by drawing and flushing the solution through the needle 3 times. The isolated cells from up to 4 mice were pooled together, strained through a 70 μm cell strainer, and centrifuged at 300g for 10 min at 4C. A 10^8 cells/mL suspension of cells was prepared in EasySep buffer (StemCell Technologies, #20144), and plasma cells were isolated using a EasySep mouse CD138 positive selection kit (StemCell Technologies, #18957) according to the manufacturer's protocol. The isolated cell suspensions were then placed on ice until use. For B cell isolation, spleen was removed, cut into small pieces with scissors, and pushed through a 70 μm cell strainer in a 10 cm petri dish containing 10 mL cold PBS, using the plunger of a 10 mL syringe. The same syringe was then used to dissociate tissue clumps by drawing and flushing the solution through a 25-gauge needle 3 times. Cells were pelleted by centrifugation at 300g for 10 min and resuspended at 10^8 cells/mL in EasySep buffer and B lineage cells were isolated using an EasySep mouse B cell negative isolation kit (StemCell Technologies, #19854). For serum, blood was collected directly from left ventricle via cardiac puncture immediately after euthanasia. Blood was allowed to clot at room temperature for 4 hours, before centrifuging at 10,000 g for 10 min to separate serum.

3.2.15. B cell and plasma cell cultures

All efforts were made to use plasma and B cells fresh after isolation. Excess cells were frozen in FBS containing 10% DMSO at 1 million cells per mL. After thawing, cells were allowed to recover for one hour in media before further use. Cells were grown in RPMI, containing 10% FBS, 1% of each of penicillin/streptomycin, L-Glutamine, HEPES buffer, minimum essential medium nonessential amino acids, sodium pyruvate (ThermoFisher Scientific 15070063, A2916801, 15630130, 11140050, 11360070), and 50 M beta mercapto-ethanol. For any incubation time over 1 hour, the plasma cell media was supplemented with IL-6 and APRIL (GenScript Z03189 and Z02969) at 50 and 100 ng/mL respectively. Isolated B cells from spleen of vaccinated mice were cultured at 500k cells per mL in vitro for 3 days in media supplemented with LPS and CpG ODN 1826 at 5 and 1 μg/μL, respectively.

3.2.16. Plasma cell secretion assay

To minimize manipulation of primary plasma cells in antibody secretion assays, particle labeling was performed prior to seeding the cells. To reduce sample loss, as mentioned above, all conical tubes and pipette tips were precoated with washing buffer prior to handling particle containing solutions. Biotinylated particles were labeled with streptavidin (Thermo Fisher, 434302) by adding 150 ng per μL of concentrated particle solution and incubating for 10 min. Samples were then washed 3X with washing buffer and resuspended. Particles were then labeled with biotinylated anti-CD45 and biotinylated goat anti-mouse IgG H&L chain antibodies (Invitrogen 13045182 and SouthernBiotech 1034-08) by adding 40 ng and 60 ng of the respective antibodies per μL of concentrated particle solution and incubating for 30 min. After incubation, particles were washed and resuspended in EasySep buffer containing IL6 and APRIL, respectively. 9 μL of 55 μm nanovials and 85000 plasma cells were seeded into a 24-well plate as described above and then incubated at 37°C for 1 hours to allow cells to adhere to

the particles. Particles were then recovered by tilting the well plate and transferring by pipetting. To remove unattached cells from the background, samples were strained using a 37 or 20 μm reversible cell strainer for 55 and 35 μm particles, respectively (STEMCELL Technologies or Partec North America CELLTRICS) and then particles were recovered by flipping the cell strainer and washing with washing buffer. After recovering, samples were concentrated by centrifuging particles and associated cells at 300 g for 3 min, aspirating, and then resuspending in 1 mL EasySep buffer containing IL6 and APRIL. After re-suspending, samples were compartmentalized by pipetting with oil and surfactant as described above to create dropicles. Samples were then incubated for 2 hours to allow cells to secrete and to facilitate capture of secreted antibodies onto the associated particle matrix via goat anti-mouse IgG H&L sites. After the incubation period, particles and associated cells were transferred back into media by breaking the emulsions (see live dead section). Samples were then washed, and captured secretions were stained with Alexa Fluor 647 conjugated ovalbumin (Invitrogen O34784) at a final concentration of 50 ng per μL of initial concentrated particle solution. After 30 min of staining, samples were washed 3X a large volume of EasySep buffer and optionally stained with propidium iodide. An aliquot of the sample was then either sorted using a Sony SH800 FACS system or imaged with a fluorescent microscope in both brightfield and fluorescence channels in a well plate for quality control, or analysis in MATLAB.

3.2.17. Serum measurements, LOD and Dynamic Range Experiments

For assessment of the dynamic range of the on-particle ELISA for antibody capture and detection, 2 uL aliquots of particles were used for each condition. Biotinylated particles were labeled with streptavidin (Thermo Fisher, 434302) by adding 150 ng per μL of concentrated particle solution and incubating for 10 min. Samples were then washed 3X with washing buffer

and resuspended. Particles were then labeled biotinylated goat anti-mouse IgG H&L antibodies with or without biotinylated anti-CD45 and (SouthernBiotech 1034-08, Invitrogen 13045182) by adding 60 ng and 40 ng of the respective antibodies per μL of concentrated particle solution and incubating for 30 min. After incubation, particles were washed and resuspended in washing buffer. Serum, media, or purified antibodies at various concentrations were added to the particles and incubated for 2 hours to allow antibody capture onto the particle matrix via anti-mouse IgG H&L sites. After the incubation period, particles were washed and captured secretions were stained with Alexa Fluor 647 conjugated ovalbumin (Invitroge O34784) at a final concentration of 50 ng per μL of initial concentrated particle solution. After 30 min of staining, samples were washed 5X with washing buffer. Finally particles were analyzed by Sony SH800 FACS system or imaged with a fluorescent microscope in both brightfield and fluorescence channels in a well plate. A similar assay format was also tested for ovalbumin specific antibody capture using a reverse ELISA setup: biotinylated ovalbumin (Nanocs OVA1BN1) as capture site on particles, and Alexa Fluor Plus 555 conjugated goat anti-mouse IgG H&L antibodies (Invitrogen, A32727) for detection, with similar moles of capture and detection molecules as the first ELISA configuration.

3.3. Results

3.3.1. Precise fabrication of suspendable microcontainers

Our approach to screen single cells requires microparticles that are engineered with cavities to directly load and protect cells, functional groups to attach cells and perform chemical reactions, and which are engineered to be compatible with commercial flow cytometers. Utilizing an aqueous two-phase system combined with droplet microfluidics we fabricate hydrogel microparticles (nanovials) that meet these requirements at high throughputs (~1000 s^{-1})

(Figures 3-2, 3-3, 3-4).[28, 29] By tuning the fabrication parameters, we achieve highly monodisperse polyethylene glycol (PEG)-based nanovials with accessible internal cavities (outer diameter CV of 1.5%, cavity opening diameter CV of 2.1%, Figure 3-2F). Particles are easily modified with various cell adhesion moieties (e.g. arginine-glycine-aspartate (RGD), poly-L-lysine). Biotin conjugated within the nanovial matrix allows for facile surface decoration with streptavidin (Figure 3-2G) which allows linkage with biotinylated antibodies or antigens for desired secretion assays. This linkage can also be used for antibodies specific to cell surface proteins (e.g. CD45 and CD19) for cell binding. We fabricate monodisperse nanovials to achieve a range of mean diameters (Figure 3-4) from 35 to 105 μm which are compatible with a range of cell types and common lab instruments FACS instruments (Figure 3-4). The morphology of the cavity and relative size can be adjusted by tuning the concentration of components in the particle precursor solutions (Figure 3-3). Importantly, this fabrication step is the only part of the process that requires use of a specialized microfluidic device and is completely separate from the assays themselves. All parts of the single cell assay workflows are performed directly with prefabricated nanovials and standard lab equipment. This is a critical feature of our platform as it enables the more complex microfluidic/particle fabrication work to be centralized and performed in advance.

3.3.2. Nanovials as modular single-cell carriers

Loading of cells into the cavities of the nanovials utilizes simple pipetting steps followed by incubation to allow cell binding. Nanovials can be first loaded into a standard well plate by pipetting and due to their unique morphology settle with their cavities mostly upright , forming a monolayer of particles with exposed cavities at the bottom of the well (Figure 3-2H, 3-5).[30]

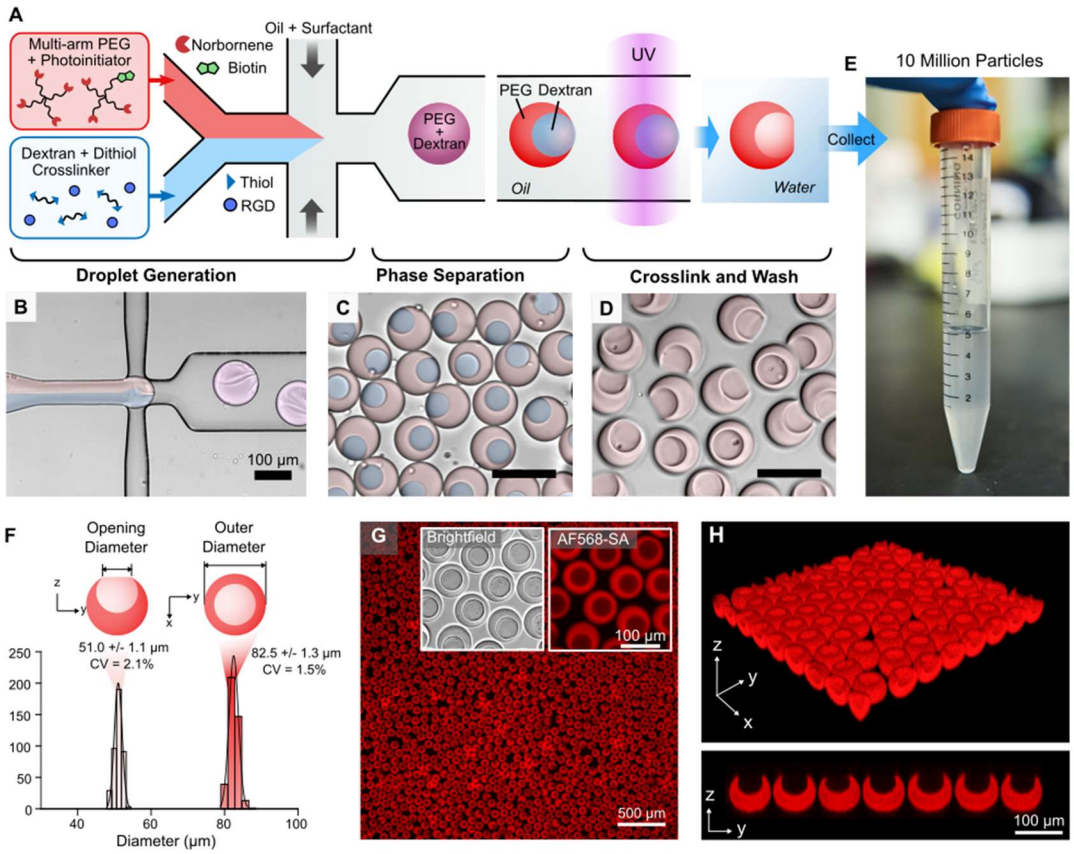

Figure 3-2 Nanovial formed via aqueous two-phase system combined with droplet microfluidics. **(A)** A solution comprised of UV reactive PEG and photoinitiator is co-flowed with a solution containing dextran, dithiol crosslinkers, and RGD peptides in a microfluidic droplet generator. **(B)** A third solution of oil and surfactant is injected into the device to generate water-in-oil droplets at a rate of ~1000 Hz. **(C)** Downstream on the device PEG and dextran undergo phase separation resulting in two distinct regions in the droplet. The droplets are exposed with UV light at the end of the device to crosslink the PEG rich portion of the droplet, while the dextran rich region remains as a liquid. **(D)** The resulting microparticles are then collected, washed to remove oil and dextran, and stored for later use. **(E)** Photograph of a 15 mL conical tube with 10 million drop-carrier particles fabricated in ~3 hours. **(F)** Nanovials fabricated using this approach are highly monodisperse with outer diameter CV of 1.5% and cavity opening diameter CV of 2.1% (n = 409). Particle uniformity was calculated by analyzing fluorescence microscopy images using a custom image analysis algorithm in MATLAB. **(G)** Fluorescence microscopy image of biotinylated drop-carrier particles stained with Alexa Fluor 568 Streptavidin (AF568-SA). A large fraction of the seeded particles settles with their cavities exposed upright. **(H)** Nanovial cavity morphology and upright orientation was confirmed using confocal microscopy. Microscopy images in B, C, and D have overlayed color to aid in visualization.

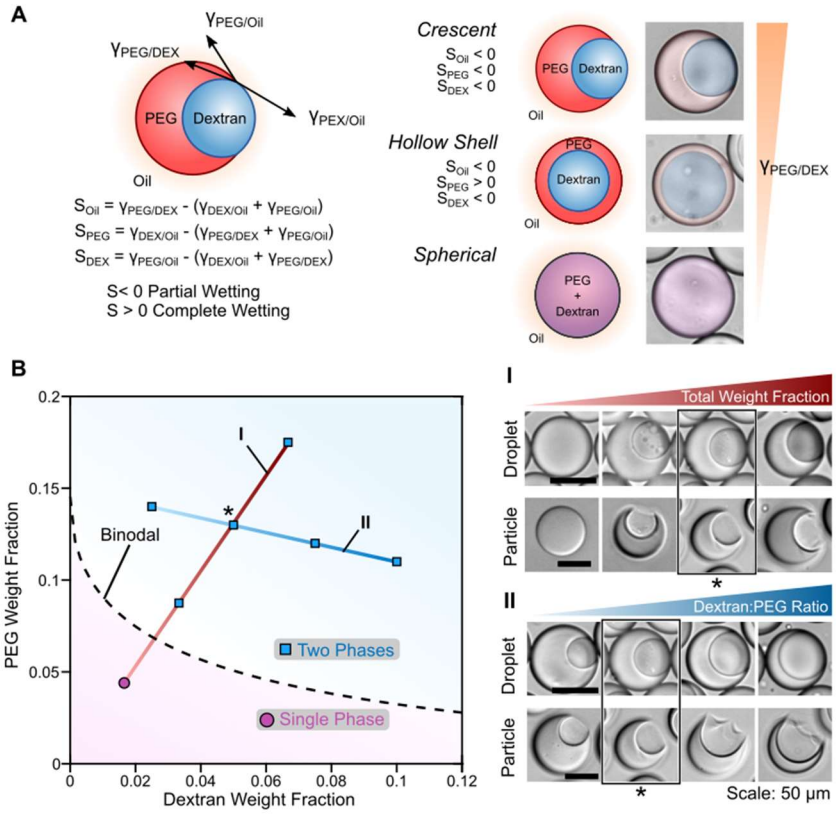

Figure 3-3 Morphology is tuned by adjusting the concentration of PEG and dextran in the droplets. (**A**) The morphology of nanovials is dictated by a balance of interfacial tensions (γ) between the different phases. $\gamma_{PEG/Oil}$ and $\gamma_{DEX/oil}$ are expected to vary minimally, the balance of interfacial tensions and the resulting morphology is expected to be dictated mostly by a change in $\gamma_{PEG/DEX}$. (**B**) Experimentally determined phase diagram of 4-Arm PEG Norbornene, and dextran. At very low concentrations phase separation does not occur resulting in a spherical particle (**i**). As the total concentration of PEG and dextran is increased above the binodal line, phase separation occurs enabling fabrication of cavity-containing microparticles. (**I**) The relative opening diameter of the particle cavity is increased by increasing the total polymer concentration and thus $\gamma_{PEG/DEX}$ resulting in relative opening size of 48 – 63% of the outer diameter. (**II**) By adjusting the concentration ratio of dextran and PEG, particles can be fabricated with different relative cavity sizes. Here the relative cavity diameter is from 34 – 76% the outer diameter Particles fabricated using a PEG concentration of 13% and dextran concentration of 5% (denoted by *) were found to have high structural integrity while maintaining a relatively large cavity opening to enable efficient cell loading. This condition was used for all other experiments in this work.

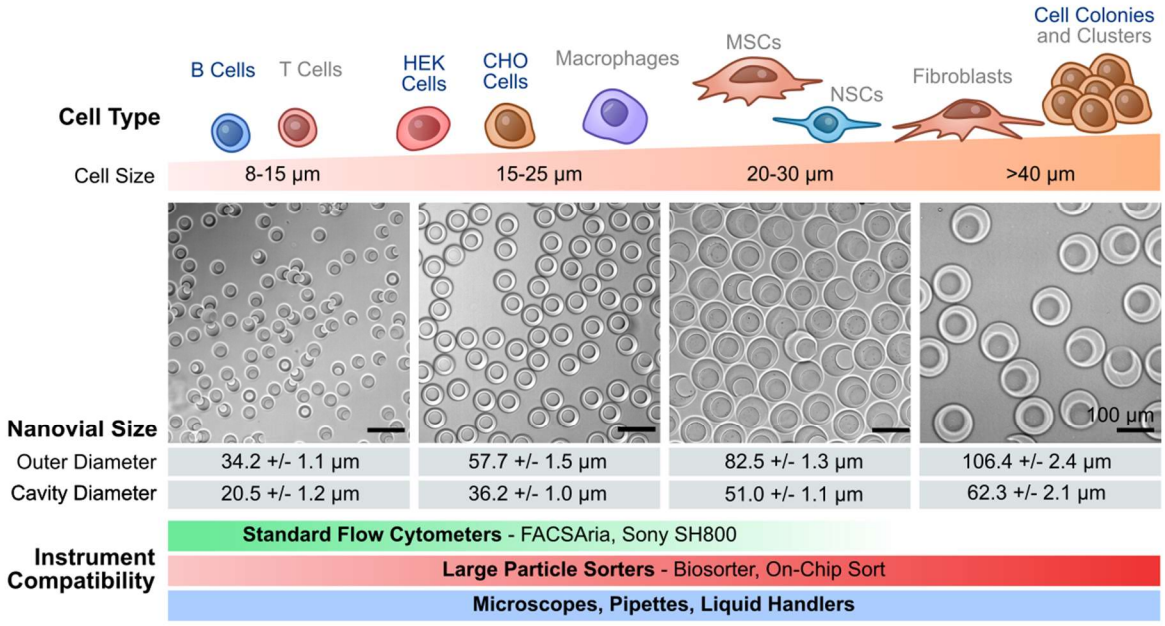

Figure 3-4 Compatibility of a range of nanovial sizes with different cell types and instruments. Nanovials with high uniformity were fabricated with mean outer diameters ranging from 35 to 105 µm and respective mean cavity diameters of 20 to 62 µm. Smaller nanovials are more compatible with standard flow cytometers which are more accessible and allow higher throughputs, but are limited to smaller cell types. Larger nanovials are compatible with larger cells and cell colonies/clusters, but have fewer commercially available flow sorters. Notably all sizes are compatible with microscopy imaging, pipettes and liquid handlers. Cell labels in blue identify cells that were demonstrated in this work. Scale = 100 µm.

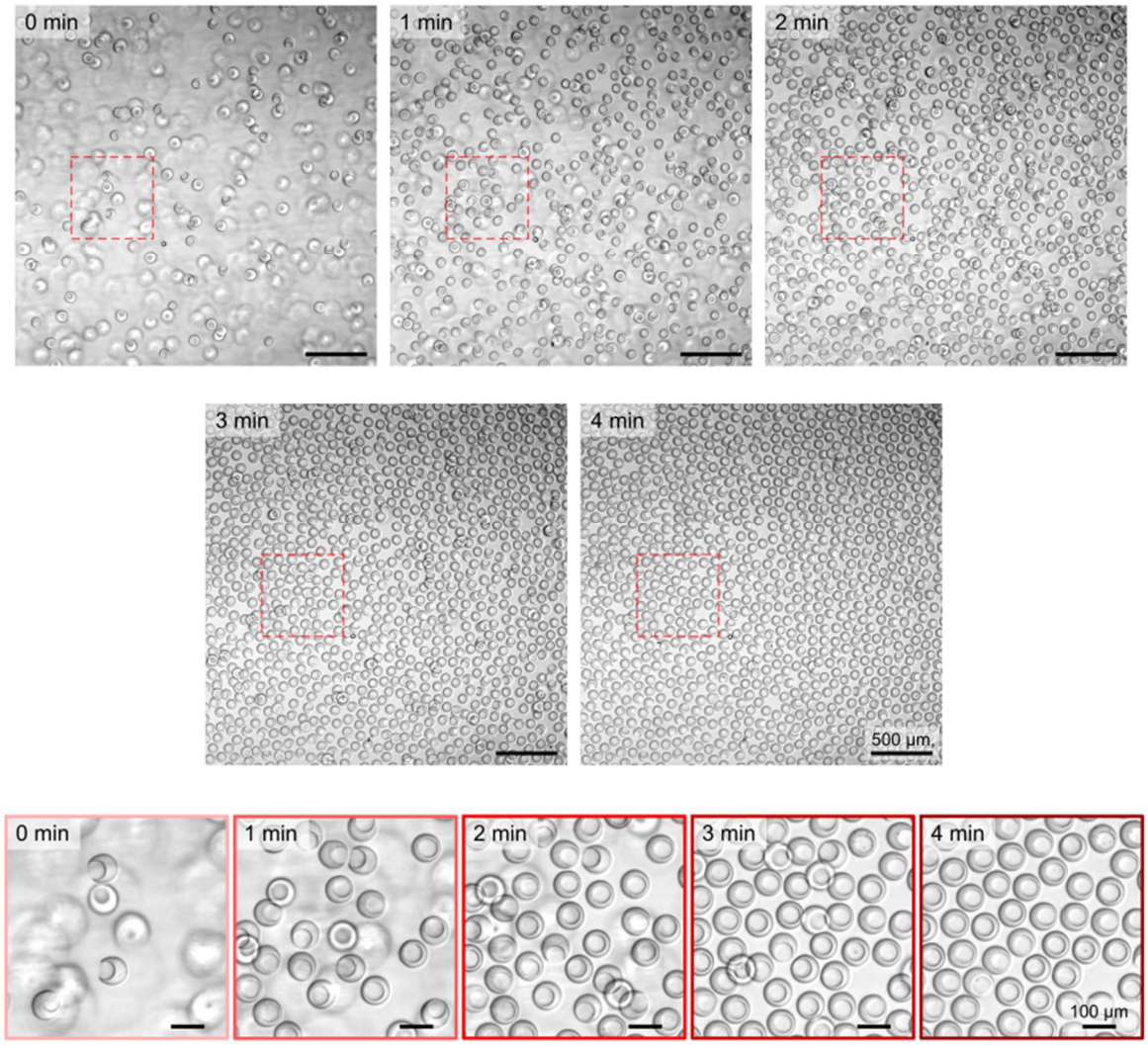

Figure 3-5 Time-lapse images of nanovials seeded into a well plate.

To prepare nanovials for cell seeding they are pipetted into a well plate by dispensing liquid up and down in circular motions. Due to the unique morphology of the nanovials they tend to settle with their cavities oriented upright and displace adjacent nanovials aside to form a monolayer.

Cells are then seeded over the particles and settle with a sizeable fraction coming to rest in the particle cavities (Figure 3-6). It was noted that this seeding approach led to cell occupancies that closely followed Poisson statistics (Figure 3-6D), as is expected for loading of single cells into microfluidically-generated droplets.[31, 32] By controlling the cell seeding density, we can control occupancy such that most particles have either 0 or 1 cells associated with them. Following seeding, cells are bound to the nanovials through a variety of cell-surface interactions, depending on the cell type of interest. Adherent producer cell lines used for the production of mAbs and other biologics can be adhered through cell surface interactions with RGD, a well-known cell-binding motif present in fibronectin. CHO DP12 and HEK293 cells adhered (Figure 3-6B,C) and maintained high levels of single cells within cavities following vigorous wash steps. Suspension-adapted cell lines, like ExpiCHO cells, did not adhere well to RGD alone. However, increased adhesion similar to other cell lines was achieved by modifying particles to also contain poly-L-lysine (PLL) (Figure 3-6B). For other primary suspension cell populations, such as B cells, we found that antibodies against cell surface proteins led to optimum adhesion in nanovial cavities even after vigorous washing and sorting. Antibodies against CD45, CD19 and their combination all yielded high levels of B cell adhesion and maintenance that followed Poisson loading statistics (Figure 3-6C).

3.3.3. Sealing of nanovials using biocompatible oil and surfactants to prevent cross-talk

By exploiting the structure of the nanovials, uniform droplets are formed around the particles via simple pipetting steps with oil and surfactant to seal them and prevent cross-talk between samples (Figure 3-7). An aqueous solution of nanovials is first concentrated in a conical or microcentrifuge tube by centrifuging and aspirating the supernatant.

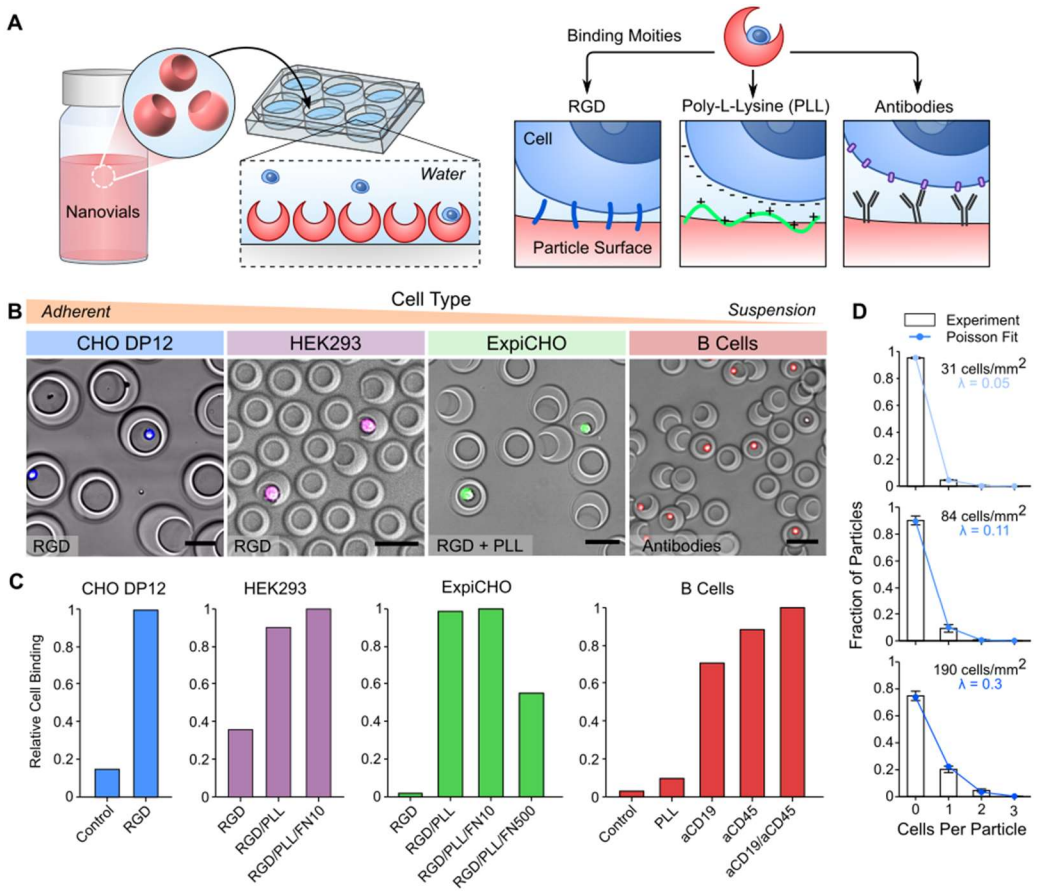

Figure 3-6 Loading and binding of single cells into nanovials.

(A) Particles are loaded into wells and settle with their cavities oriented upright due to their asymmetric center of mass. Cells are then seeded into the open cavities and attaching using various binding moities. Unbound cells are washed away using a reversible cell strainer and recovered particles and associated cells are analyzed. **(B)** Example microscopy images of fluorescently tagged cells bound to nanovials. **(C)** Comparison of cell binding is plotted below for different cell types and binding moieties. Adherent producer cells such as CHO DP12 (Blue) and HEK293 cells (magenta) bound to particle cavities through integrin binding sites (RGD peptide) linked to the particle matrix. Cell retention for suspension adapted ExpiCHO (green) was increased by introduction of positively charged poly-L-lysine (PLL). Inclusion of surface marker specific antibodies on the nanovial surface increased retention of B-Cells (red). **(D)** Loading of cells into nanovial cavities follows Poisson statistics. Error bars represent SD of n = 3 samples for loading distribution.

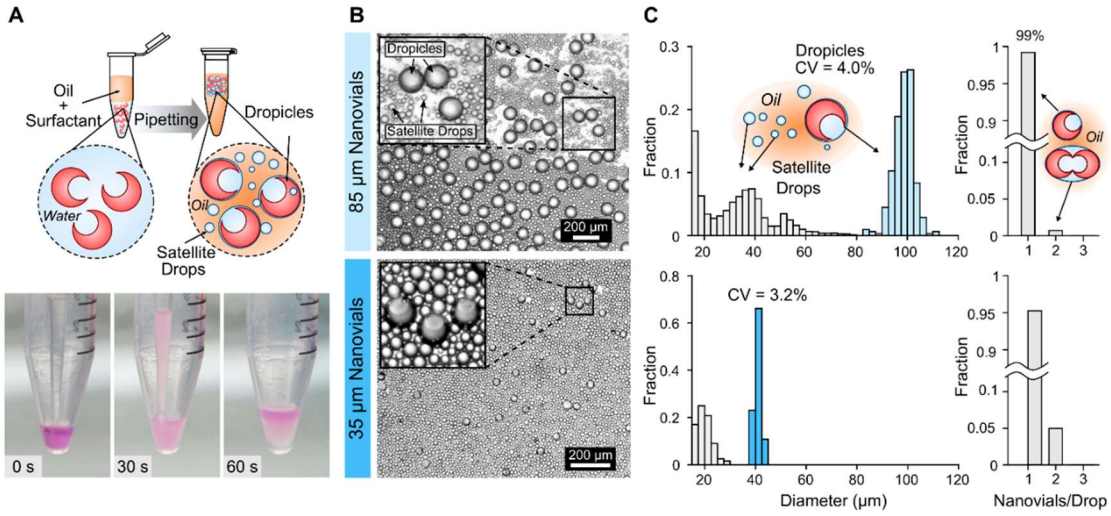

Figure 3-7 Massively parallel device-free formation of uniform droplets.

(A) Biocompatible oil and surfactant are added to a tube containing concentrated particles. The suspension is pipetted vigorously for 1 minute to generate smaller and smaller emulsions. **(B)** Microscopy images of the emulsion shows a uniform population of droplets containing particles and smaller background satellite droplets. **(C)** Histograms of dropicle diameter for different nanovial sizes. Nanovial containing droplets are highly-uniform and comparable to advanced microfluidic techniques (CV<5%). **(D)** For both nanovial sizes nearly all droplets formed have either 0 or 1 particle encapsulated, with only a small fraction (<1%) containing 2 or more particles per droplet. Scale bars, 500 µm.

A layer of biocompatible oil with surfactant is added and the suspension is then pipetted vigorously for 1 min to create smaller and smaller water-in-oil droplets. Eventually the droplet size is maintained by the outer periphery of the microparticle and we find that, in agreement with minimal energy considerations (Figure 3-8),[33] uniform volumes of fluid remain stably trapped within the cavity by the hydrophilic particle. Any excess fluid in the suspension is partitioned into much smaller satellite droplets (Figure 3-7B). The resulting emulsion shows two unique distributions; (1) small non- uniform satellite droplets and (2) monodisperse droplets each templated by single nanovials (Dropicles) (Figure 3-7C). The compartmentalization process was tested over a range of nanovial sizes (35-85 μm diameters). For larger particles it was found that uniform emulsions (CV = 4%) could be formed with minimal aggregates (<1%, Figure 3-7D) from the concentrated nanovials directly.

Spherical gel particles have previously been used to template emulsions,[26, 27] however, the lack of a cavity precluded use with mammalian cells, and no secretion assays or compatibility with flow cytometry were demonstrated. We have also previously used amphiphilic cavity-containing particles to form uniform emulsions and perform molecular and cellular assays,[23-25] however, these previous systems were not compatible with commercial flow cytometers due to their hydrophobic components.

Importantly nanovials can be recovered from the oil while still retaining functional cells. To recover nanovials a biocompatible destabilizing agent is used to coalesce the droplets together. Live/dead analysis of CHO cells following encapsulation and subsequent emulsion breaking shows high viability over a 24-hour period (>80%) indicating that the workflow is biocompatible (Figure 3-9A,B).

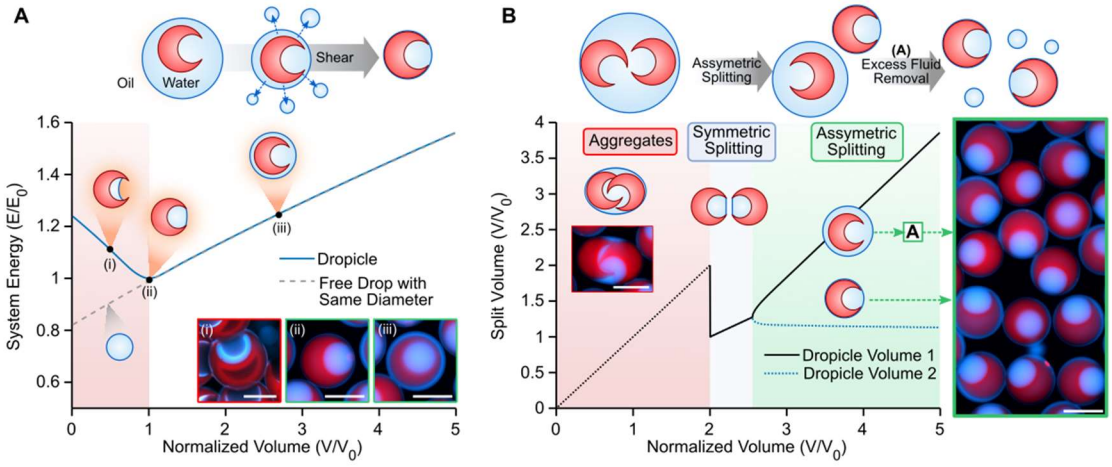

Figure 3-8 Energy minimization theory supports monodisperse dropicle formation.

(A) Simulated volume-energy (V-E) curves show that droplets formed with nanovials (dropicles) have a minimal energy configuration when the size of the droplet surrounding it approaches the size of the nanovial. Here the system energy and volume are normalized by the minimum energy values (E0 and V0, respectively). A free droplet of the same outer diameter follows along the same energy curve until the minimal energy point. As energy is added to the system (e.g. by shearing with a pipette) excess fluid is shed from the nanovial (iii), until the minimal energy volume is reached (ii). Lower volumes could only be achieved by drying out excess fluid via evaporation (i). (B) On the basis of the V-E curve in (A), splitting of a drop containing two nanovials is theoretically expected to depend on the total fluid volume. At volumes below twice V0 nanovials are expected to remain as aggregates. At slightly larger volumes if enough energy is added volume is expected to split evenly based on energy minimalization theory. At larger volumes the fluid is expected to distribute asymmetrically between nanovials; one with a smaller volume approaching V0 and one with the remainder of the fluid. The nanovial with the larger volume may undergo additional volume reduction via shearing until reaching V0.

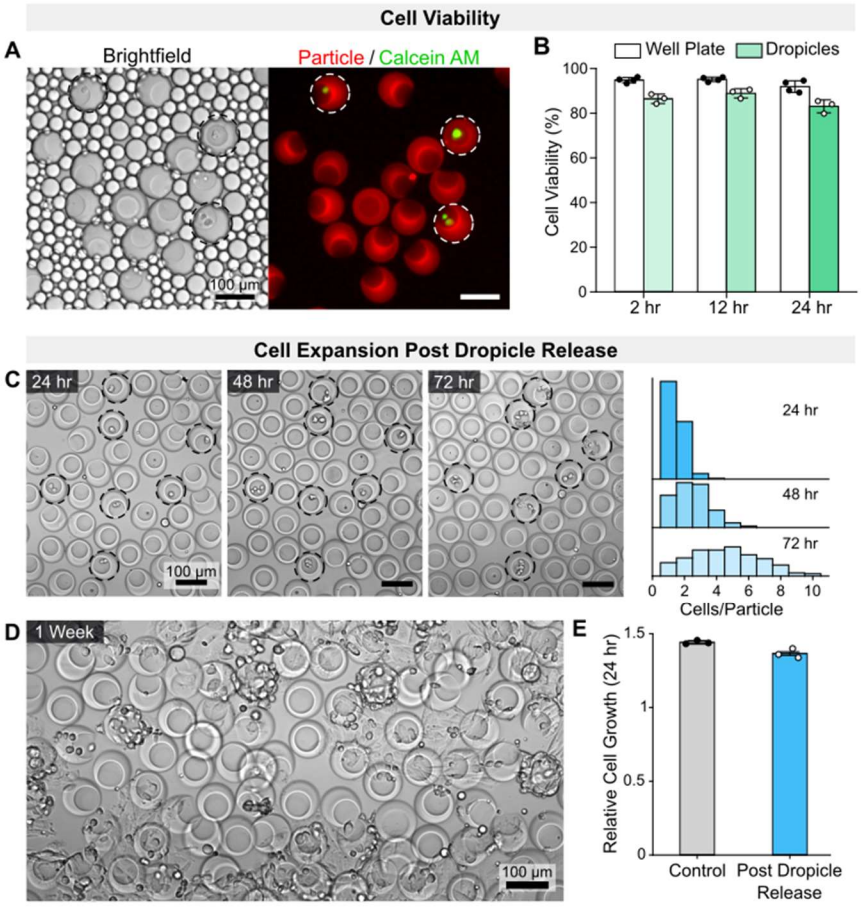

Figure 3-9 Characterization of cell viability and growth after dropicle formation and release. **(A)** Brightfield and fluorescence microscopy image of cells encapsulated in dropicles. Biotinylated drop-carrier particles are stained with Alexa Fluor 568 streptavidin and cells are stained with calcein AM. **(B)** Cells maintained high viability after dropicle formation and release. Viability was assessed by staining with calcein AM and propidium iodide after recovering particles and cells from droplets. Live/dead assay was performed with a minimum of n =3 samples, cell number > 1000 per condition. **(C)** Cells initially remain in the drop-carrier particle cavities after releasing them. Colonies derived from single cells remain in the particle cavities during initial expansion. **(D)** After significant accumulation of cells in the cavities, cells begin to spread to the outside of the cavities and onto the well plate surface. **(E)** Cell growth in drop-carrier particles post dropicle release is comparable to cell growth on standard well plates (control) (n = 3). Growth is characterized by fold change in cell number over a 24 hr period as characterized by counting cell number using CellTracker staining.

Further, we observe similar growth rates from cells expanded after dropicle release in comparison to cells seeded directly into a well plate. (Figure 3-9C,D). After washing and emulsification steps very few cells are found bound to the external region of the nanovials suggesting that the cavity potentially protects cells from shear forces during processing.

3.3.4. Single cell secretion analysis and sorting using nanovials

Using the nanovial platform we demonstrate a device free workflow to perform single-cell secretion assays with minimal crosstalk (Figure 3-10). Given the importance of selecting high antibody titer cell lines for therapeutic production,[34] we chose a Chinese hamster ovary (CHO) cell line that produces human IgG targeting interleukin 8 (IL-8) as our model system. Cells are first loaded into the microparticle cavities and adhere via integrin binding sites as previously described. After initial cell seeding, particles and associated cells are collected and washed to remove background secretions. Particles are then coated with anti-human IgG Fc antibodies by binding to biotin groups linked to the particle matrix. Following this step, the nanovials and associated cells are rapidly compartmentalized in less than 1 minute by pipetting with oil and surfactants. The compartmentalized CHO cells are then incubated, and the secreted antibodies are captured onto the associated particle matrix. After incubation, the emulsions are broken and the nanovials with attached cells and secretions are collected and washed. The nanovials with the associated cells and secretions are then labeled with secondary fluorescent antibodies targeting the secreted anti-IL-8 antibodies. Using fluorescence microscopy, we confirmed retention of cells and associated secretion signal on the particle surface after recovering out of oil into an aqueous phase (Figure 3-1C).

Because of the heterogeneity across cell populations, preventing secretion cross-talk between particles is critical to enabling quantitative analysis and sorting.

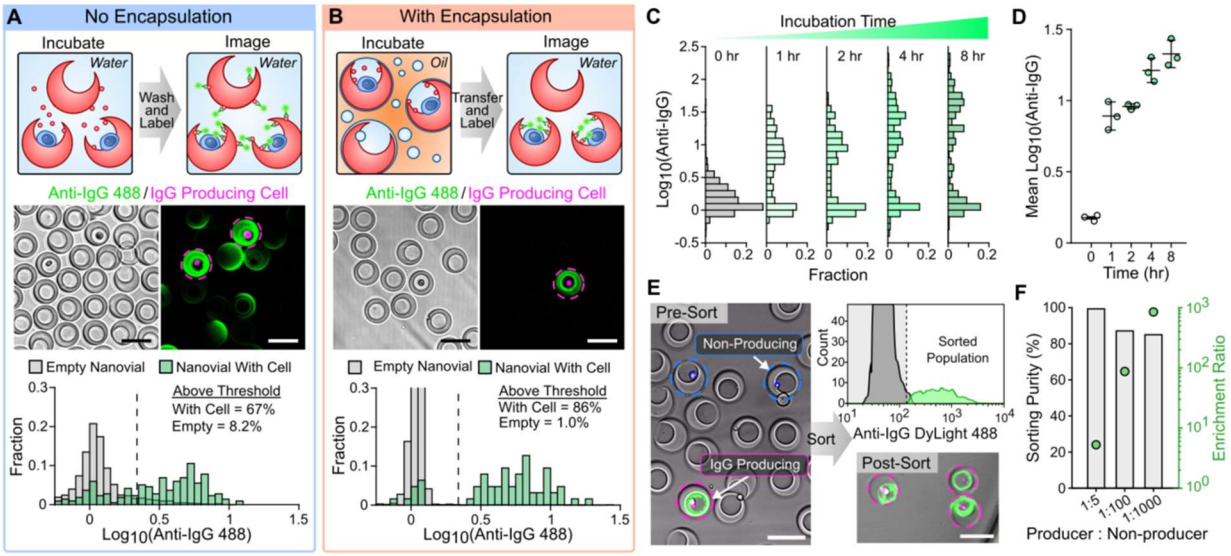

Figure 3-10 Analysis of single cell secretions using dropicles.

(A-B) Characterization of cross-talk when performing a secretion assay with human IgG producing CHO cells with and without an encapsulation step. **(A)** Significant crosstalk is observed when cells and particles are left in an aqueous phase during secretion incubation. **(B)** Minimal cross-talk is observed when cells and associated particles are encapsulated in oil during the secretion incubation step. Thresholds in both **(A)** and **(B)** are set at 3 standard deviations above empty particle signal for the encapsulation condition. **(C)** Measured secretion signal increases with incubation time due to accumulation of more molecules. As the secretion incubation time is increased, the distribution in measured secretions increases as expected. **(D)** Averaged secretion measurements across the producing population shows signal increasing proportionally with time across 3 separate samples. **(E)** A secretion assay was performed on a mixture of human IgG producing CHO cells (magenta) spiked into a non-producing CHO cell population (blue). Samples were sorted based on positive IgG signal using FACS and imaged using fluorescent microscopy to determine purity and enrichment ratio. **(F)** Spiked target cells were successfully isolated across a range of dilutions (1:5 – 1:1000) at purity up to 99% and nearly 1000-fold enrichment. 100,000 single cells were sorted during the enrichment study.

Rapid encapsulation is key to preventing crosstalk of secretions as demonstrated by a side-by-side comparison of the secretion assay with and without the oil encapsulation step (Figure 3-10 A-B). When secretions are captured on particles without the encapsulation step, particles without associated cells show high secretion signals indicating significant crosstalk (8.2% of empty particles have signal above threshold) (Figure 3-10A). Conversely, with the oil encapsulation step there are two visibly distinguishable populations, nanovials with and without secreting cells, and only 1% of nanovials without cells have signal above the cut off threshold (Figure 3-10B). Minimizing the fraction of false positives is particularly critical when secretions can spill over into neighboring nanovials containing non-secreting cells that would contaminate downstream cultures or sequencing assays.

We observe an increase in mean accumulated fluorescence signal on the 85 μm diameter particles that trends, as expected, with increasing incubation time and corresponding antibody production (Figure 3-10C,D). Using fluorescence microscopy, we are able to measure significant signal over background (3 standard deviations) after 1 hour of incubation. Interestingly, we note across all incubation times that there are a sizeable population of cells (~25%) that have no measurable secretion signal (Figure 3-10C). Viability analysis of this population revealed that >50% of these cells were still alive indicating that the lack of signal is likely due to a fraction of the cell population no longer expressing the antibody production gene or secreting the produced antibodies.

To further validate the capability of the system to identify rare subpopulations based on secretions, a FACS enrichment experiment was performed. We performed secretion-based sorting with a mixed population of the anti-IL-8 producing CHO cells and non-producing CHO cells each labeled with a separate Cell Tracker™ dye (Figure 3-10E). After the secretion assay

and prior to sorting, fluorescence imaging of the stained 85 μm diameter particles shows increased signal on particles containing the antibody-secreting cells of interest compared to those containing non-secreting cells (Figure 3-10D). This further demonstrates the lack of cross-talk in our system as well as the specificity of the labels only to the secretions of interest. The particles with associated cells and secretions were then sorted based on the labeled secretion intensity (Figure 3-10d). Downstream analysis shows effective isolation of the sub-population of interest with high-purity (85-99%) (Figure 3-10F) over a range of target cell dilutions. In the most dilute case (1:1000) an enrichment ratio of 850X was achieved indicating the capability to isolate rare target cell events. Cells isolated using this approach can be expanded directly from the particle matrix enabling a streamlined workflow with minimization of trypsinization steps (Figure 3-9C,D).

3.3.5. Viable enrichment of high-titer subpopulations using FACS

Sorted cells maintain the ability to produce antibodies at levels correlating with the mean intensity of initial secreted signal. In a separate set of experiments with 85 μm nanovials, we performed a secretion assay on human anti-IL8 producing CHO cells and selected out sub-populations based on level of secretion signal using FACS (Figure 3-11). Cells secreting antibodies were sorted in high-throughput (>200 events/s) by gating off both the fluorescently labeled secretion channel as well as CellTracker™ dye (Figure 3-11A, Figure 3-12). For each separate passage of cells analyzed (n = 4) we sorted two sub-populations: (1) all particles with cells and detectable secretion signal above background and (2) particles with cells and the top 20% of antibody secretion signal. Microscopy images of the sorted nanovials and associated cells show successful isolation of secreting cells with signal proportional to their respective FACS gating (Figure 3-11B).

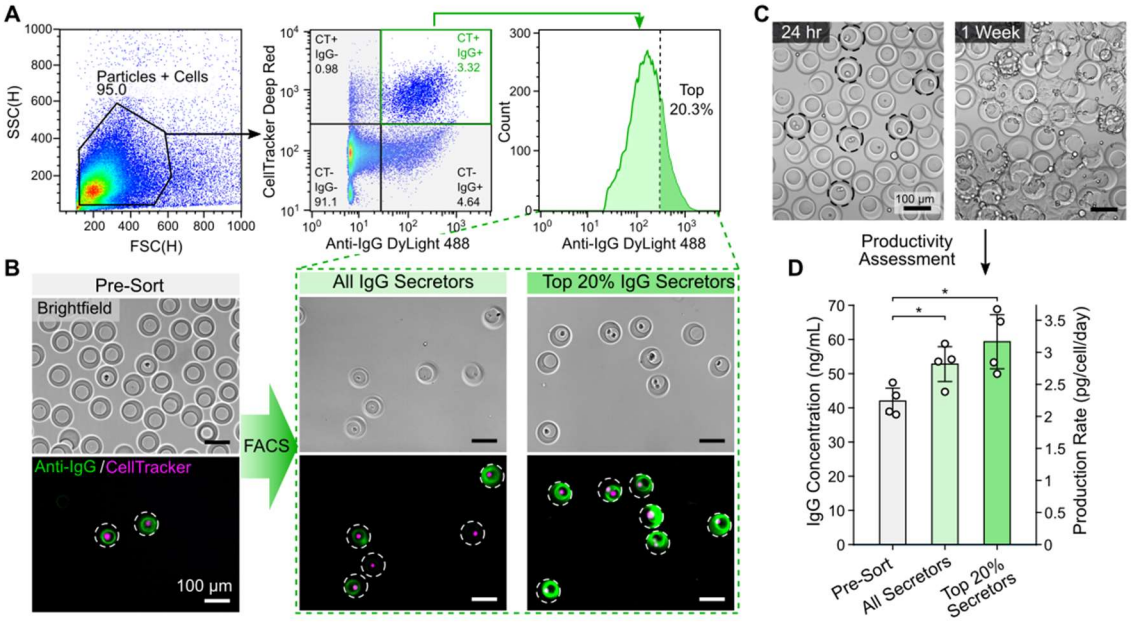

Figure 3-11 Selection of high secreting cell sub-populations using FACS.

(A) The secreting population of cells were gated and sorted based on IgG secretion signal and CellTracker (CT) labelling. Both cells with any secretion signal disparate from background as well as the top 20% of secretors were separately sorted. **(B)** Microscopy images before and after sorting show enrichment of secreting cells with fluorescence intensity proportional to the selection criteria. **(C)** Example images of cells expanded out of nanovials after encapsulation and release. **(D)** After expanding isolated cells for 10 days, bulk ELISA was performed to determine the production rate for the different sub-populations. Full experiment was performed with separate cell passages (n = 4). Error bars represent s.d.

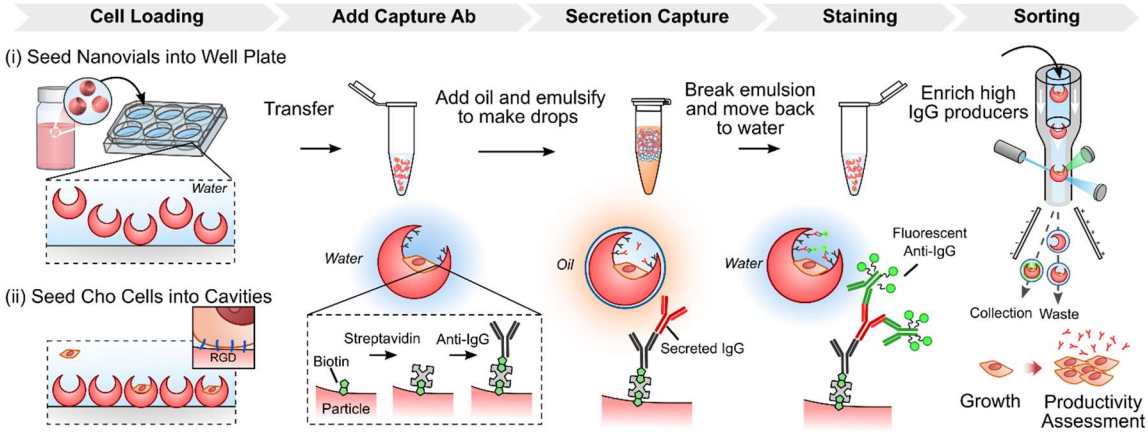

Figure 3-12 Detailed overview of high IgG producer enrichment workflow.

RGD coated nanovials are first seeded into a well plate and settle with cavities exposed upright. CHO cells are then seeded into the exposed cavities and incubated to allow attachment via integrin binding. Nanovials and attached cells are recovered by pipetting and transferred into a centrifuge or conical tube. Nanovials are then modified sequentially with streptavidin and biotinylated anti-IgG antibodies. The nanovials are then emulsified to prevent crosstalk and incubated in a CO2 incubator and accumulated secreted antibodies from cells. Nanovials, cells, and associated secretions are transferred back into water phase, labeled with fluorescent secondaries and analyzed with flow to measure amount of secreted product. The higher producing cells, as measured by fluorescence are sorted out and expanded in a well plate for downstream productivity assessment. The full secretion assay workflow is completed in a single day and cells are expanded for a week after enrichment for downstream assessment via bulk well plate ELISA.

The sorted sub-populations were seeded into a 96-well plate and expanded out of the particles over the course of ~10 days (Figure 3-11C). Samples were then plated at the same cell density and bulk antibody production of the different subpopulations was measured by ELISA and compared with non-sorted control samples. We observed a 26% increase in total IgG production for the sorted sub-population 1 (all secreting cells) in comparison to the pre-sort control population (Figure 3-11D). This increase is most likely due to the removal of cells that are no longer secreting IgG following the sort, which was measured to be ~25% based on microscopy analysis (Figure 3-10C) as well as flow analysis (Figure 3-11A). For sorted sub-population 2 (the top 20% of secretors) we measured an average increase of 41% in total IgG production (n =4) with a maximum increase among the samples of 58% (Figure 3-11D), indicating the capability of the platform to select out functionally higher producing sub-populations that maintain the phenotype for at least 10 days.

3.3.6. Isolation of Antigen Specific IgG Secreting Cells

In a final application, we tested the feasibility of using our nanovial platform to screen and isolate antigen-specific antibody producing cell clones out of a background of similar, non-specific, antibody producers (Figure 3-13). Rather than selecting simply for high secretion rates, this type of assay replicates strategies taken for antibody discovery using our nanovial secretion screen. HyHel-5 hybridoma cells secreting anti-hen egg lysozyme (anti-HEL) antibodies (IgG1) were used as our target cell population and were diluted into a background of similar, CellTracker^{TM} Blue (CTB) labeled, 9E10 hybridoma cells producing anti-myc antibodies (IgG1).

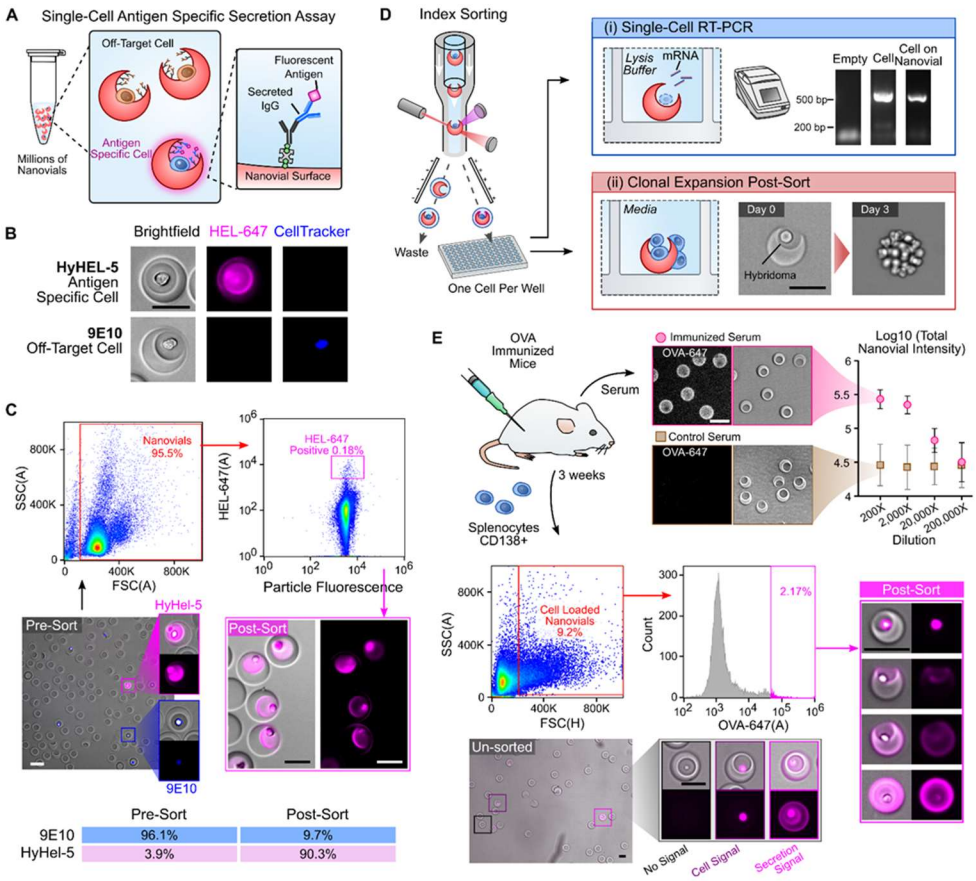

Figure 3-13 Detection and sorting of antigen-specific antibody secreting cells.

(A) Hybridomas or B cells loaded into nanovials secrete antibodies which are captured via biotinylated antibodies and subsequently labeled with fluorescent antigen to assess specificity of the secreted IgG. (B) Fluorescence microscopy images reveal specific signal from binding to AlexaFluor™ 647 conjugated hen egg lysozyme (HEL-647) on nanovials containing a hybridoma line (HyHEL-5) secreting IgG HEL while a cell line (9E10) secreting an off-target IgG results in no signal. (C) HyHel-5 hybridomas spiked into 9E10 hybridomas (CellTracker™ Blue) were assayed by fluorescence microscopy for HEL-specific signal before and after FACS sorting. (D) Sorted single hybridomas loaded onto nanovials can be (i) reverse transcribed and amplified from single cells loaded on nanovials, (ii) or expanded into a clonal colony directly from the nanovials following sorting. (E) Antibody-secreting B cells from OVA-immunized mice are assayed for antigen specificity using nanovials. OVA-specific signal is observed directly on the nanovials by fluorescence microscopy down to 20,000X dilution of serum from OVA-immunized mice but not control mice. Splenocytes loaded on nanovials were observed to have both cell surface signal and OVA-specific signal by fluorescence microscopy. Following FACS sorting, OVA-specific antibody-secreting cells were successfully imaged possessing minimal cell surface staining with OVA, along with some cells staining strongly but possessing no OVA-specific secreted antibody signal.

Mixed populations of HyHel-5 and 9E10 hybridoma cells were loaded and bound to nanovials using anti-CD45 cell capture antibodies as described previously, and all antibodies secreted from both cell types were captured non-specifically onto the nanovial surfaces using biotinylated secretion capture antibodies targeting mouse IgG heavy and light chains (Figure 3-13A). Following incubation to capture secreted IgG, we labeled particles with fluorescently conjugated HEL antigen (HEL-647), revealing the presence of only the antigen-specific antibody secretions (Figure 3-13A). When assaying mixed hybridoma populations, this assay format yielded strong and specific signal with over 80% of nanovials containing HyHel-5 hybridoma cells staining positively for antigen specific secretion after one hour, while no detectable signal was present on nanovials containing 9E10 cells (Figure 3-13B). The top 0.18% of the nanovial population was sorted based off of their high HEL fluorescence area.

Subsequent microscopic analysis confirmed highly enriched populations of strongly labeled HEL-647+/CTB- cell-loaded nanovials in the post-sort population (>90% purity), confirming that the entire analysis and sorting workflow was compatible with antigen-specific antibody detection produced by suspension cell types (Figure 3-13C). In addition to bulk recovery of enriched cell samples producing antigen-specific antibodies, we recovered single hybridoma-loaded nanovials directly into individual wells of a 96-well plate for downstream sequence recovery and re-growth (Figure 3-13D). We were able to lyse individual cells loaded on nanovials that were deposited into wells and amplify antibody sequence information through standard single-cell RT-PCR (Figure 3-13D), indicating that nanovial materials do not interfere with the RT-PCR chemistry. We were also able to sort single hybridoma clones loaded on nanovials into individual wells, culture and expand them into clonal sub-populations (Figure 3-13D).

The antigen binding assay was also extended to a second antigen and to primary B cells from ovalbumin (OVA) immunized mice. We first confirmed that OVA immunized mice produced IgG that were OVA-specific by incubating nanovials in serum from either immunized or control mice. Anti-IgG coated particles incubated in serum of immunized mice and exposed to fluorescent OVA yielded differentiable fluorescence signal down to a 20,000X serum dilution, whereas no detectable signal was generated from control serum at any concentration (Figure 3-13E). We then loaded and sorted ovalbumin (OVA)-specific antibody-secreting CD138+ splenocytes (Figure 3-13E).

A subset of the analyzed and sorted cells were associated with strong OVA-specific signal on the nanovials reflecting secreted antibodies but little to no surface stain (Figure 3-13E), suggesting we isolated plasma B cells which lack high levels of the B cell receptor (BCR) expressed on the cell surface. Another subset of the CD138+ splenocytes acquired strong surface fluorescence after exposure to fluorescent antigen but did not secrete detectable levels onto the nanovial surface, suggesting direct binding to BCRs, or non-specific binding to membrane compromised cells. A third population of cells had both surface BCR staining and staining on the nanovial surfaces reflecting secreted antibodies. The top ~2% of nanovials with the highest OVA staining were sorted by FACS and visualized, yielding the same mixture of cell types that likely reflects the ability to isolate a larger repertoire of B cell populations, including plasma B cells difficult to isolate with standard antigen baiting workflows.

3.4. Discussion

The dropicle platform provides specific advantages in sorting cells based on secretions, but also lays the foundation for the next generation of microfluidic assays on single cells and molecules without new instruments. We show that two key features of the dropicle platform

allow for widely accessible analysis and sorting of cells based on secretions: (i) the ability to form uniform compartments containing single cells in small volumes with minimal crosstalk using simple pipetting and no devices, and (ii) the compatibility of the nanovials with commercially available flow sorters such that viable cells can be sorted based on their associated secretions. Nanovials allow for seeding of cells into their open cavities and emulsification to form hundreds of thousands to millions of dropicles all in parallel using simple pipetting operations. Parallel encapsulation in < 1 min is an important differentiator from microfluidic techniques which often require tens of minutes to several hours to sequentially form droplets while cells remain mixed and secreting in the input sample volume.[35] Rapid emulsification minimizes cross-talk from cells secreting into the mixed input sample volume during the time over which secreting cells are encapsulated which is critical for enabling screening of large cell populations. Dropicle emulsification and analysis steps can also be more easily performed in a sterile environment (e.g. biosafety hood) using standard sterile plasticware (e.g. well plates, pipette tips), as opposed to bulkier equipment. Although microfluidics is used to manufacture the nanovials, the particles can be easily produced in batch (>10 million drop-carrier particles per batch, Figure 3-1) and provided to other labs who do not have expertise in microfluidics. Shipping of particles is significantly more cost-effective and rapid than replicating microfluidic setups for generation and sorting of droplets. Further, the amount of additional expertise required to use the nanovial system is substantially lower than microfluidic based approaches due to the familiar handling steps. Collaborators across the globe have been able to perform nanovial assays without any hands-on training.

The nanovial system is also compatible with commercial flow cytometers enabling screening across the experiments described in this report at rates of >1000 events/second. This

throughput is comparable to state-of-the-art microfluidic approaches and by further optimizing the loading of cells into the particles as well using higher-throughput FACS machines this throughput could exceed 10 million cells per day. Besides increasing availability to labs without expertise in microfluidics or specialized commercial instruments, there are some unique advantages of this new approach for encapsulation of mammalian cells.

The structure and surface of the drop-carrier particles provide unique capabilities for tuning the number and type of captured cells, analysis of adherent cell secretions, and analysis and sorting of clonal colonies. The size and opening diameter of the cavity within a drop-carrier particle can be tuned (Figure 3-3), potentially enabling deterministic loading of single cells based on size exclusion effects. This could enable more rapid screening because cell loading rates may not be limited by Poisson statistics. Besides structural changes to the particles, the surface of particles can also be functionalized with affinity agents that specifically enrich certain populations of cells, such as antibodies to CD3 that enrich T cells from a mixed population. The surface of the particle also enables the attachment and growth of adherent cell populations, such as the CHO cells used herein. Analysis of secretions from adherent cells can be challenging with other microfluidic techniques which require cells to be in suspension to flow into devices and sort afterwards. Adherent cells begin to undergo apoptosis when remaining in suspension and it is expected that secretion rates of biomolecules would change in this condition.[36] The inability to perform these assays has led to a dearth of information on the secretion phenotypes and heterogeneity of adherent cells with important secretion products in health and disease, such as mesenchymal stem cells, glandular epithelial cells, endothelial cells, glial cells, and even adherent bacterial biofilms. Further, in the dropicle system, when single cells are initially seeded onto particles they adhere and grow without nutrient limitations. The clonal colonies can then be

encapsulated to form dropicles, enabling high-throughput screening based on the combination of growth and per cell secretion (i.e. overall biomass produced per unit time), potentially overcoming previous challenges in cell line selection in which growth and biologic production can be in a trade-off relation.[12]

Sorting based on secretions extends beyond selection of high antibody-titer cell lines to many applications of importance in life sciences and biotechnology. Discovering high affinity mAb therapeutics relies on the selection of B and plasma cells producing antibodies with high affinity amongst a large background.[6] The activity of immune cells is largely connected to their secretion profiles, which direct communication and effector functions and can be better studied by sorting out specific sub-populations for further functional testing in vivo or in vitro. The effectiveness of chimeric antigen receptor-T cell batches also appears to depend on a multifunctional secretion of cytokines, such that sorting populations based on secretion profiles may enhance therapeutic activity.[37, 38] Finally, processes of directed evolution of cell products and cells themselves can benefit from larger numbers of clones being screened, mutagenized, and expanded across multiple cycles using an efficient process relying on standard equipment and expertise.[39]

More broadly, our new approach to encapsulate single entities into uniform compartments with a solid phase can enable a centralized “lab on a particle” platform for a number of single-cell and single-molecule assays. Encapsulation is a key component for single-cell nucleic acid sequencing. Clonal colonies of bacteria, yeast, or algae producing engineered proteins (e.g. fluorescent proteins) can also be maintained in dropicles and sorted based on desirable features (e.g. intensity at particular excitation/emission wavelengths). Moving beyond cells, the compartments formed can enable digital nucleic acid amplification assays and

immunoassays, where the solid phase provides potential for barcoding and capturing of amplified assay signals. Given the ability to rapidly deploy our approach with established lab infrastructure we anticipate widespread applications of lab on a particle technology across a range of these single cell and single molecule assays in the near future. Rapid deployment across the world is of particular importance during emerging pandemics, enabling collective distributed research and development, and removing the bottlenecks of only a few skilled groups being able to contribute to key points in therapeutic and diagnostic pipelines.

3.5. References

[1] T. Tiller, E. Meffre, S. Yurasov, M. Tsuiji, M.C. Nussenzweig, H. Wardemann, Efficient generation of monoclonal antibodies from single human B cells by single cell RT-PCR and expression vector cloning, J Immunol Methods, 329 (2008) 112-124.

[2] T. Tiller, C.E. Busse, H. Wardemann, Cloning and expression of murine Ig genes from single B cells, J Immunol Methods, 350 (2009) 183-193.

[3] B. DeKosky, High-Throughput Sequencing of the Paired Human Immunoglobulin Heavy and Light Chain Repertoire, Springer Theses-Reco, (2017) 21-28.

[4] B.J. DeKosky, T. Kojima, A. Rodin, W. Charab, G.C. Ippolito, A.D. Ellington, G. Georgiou, In-depth determination and analysis of the human paired heavy- and light-chain antibody repertoire, Nat Med, 21 (2015) 86-91.

[5] J.R. McDaniel, B.J. DeKosky, H. Tanno, A.D. Ellington, G. Georgiou, Ultra-high-throughput sequencing of the immune receptor repertoire from millions of lymphocytes, Nat Protoc, 11 (2016) 429-442.

[6] C. Parola, D. Neumeier, S.T. Reddy, Integrating high-throughput screening and sequencing for monoclonal antibody discovery and engineering, Immunology, 153 (2018) 31-41.

[7] F.M. Wurm, Production of recombinant protein therapeutics in cultivated mammalian cells, Nature Biotechnology, 22 (2004) 1393-1398.

[8] B. Sander, J. Andersson, U. Andersson, Assessment of Cytokines by Immunofluorescence and the Paraformaldehyde-Saponin Procedure, Immunol Rev, 119 (1991) 65-93.

[9] G. Freer, L. Rindi, Intracellular cytokine detection by fluorescence-activated flow cytometry: Basic principles and recent advances, Methods, 61 (2013) 30-38.

[10] R. Manz, M. Assenmacher, E. Pflüger, S. Miltenyi, A. Radbruch, Analysis and sorting of live cells according to secreted molecules, relocated to a cell-surface affinity matrix, P Natl Acad Sci USA, 92 (1995) 1921-1925.

[11] M. Assenmacher, A. Scheffold, A. Radbruch, Cytometric cytokine secretion assay: Detection and isolation of cytokine-secreting T cells, Method Microbiol, 32 (2002) 59-75.

[12] N. Borth, M. Zeyda, H. Katinger, Efficient selection of high-producing subclones during gene amplification of recombinant Chinese hamster ovary cells by flow cytometry and cell sorting, Biotechnol Bioeng, 71 (2000) 266-273.

[13] Z. Chen, J.J. Chen, R. Fan, Single-Cell Protein Secretion Detection and Profiling, Annu Rev Anal Chem, 12 (2019) 431-449.

[14] L. Mazutis, J. Gilbert, W.L. Ung, D.A. Weitz, A.D. Griffiths, J.A. Heyman, Single-cell analysis and sorting using droplet-based microfluidics, Nat Protoc, 8 (2013) 870-891.

[15] K. Ahn, C. Kerbage, T.P. Hunt, R.M. Westervelt, D.R. Link, D.A. Weitz, Dielectrophoretic manipulation of drops for high-speed microfluidic sorting devices, Appl Phys Lett, 88 (2006) 1-3.

[16] J.C. Baret, O.J. Miller, V. Taly, M. Ryckelynck, A. El-Harrak, L. Frenz, C. Rick, M.L. Samuels, J.B. Hutchison, J.J. Agresti, D.R. Link, D.A. Weitz, A.D. Griffiths, Fluorescence-activated droplet sorting (FADS): Efficient microfluidic cell sorting based on enzymatic activity, Lab on a Chip, 9 (2009) 1850-1858.

[17] M. Li, M. van Zee, C.T. Riche, B. Tofig, S.D. Gallaher, S.S. Merchant, R. Damoiseaux, K. Goda, D. Di Carlo, A Gelatin Microdroplet Platform for High-Throughput Sorting of Hyperproducing Single-Cell-Derived Microalgal Clones, Small, 14 (2018).

[18] J.C. Love, J.L. Ronan, G.M. Grotenbreg, A.G. Van Der Veen, H.L. Ploegh, A microengraving method for rapid selection of single cells producing antigen-specific antibodies, Nature Biotechnology, 24 (2006) 703-707.

[19] S. Park, J. Han, W. Kim, G.M. Lee, H.S. Kim, Rapid selection of single cells with high antibody production rates by microwell array, J Biotechnol, 156 (2011) 197-202.

[20] K. Le, C. Tan, S. Gupta, T. Guhan, H. Barkhordarian, J. Lull, J. Stevens, T. Munro, A novel mammalian cell line development platform utilizing nanofluidics and optoelectro positioning technology, Biotechnology Progress, 34 (2018) 1438-1446.

[21] A. Winters, K. McFadden, J. Bergen, J. Landas, K.A. Berry, A. Gonzalez, H. Salimi-Moosavi, C.M. Murawsky, P. Tagari, C.T. King, Rapid single B cell antibody discovery using nanopens and structured light, mAbs, 11 (2019) 1025-1035.

[22] D. Josephides, S. Davoli, W. Whitley, R. Ruis, R. Salter, S. Gokkaya, M. Vallet, D. Matthews, G. Benazzi, E. Shvets, F. Gesellchen, D. Geere, X. Liu, X. Li, B. Mackworth, W. Young, Z. Owen, C. Smith, D. Starkie, J. White, B. Sweeney, M. Hinchliffe, S. Tickle, D.J. Lightwood, M. Rehak, F.F. Craig, D. Holmes, Cyto-Mine: An Integrated, Picodroplet System for High-Throughput Single-Cell Analysis, Sorting, Dispensing, and Monoclonality Assurance, Slas Technol, 25 (2020) 177-189.

[23] G. Destgeer, M.X. Ouyang, C.Y. Wu, D. Di Carlo, Fabrication of 3D concentric amphiphilic microparticles to form uniform nanoliter reaction volumes for amplified affinity assays, Lab on a Chip, 20 (2020) 3503-3514.

[24] C.Y. Wu, M.X. Ouyang, B. Wang, J. de Rutte, A. Joo, M. Jacobs, K. Ha, A.L. Bertozzi, D. Di Carlo, Monodisperse drops templated by 3D-structured microparticles, Sci Adv, 6 (2020).

[25] G. Destgeer, M.X. Ouyang, D. Di Carlo, Engineering Design of Concentric Amphiphilic Microparticles for Spontaneous Formation of Picoliter to Nanoliter Droplet Volumes, Anal Chem, 93 (2021) 2317-2326.

[26] R. Novak, Y. Zeng, J. Shuga, G. Venugopalan, D.A. Fletcher, M.T. Smith, R.A. Mathies, Single-Cell Multiplex Gene Detection and Sequencing with Microfluidically Generated Agarose Emulsions, Angew Chem Int Edit, 50 (2011) 390-395.

[27] M.N. Hatori, S.C. Kim, A.R. Abate, Particle-Templated Emulsification for Microfluidics-Free Digital Biology, Anal Chem, 90 (2018) 9813-9820.

[28] S.H. Ma, J. Thiele, X. Liu, Y.P. Bai, C. Abell, W.T.S. Huck, Fabrication of Microgel Particles with Complex Shape via Selective Polymerization of Aqueous Two-Phase Systems, Small, 8 (2012) 2356-2360.

[29] B.D. Fairbanks, M.P. Schwartz, A.E. Halevi, C.R. Nuttelman, C.N. Bowman, K.S. Anseth, A Versatile Synthetic Extracellular Matrix Mimic via Thiol-Norbornene Photopolymerization, Adv Mater, 21 (2009) 5005-+.

[30] Q. Liu, M. Zhao, S. Mytnyk, B. Klemm, K. Zhang, Y.M. Wang, D.D. Yan, E. Mendes, J.H. van Esch, Self-Orienting Hydrogel Micro-Buckets as Novel Cell Carriers, Angew Chem Int Edit, 58 (2019) 547-551.

[31] D.J. Collins, A. Neild, A. deMello, A.Q. Liu, Y. Ai, The Poisson distribution and beyond: methods for microfluidic droplet production and single cell encapsulation, Lab on a Chip, 15 (2015) 3439-3459.

[32] A.S. Basu, Digital Assays Part II: Digital Protein and Cell Assays, Slas Technol, 22 (2017) 387-405.

[33] K. Ha, J. de Rutte, D. Di Carlo, A. Bertozzi, Minimal surface configurations for axisymmetric microparticles, Prep.

[34] J.K. Hong, M. Lakshmanan, C. Goudar, D.Y. Lee, Towards next generation CHO cell line development and engineering by systems approaches, Curr Opin Chem Eng, 22 (2018) 1-10.

[35] K. Eyer, R.C. Doineau, C.E. Castrillon, L. Briseño-Roa, V. Menrath, G. Mottet, P. England, A. Godina, E. Brient-Litzler, C. Nizak, Single-cell deep phenotyping of IgG-secreting cells for high-resolution immune monitoring, Nature biotechnology, 35 (2017) 977.

[36] X.L. Zhong, F.J. Rescorla, Cell surface adhesion molecules and adhesion-initiated signaling: Understanding of anoikis resistance mechanisms and therapeutic opportunities, Cell Signal, 24 (2012) 393-401.

[37] J.A. Fraietta, S.F. Lacey, E.J. Orlando, I. Pruteanu-Malinici, M. Gohil, S. Lundh, A.C. Boesteanu, Y. Wang, R.S. O'Connor, W.T. Hwang, E. Pequignot, D.E. Ambrose, C.F. Zhang, N. Wilcox, F. Bedoya, C. Dorfmeier, F. Chen, L.F. Tian, H. Parakandi, M. Gupta, R.M. Young, F.B. Johnson, I. Kulikovskaya, L. Liu, J. Xu, S.H. Kassim, M.M. Davis, B.L. Levine, N.V. Frey, D.L. Siegel, A.C. Huang, E.J. Wherry, H. Bitter, J.L. Brogdon, D.L. Porter, C.H. June, J.J.

Melenhorst, Determinants of response and resistance to CD19 chimeric antigen receptor (CAR) T cell therapy of chronic lymphocytic leukemia, Nat Med, 24 (2018) 563-+.

[38] J. Rossi, P. Paczkowski, Y.W. Shen, K. Morse, B. Flynn, A. Kaiser, C. Ng, K. Gallatin, T. Cain, R. Fan, S. Mackay, J.R. Heath, S.A. Rosenberg, J.N. Kochenderfer, J. Zhou, A. Bot, Preinfusion polyfunctional anti-CD19 chimeric antigen receptor T cells are associated with clinical outcomes in NHL, Blood, 132 (2018) 804-814.

[39] D. Di Carlo, Technologies for the Directed Evolution of Cell Therapies, Slas Technol, 24 (2019) 359-372.

Chapter 4. Assessment of dropicle compatibility across commercially available flow cytometers

4.1. Introduction

The ability to precisely manipulate and partition individual cells within miniaturized fluid volumes has expanded biological discovery to encompass the heterogeneity across cell populations[1-3]. Traditional workflows focused on measuring bulk properties of interest from populations of cells have given way to novel microfluidic technologies enabling the parallelized assessment of these same features from each cell in a population simultaneously. Cursory insights gleaned from population averages are now being refined with a tremendous amount of single cell multi-omics data, fostering nuanced understandings of phenotypic heterogeneity and population dynamics[4]. Early-stage adoption of these novel single cell functional screens have already proved critical across all stages of modern drug development, from antibody discovery[5-7] to cell line development[8, 9]. Unfortunately, even with the technical progress that has been achieved, single-cell screening capabilities are often limited in scale and restricted to researchers who have the capability to implement complex microfluidic tools or have access to a few high-priced commercial platforms.

Researchers have developed techniques to address some of the challenges related to access and throughput by leveraging common flow cytometers for downstream analysis and sorting, instead of specialized instruments. For example, hybrid techniques using microfluidics to encapsulate cells within hydrogel particles[10-14], double emulsions[15-17], or hollow particle shells[18] have been developed to create small single-cell containers that can be analyzed and sorted with standard fluorescent activated cell sorters (FACS). Still, widespread adoption of

these approaches is limited due to the significant expertise and specialized equipment required for the upstream formation of compartments using microfluidic devices, and limited capability to perform standard laboratory operations such as washing and reagent exchange once compartments have been formed. Further, the serial nature of forming compartments with these approaches limit potential throughput of the systems.

Similarly, continued miniaturization of standard micro-titer plates, have significantly enhanced our ability to screen individual cells in parallel. However, the advantages gained from enabling direct scale down of common assay protocols utilized in more highly parallelized micro-titer plate formats are offset by the need to use liquid handlers and other automated robotics to accurately interface with the miniaturized well designs, significantly increasing assay costs and limiting throughputs. Additionally, there is a fundamental limit on the volume of these compartments as interfacial tension effects dominate at lower scales making it difficult to accurately perform liquid handling operations. To unlock the potential of single cell screening workflows, new technologies that extend compartmentalization to single-cell compatible volumes must be designed and standardized to work fully with existing infrastructure and common laboratory operations.

Recently our group has reported on novel “lab on a particle” technologies that enable users to perform the same fundamental operations as in microtiter plates, but at orders of magnitude higher throughputs and at volumes on the scale of individual cells.[19-21] These particle based platforms are unique in that they can be manufactured at scale in centralized locations and distributed to end users to perform assays utilizing existing lab infrastructure. We first applied the platform for screening and sorting individual cells based on their secreted products in high-throughput.[21] Our hydrogel nanovial technology acts as suspendable sub-

nanoliter containers that can be functionalized with chemical moieties to promote cell binding and growth (Figure 4-1). Fluids are easily exchanged around the nanovials by simple pipetting and centrifugation steps enabling exposure to different chemical stimuli or staining reagents. The cavity of the nanovials can be sealed in parallel through emulsification with biocompatible oils preventing molecular crosstalk between compartments. Like a well-plate bottom, the hydrogel surfaces of nanovials can act as a substrate for performing biomolecular assays such as sandwich immuno-assays. Importantly, the emulsification process is reversible allowing for viable recovery of cells, staining, and analysis or sorting using FACS.

Because traditional FACS systems were designed to analyze and sort lymphocytes, and our nanovials are larger and possess a unique morphology when compared to typical mammalian cells, it is important to identify the operational parameters that yield the best performance with nanovials across a range of FACS instruments. In this work we perform a comprehensive characterization of the conditions suitable to analyze and sort nanovials with three different commercial FACS instruments.

In particular, we characterized (1) the limit of detection (LOD) and dynamic range for measuring fluorescent protein binding to nanovials, (2) the sorting settings that led to optimal purity and efficiency, and (3) the ability to enrich cell-containing nanovials using scatter signals. To understand the limit of detection and dynamic range of affinity assays on nanovials we performed a dilution sweep using fluorescent streptavidin with biotinylated nanovials and compared with microscopy measurements. Using FACS we found that nanovials could bind ~10^8 fluorescent molecules and had detectable concentrations down to ~10^4 molecules, an order of magnitude improved over fluorescence microscopy measurements with a cooled, low dark noise, CMOS camera.

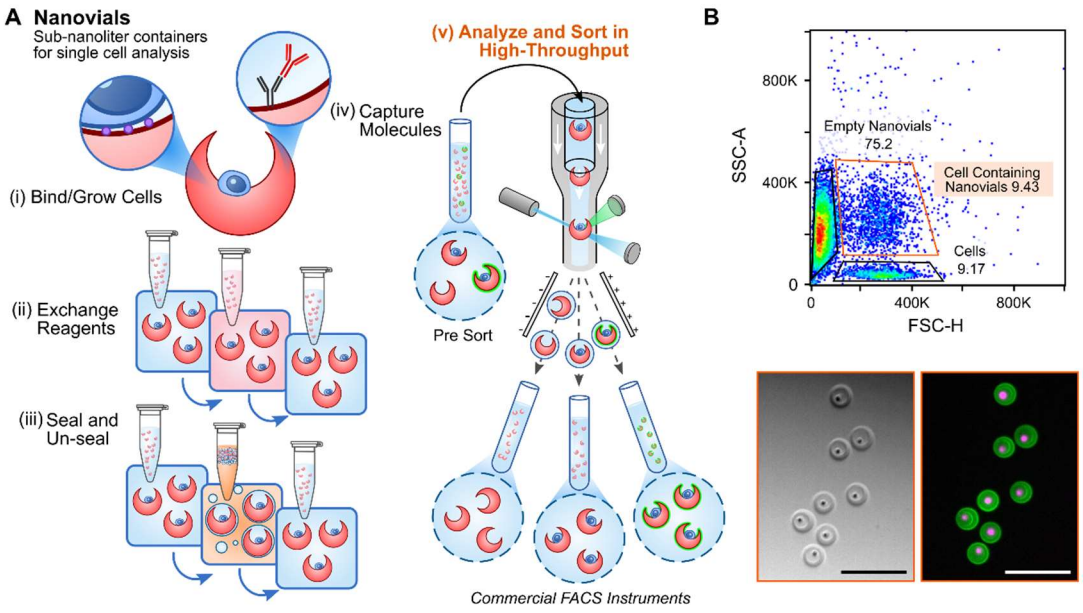

Figure 4-1 Nanovials: Sub-nanoliter containers for single cell analysis and sorting.

(A) Overview of the key features of the nanovial platform. (i) Cavity-containing hydrogel microparticles (nanovials) can be modified with various binding moieties to directly facilitate the adhesion and growth of loaded cells. (ii) Reagents can be easily exchanged around cells contained in the nanovials using simple pipetting and centrifugation steps. (iii) Nanovials can be sealed to create uniform sub-nanoliter compartments by emulsifying with biocompatible oil and surfactants using a pipette or through vortexing. Nanovials can be un-sealed to perform downstream processes using a destabilizing agent to coalesce emulsions. (iv) The surface of nanovials can be used for capturing molecules of interest such as secreted proteins. (v) Nanovials can be sized to be compatible with commercial flow cytometers and FACS machines for high-throughput analysis and sorting. **(B)** Example flow cytometry scatter plot for a sample of nanovials loaded with B lymphocytes. Highlighted region corresponds to cell-loaded nanovials shown in the bright field and fluorescence images below.

For each instrument we also systematically adjusted the sorting parameters such as drop delay, sort masks, and sample buffers to identify the optimal conditions for sorting different size ranges of nanovials. We identified conditions that enabled sorting purities as high as 99% and sort recovery efficiencies >90%. Nanovials are unique in that they are transparent and scatter only weakly due to their hydrogel composition and small index of refraction difference compared with surrounding medium. By exploiting this property, we demonstrate that a scatter signal alone can be used to identify cell-containing nanovials from a background of empty nanovials and free cells. We further demonstrate the ability to enrich these populations with purities >90%.

4.2. Materials and Methods

All materials were purchased from Sigma unless otherwise noted. Additional information on the flow cytometers used in this study is listed in table 4-1.

4.2.1. Nanovial Fabrication and Modification

Biotinylated nanovials were fabricated using approaches described previously.[21] Briefly an aqueous two-phase system combined with droplet microfluidics was employed to create hydrogel particles with exposed cavities. The hydrogel precursor component was composed of a 29 % w/v solution of 10 kDa, 4 arm PEG norbornene, premixed with 10 mg/mL of 5 kDa biotin-PEG-thiol (Nanocs) to add biotin handles to the nanovial matrix. Different sizes of nanovials (35, 55, and 85 μm) were achieved by adjusting both the size of the droplet generators and the flow rates used to generate droplets. Intra-batch variation in the outer diameter of the nanovials was measured to be <5% for each size condition tested in this work as measured by brightfield microscopy.

Nanovials were modified using fluorescent streptavidin for microscopy and flow cytometry experiments.

Table 4-1 Hardware comparison for the three different flow cytometers used in this work.

Property	FACS Aria II	Sony SH800	On-chip Sort
Laser Interrogation Vessel	Rectangular Cuvette	Microfluidic Chip	Microfluidic Chip
Nozzle Size	100, 130 µm	130 µm	80, 150 µm
Nozzle Type	Ring	Chip Integrated	Chip Integrated
ND Attenuation	Yes (1.5 OD)	No	No
Number of Lasers	4 (355,488,561,640 nm)	4 (405,488,561,638 nm)	3 (405,488,637 nm)
Laser Power	50-100 mW	30 mW	10-30 mW
Laser Geometry	Spatially Separated	Colinear	Colinear
Sort Method	Jet-in-air	Jet-in-air	Hydraulic
Ease-of-Use	Trained operator required	Easy to use	Easy to use

A volume of concentrated nanovials was first diluted 5-10X in PBS containing 0.05% w/v Pluronic F-127. An equal volume of solution containing fluorescent streptavidin was added to the diluted solution of nanovials and incubated for a minimum of 15 minutes to allow binding of streptavidin to the biotin groups on the nanovials. Before analysis the nanovial solution was washed 3 times with PBS/Pluronic solution by centrifuging, aspirating supernatant, and resuspending. During all particle handling steps, tubes and pipette tips were precoated with PBS + 0.05% Pluronic solution to reduce unwanted sticking of nanovials onto surfaces.

4.2.2. LOD and Dynamic Range Measurements

Biotinylated nanovials modified with AlexaFluor™ 488 Streptavidin (Invitrogen) were prepared over a range of concentrations using the methods described above. A fixed number of nanovials were added to various concentrations of fluorescent streptavidin solutions and incubated for 15 minutes to allow for binding. Nanovials were then washed in a large excess of PBS + 0.05% Pluronic solution 3 times to remove any unbound streptavidin molecules.

Microscopy – The intensity of each particle was measured with an automated image analysis algorithm to detect each nanovial in the image and integrate the intensity across the particle. Localized background subtraction in our automated analysis algorithm was required to reach this performance level by reducing variation due to illumination non-uniformity across the images (Figure 4-2). Brightfield and fluorescent images were taken using a Nikon Eclipse TI-S fluorescence microscope equipped with a Photometrics® PRIME™ cooled CMOS camera and SOLA Light Engine LED light source. All images were taken using a 20X objective lens (Nikon CFI S Plan Fluor ELWD 20XC, 0.45 NA) with a 1 second exposure time. For quantification of fluorescence intensity a custom MATLAB script was developed.

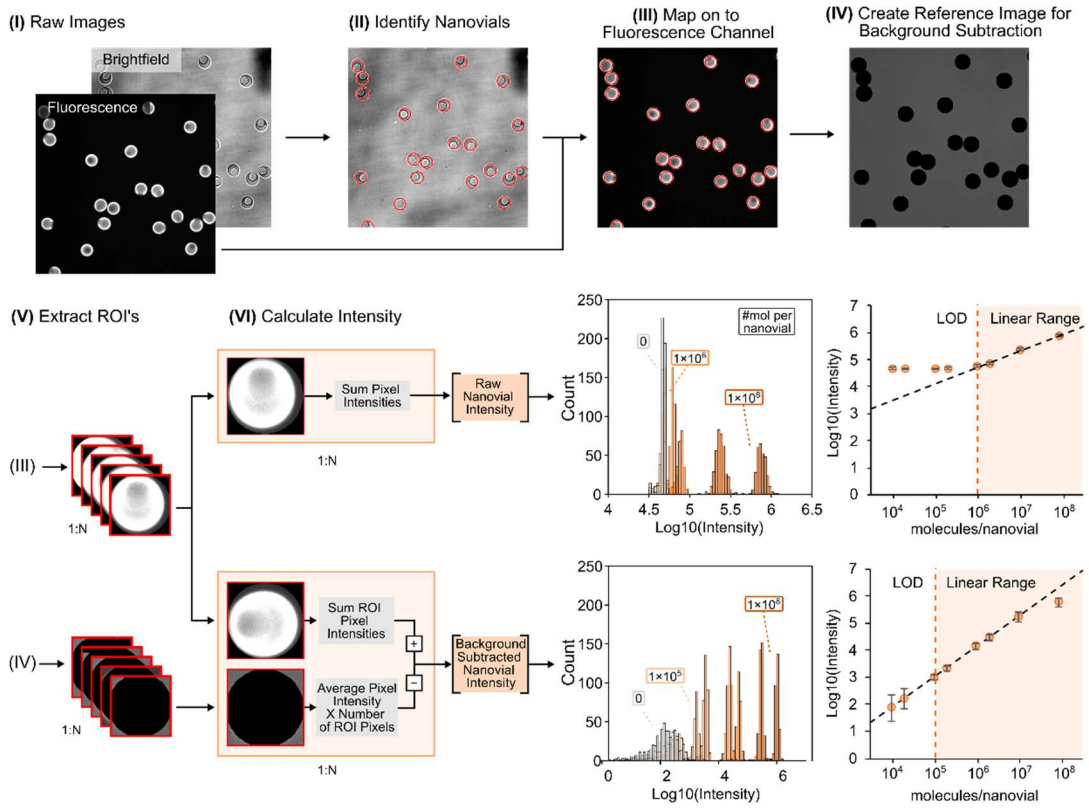

Figure 4-2 Image analysis workflow to quantify nanovial intensity from fluorescence microscopy. **(I)** Fluorescence and bright field images are imported into MATLAB. **(II)** Nanovials are identified using a Hough transform algorithm and locations are mapped onto the fluorescence channel **(III). (IV)**A background reference image is constructed by taking the fluorescence image and setting the intensity of the nanovial region of interest (ROI) to zero. **(V)** Fluorescence image and background images are cropped at each particle location. **(VI)** Side by side comparison of the raw intensity measurement and background subtracted intensity. For raw intensity the pixel values are summed in the ROI. For the background subtracted intensity the average pixel intensity of the background corner regions is multiplied by the number of pixels in the ROI and then subtracted from the total intensity of the ROI. Distributions from Figure 4-3 are shown with and without the localized background subtraction process. Background subtraction improves the limit of detection (LOD) and linear portion of the dynamic range by an order of magnitude.

Briefly, nanovial locations were identified using a brightfield image and regions of interest were mapped onto a fluorescent image of the same location. Pixels within the border of the nanovial were integrated to obtain a calculated intensity and then subtracted from local background intensity to compensate for spatial background variation in illumination. >200 nanovials were quantified for each condition.

Flow Cytometry – Nanovials were assessed for fluorescence signal using three different commercially available flow cytometers. For each trial nanovials were diluted into a 50-fold excess volume of PBS containing 0.05% w/v Pluronic F-127. PMT voltage/gain settings were optimized to ensure that the sample peak from the most concentrated particle sample was completely present within the bounds of the flow plot and unstained samples were between the first and second decades in the fluorescence histogram. Samples were gated based on FSC area and SSC area values and analyzed for Alexa Fluor™ 488 signal area. At least 10,000 events were quantified for each condition.

4.2.3. Sorting Optimization

General sample preparation – To compare the nanovial sort efficiency across FACS machines we created mixtures of nanovials containing a defined subpopulation with a unique fluorescent label. Labeled nanovials were modified as described above. Labeled target nanovials were then mixed with an excess of background nanovials, labeled with a non-overlapping fluorophore, at desired concentrations.

FACSAria – Nanovial samples were sorted on a FACSAria™ II instrument using a 130 μm nozzle. To optimize sorting efficiency the machine's drop delay values and sorting masks were adjusted until maximum target yields were obtained. Briefly, the instrument drop delay was initially set according to manufacturer instructions using Accudrop calibration beads. Drop delay

was then offset +2.0 to -2.0 units from the set point in increments of 0.25. At each drop delay value a 1:5 mixture of unlabeled to fluorescently labeled particles was analyzed and 100 fluorescent target particles were sorted using a single-cell sort mask. Sorted samples were imaged to quantify the total number of recovered particles as well as the fraction of target vs off-target particles sorted. In general, optimal drop delay values shifted slightly between runs and a similar rapid test is recommended before each nanovial sort.

The stringency of yield, purity, and phase mask settings were also calibrated to identify the optimal sort mask conditions for nanovial recovery. The FACS Aria II system discretizes droplets into 32 segments, and each mask can be varied between the values of 0 and 32 depending on how large a fraction of each interrogated droplet it is desired to affect. Each of the three masks was adjusted in units of 8 between the values of 0-32 (yield and purity) or 0-16 (phase). At each condition an identical mixture of AlexaFluor™ 488 streptavidin and AlexaFluor™ 568 streptavidin labeled particles (1:5 ratio) was analyzed and 100 AlexaFluor™ 488 Streptavidin labeled target particles were sorted into a single well of a well-plate. Total recovery and sample purity were determined using fluorescence microscopy.

Sony SH800 – Samples were sorted using a 130 μm chip. Because the single cell sort mask on the Sony instrument is more lenient and sorts all droplets in the vicinity of detected target events as long as off target events are not nearby, we found calibration of drop delay values unnecessary. Instead the sort recovery and purity of nanovial sorts was evaluated using the four primary sort masks, yield, normal, purity, and single cell. In each condition 200 AlexaFluor™ 488 Streptavidin target nanovial events were sorted from a background of AlexaFluor™ 647 Streptavidin labeled particles. Recovered samples were analyzed using fluorescent microscopy. Note, the Sony SH800 sorter by default reports forward and back scatter data. Generated back

scatter data was converted to side scatter upon export and is referred to as such throughout the manuscript.

On-Chip Sort – 35 μm nanovial samples were sorted using an 80 μm chip following similar procedures outlined above. Larger nanovials (55 and 85 μm) were sorted using a 150 μm chip following similar procedures outlined above. Nanovials labeled with AlexaFluor™ 647 streptavidin were spiked into an unlabeled population at a ratio of 1:10. PBS containing 0.05% w/v Pluronic™ F-127 was used as a sheath fluid for the sorts. For the sample solution study, we used PBS + 0.05% w/v Pluronic, Ficoll Paque Plus diluted to 40% v/v with PBS + 0.5% Pluronic, Optiprep™ diluted to 44% with PBS + 0.05% w/v Pluronic, and On-chip sample buffer (On-chip Bio). Particle samples were diluted approximately 1, 0.5, and 0.25 million nanovials per mL for 35, 55, and 85 μm nanovials respectively. Event rates were tracked by manually recording at fixed intervals during the sort. Samples were excited with a 637 nm laser and particles containing fluorescent streptavidin were gated based on peak fluorescence height collected through a 676/37 nm emission filter. Sorted samples were transferred from the collection reservoir into a well plate with a pipette and then imaged using a fluorescence microscope. Purity and recovery were quantified using a custom MATLAB image analysis code.

4.2.4. Assessment of the amount of accessible biotin on particles

To quantify the number of biotin available per nanovial an HRP ELISA was utilized. Evaluated nanovials were fabricated with 1 or 10 mg Biotin-PEG-thiol per mL of gel precursor material. For each condition, 2 μL of particles were first labeled with various amounts of unconjugated streptavidin ranging from 1 to 31000 ng SA per μL particle solution in 60 μL buffer to cap available biotins. After 45 min of incubation, 80 ng SA-3HRP was added to each vial and allowed to incubate an additional 30 min to allow binding to any free biotin. Particles

were then washed 5 times with 1 mL PBS containing 0.05% Pluronic and 0.5% Bovine Serum Albumin (BSA), and aliquots of the supernatant of each wash were collected to confirm the level of remaining HRP is not biasing the experiment in any way. Following the last wash particles from each condition were resuspended in 50 µL washing buffer and moved to a 96 well plate and mixed with 100 µL of HRP substrate. To create a standard curve, 50 µL of washing buffer containing known amounts of SA-3HRP from 0.05 to 30 ng were mixed with 100 µL of substrate. Reactions were allowed to occur for 25 min on a shaker before proper development was observed. Reaction was stopped with 100 µL of 3N NaOH, and the absorbance was measured at 405 nm using a Gen5 plate reader. The high unconjugated SA concentrations was considered to saturate particles, practically not allowing any additional SA-3HRP being adsorbed to the particles, leading to no HRP signal in ELISA. The concentration of unconjugated SA below which the HRP signal started to appear was considered the lowest to saturate the particles and was used to estimate the capacity of particles for binding streptavidin.

4.2.5. Scatter profiling and scatter-based enrichment of cell-containing nanovials

All experiments involving animals and animal cells were performed in accordance with the Chancelor's Animal Research Committee ethical guidelines at the University of California Los Angeles under protocol no ARC-2015-125. Primary mouse B cells were isolated from spleen using an EasySep™ Mouse Pan-B cell isolation kit (STEMCELL Technologies) according to manufacturer instructions. Prior to conducting experiments, cells were labeled with a 1 µM solution of CellTracker™ deep red dye at 37ºC over a period of 30 minutes. Nanovials were also labeled during this time first through a 15 minute incubation within a 2 µg/mL solution of Alexa Fluor™ 488 streptavidin and subsequently through a 45 minute incubation in a 40 µg/mL

solution of biotinylated anti-CD45 cell capture antibodies. After each conjugation step particles were washed three times in an excess of PBS + Pluronic F-127 solution.

Once labeled with capture antibodies, 6 μL of nanovials were added into individual wells within a 24-well plate. Samples were incubated for 30 minutes to allow nanovials to settle uniformly on the bottom of each well with their cavities oriented upwards to promote cell capture. Cells were counted on a hemocytometer and roughly 125,000 cells were added into each well. Cells were co-incubated with particles for 1 hour to allow adhesion onto the nanovial surfaces. After incubation samples from each well were pooled together and strained through a cell strainer (20 μm, CellTricks™) to remove unbound cells from the suspension and nanovials and cell loaded nanovials were recovered by flipping the cell strainer and washing with buffer solution.

Recovered nanovials were sorted via flow cytometry using a 130 μm nozzle on the Sony SH800 system in single cell mode. For fluorescence-based sorting, Alexa Fluor™ 488 and CellTracker™ deep red fluorescence was evaluated for all detected events and cell loaded nanovials were gated based on high fluorescence in both channels. For scatter-based sorting, samples were evaluated either using plots of FSC-A/SSC-A or FSC-H/SSC-A and cell-loaded nanovials were gated based on high scatter. For each gating strategy 500 events were sorted into a single well of a 96-well plate in triplicate. Post sort images were taken using fluorescence microscopy and the fraction of free cells, empty nanovials and filled nanovials was counted manually.

4.3. Results

In our studies we characterized the use of nanovials with three separate commercially available fluorescence activated cell sorters: (1) BD FACSAria™ II (BD Biosciences), (2) Sony

SH800 (Sony Biotechnology), and (3) On-chip Sort (On-Chip Biotechnologies). We compared each instrument's ability to detect fluorescence signal on nanovials with fluorescence microscopy, identified parameters to maximize the purity and efficiency of nanovial sorting, and characterized the ability to identify cell-loaded nanovials using scatter measurements alone. By identifying the optimal instrument parameters and trade-offs between each system, we aim to guide future experimental effort by easing cross-platform accessibility and aiding the selection of appropriate instrumentation to meet experimental needs.

4.3.1. Dynamic range and limit of detection for microscopy and flow cytometry analysis of nanovials

We found that nanovials could be analyzed over a large dynamic range using fluorescence microscopy with a cooled CMOS camera as well as flow cytometry. As previously shown, a unique feature of the nanovials is the ability to bind biomolecules to affinity reagents attached to the hydrogel matrix and detect their presence using fluorescent labels.[21] A core advantage of flow cytometers is their ability to measure fluorescence signals associated with 100,000's to 10's of millions of unique events, such as microbeads and cells, easily and with limits of detections below 2000 molecules for common stains and down to 100's of molecules for optimized systems.[22] We assessed the ability to detect fluorescent protein bound to nanovials using flow cytometry mimicking the signal from a biomolecular assay on a nanovial (e.g. single cell secretion assay). We bound fluorescent streptavidin to biotinylated nanovials across a 4-log range of concentrations to characterize the limit of detection and the maximum dynamic range of nanovial measurements with the instruments (Figure 4-3). Fluorescence microscopy measurements were performed in parallel as a baseline reference.

Using fluorescence microscopy, we found that signal could be detected on the nanovials, with 3 standard deviations above background noise, which we define as the limit of detection (LOD), starting at around 100,000 molecules per particle after background subtraction (Figure 4-2). Fluorescence images reveal that the streptavidin first binds to the outer surface of the nanovials at lower concentrations and then can transport and react further into the hydrogel matrix of the particles as biotin groups become saturated. It was found that biotin groups were saturated at ~10^8 molecules per nanovial for the fabrication conditions used as confirmed by both fluorescence measurements (Figure 4-3) and colorimetric assay (Figure 4-4). Of note, to calculate the number of bound molecules per nanovial we assume that nearly all fluorescent streptavidin in solution binds to the particles which is likely an overestimate. Thus, the values reported herein may be a slight underestimate of the true sensitivity of the system. We found that measurements with the flow cytometers yielded comparable, and in some instances improved the limit of detection readings when compared to fluorescence microscopy setup (Figure 4-3). Both the FACS Aria II and Sony SH800 sorters were able to detect as few as ~ 10,000 molecules / nanovial. This corresponds closely to the expected LOD for measurements of cell surface markers with similar fluorophores using flow cytometry.[23] In order to capture the high signal intensity of our high concentration positive labeled samples, particles labeled with <10^5 molecules were initially difficult to distinguish from non-labeled controls. However, through adjustment of the PMT voltage or gain parameters lower signal samples could be clearly resolved (Figure 4-3B, 4-3C). This suggests that optimal parameters should be selected based on experimental need, with lower PMT voltage favoring increased resolution and higher values providing greater dynamic range. The FACSAria™ instrument was able to resolve the lowest concentration tested with minor gain adjustments indicating a higher sensitivity.

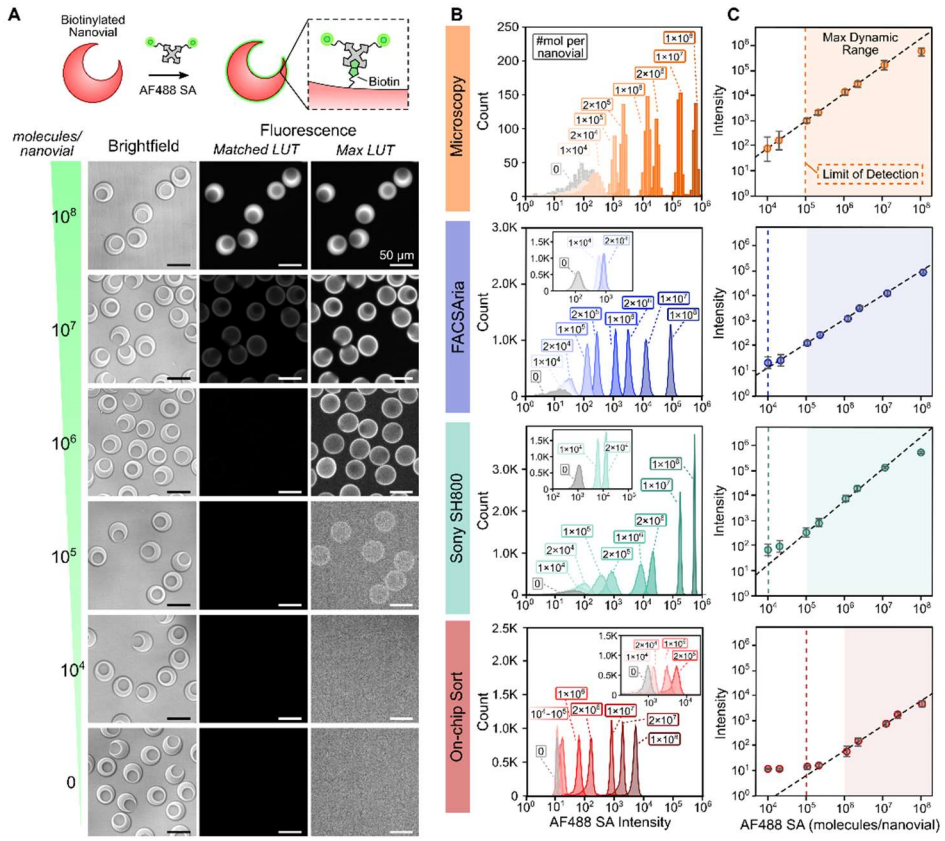

Figure 4-3 LOD and dynamic range for detecting nanovials using microscopy and flow cytometry. **(A)** Biotinylated 35 µm nanovials were labeled with Alexa FluorTM 488 streptavidin (AF488 SA) across a 4-log range of molecules per nanovial. Example brightfield and corresponding fluorescence images are shown over the range of conditions. Fluorescence images of particles with the same LUT values are shown in the middle column and images with LUTs maximized for contrast are shown to the right. **(B)** The fluorescently-labeled nanovials were analyzed using fluorescence microscopy and three flow cytometers (BD FACSAriaTM II, SONY SH800, On-chip Sort). Intensity distributions for each condition are shown. Inset graph show intensity distributions at the lower concentration range using increased gain/voltage settings for the flow cytometers. **(C)** The mean intensity for each condition is plotted against the number of molecules per nanovial on a log-log plot. The vertical dashed line indicates the lowest concentration detected for each instrument (LOD) using gain/voltage settings tuned for high sensitivity. The shaded region indicates the max dynamic range when gain/voltage is adjusted for low electronic noise. For microscopy measurements n > 200 nanovials were measured for each condition. For the FACSAria™ and Sony SH800 a total of 10,000 events were collected for each condition and for the On-Chip sort n > 2000 events were collected for each condition.

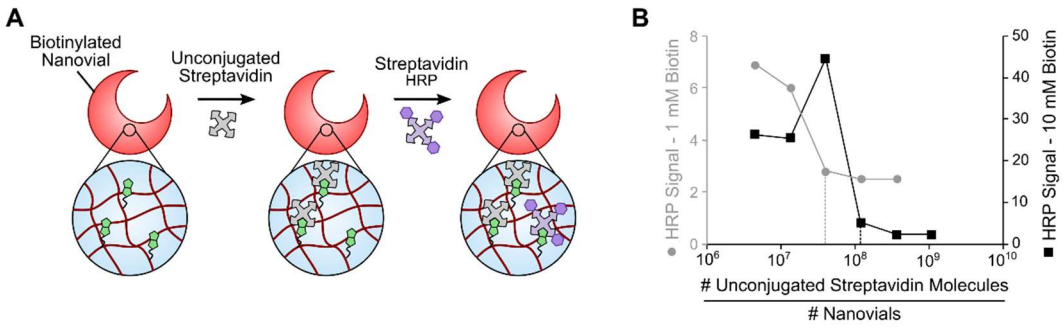

Figure 4-4 Quantification of available biotin groups using HRP colorimetric assay.

(A) Particles are first coated with unconjugated streptavidin over a range of concentrations. Samples are washed and then incubated with HRP conjugated streptavidin (SA-HRP) at a fixed concentration. After conjugation samples were washed and reacted with a colorimetric HRP substrate (2,2'-Azino-bis(3-ethylbenzothiazoline-6-sulfonic-acid, Sigma-Aldrich). The concentration of reaction product generated from conjugated SA-HRP was measured using a plate reader. **(B)** Measured HRP signal vs unconjugated streptavidin concentration for nanovials with 1 and 10 mM biotin groups in the precursor solution. Available biotin groups are saturated with streptavidin at around 4×10^7 and 1.2×10^8 molecules per nanovial for the 1 and 10 mM conditions respectively.

This is most likely due to the glass capillary used at the interrogation site as well as dedicated PMT's for each channel. Both the Sony SH800 and On-chip Sort have disposable polymer chips in the optical path which may slightly reduce the optical performance. Despite this the SH800 had a limit of detection comparable with the FACSAria™ and a 3-log max dynamic range. The measured LODs are sufficient to detect captured secretions from single cells in a reasonable time period. For example, T cells were reported to secrete cytokines at rates of ~1-10 molecules per second[24], while antibody-secreting plasma B cells can produce ~2000 antibodies per second[25]. For low abundance targets, fluorophores such as R-phycoerythrin or polymer dyes which can be an order of magnitude brighter than other common dyes may be applied to further improve the sensitivity of the system[26].

4.3.2. Sorting Nanovials using FACS

We identified optimal settings and conditions for sorting nanovials of different sizes by systematically adjusting sorting settings on the different FACS instruments. Each instrument has unique settings and parameters that can be adjusted so we discuss the characterization of each system separately.

FACSAria™ II

To test the sorting performance of the FACSAria™ II a population of fluorescently-labeled nanovials were spiked into a population of nanovials with a second label at a ratio of 1:5 and sorted into a 96-well plate (Figure 4-5). We first identified single nanovial events based on the side scatter area and forward scatter area, and then gated out target events based on high AF488 fluorescence and low AF568 fluorescence (Figure 4-5B). Gated events were sorted and then imaged using fluorescence microscopy to assess both the purity of the sort and the sort recovery efficiency as defined by:

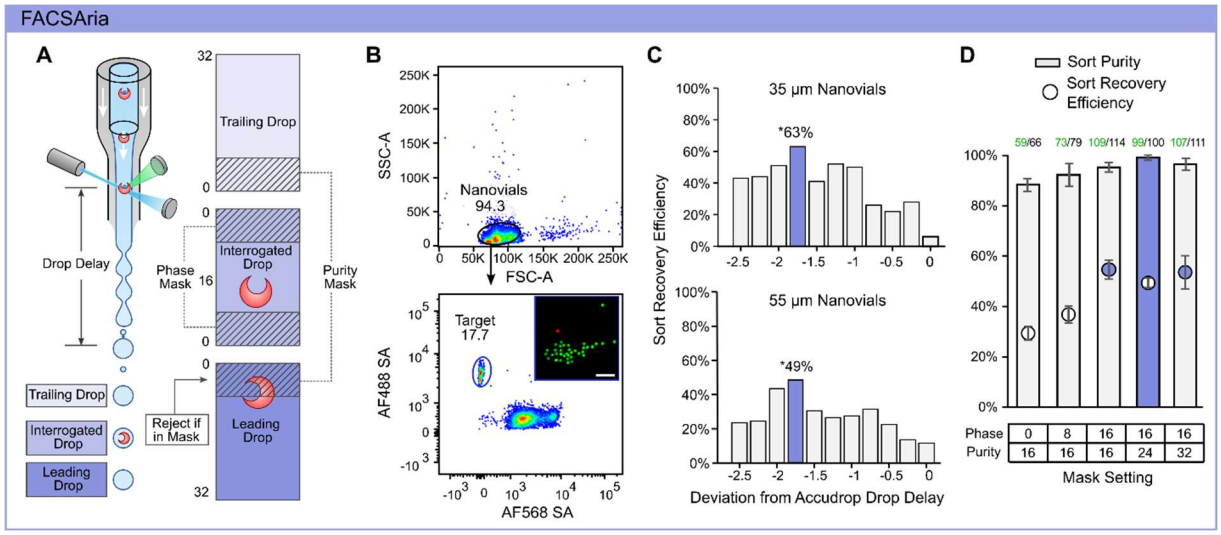

Figure 4-5 Optimized Nanovial sorting parameters on the FACSAriaTM II.

(A) Schematic showing an overview of the FACSAria™ system and important parameters that can be adjusted to fine tune sorting. The drop delay defines the expected time between the interrogation of an event and formation of the aerosol droplets. Sorting masks adjust the stringency by which an event will be sorted based on its predicted positioning. **(B)** Scatter and fluorescence plots of Alexa Fluor™ 488 streptavidin labeled nanovials (35 µm) spiked into Alexa Fluor™ 647 streptavidin labeled nanovials (1:5 ratio). Inset image shows a post sort example. Scale: 200 µm. **(C)** It was found that for both 35 and 55 µm nanovials on a 130 µm nozzle that manually adjusting the drop delay from the system calibrated baseline resulted in improved sort recovery efficiency. For each condition 100 events were sorted into different wells of a 96-well plate and performance was quantified by counting recovered events. It was found that over a 5-fold improvement in recovery was achieved by adjusting the delay settings. **(D)** Various sort masks were tested and evaluated based on both purity of the sort and the sort recovery efficiency. Fluorescently labeled nanovials were spiked into an unlabelled population at a ratio of 1:5, sorted and then characterized using fluorescence microscopy. At each condition 200 target events were sorted in triplicate. The numbers above each bar report the average number of target events recovered (green) over the average total number of recovered events over the three sorts. The optimal settings for purity and sort recovery efficiency are highlighted in purple.

$$Sort\ Recovery\ Purity = \frac{number\ of\ target\ nanovials\ in\ well}{number\ of\ total\ nanovials\ in\ well} \times 100\%$$

$$Sort\ Recovery\ Efficiency = \frac{number\ of\ target\ nanovials\ in\ well}{number\ of\ reported\ sorts} \times 100\%$$

The Aria system utilizes an integrated Accudrop system to calibrate the drop delay between the detected event and the sorting point. This value can shift from day to day and it is recommended to calibrate it before each experiment utilizing the associated Accudrop calibration beads. We found that the sort recovery efficiency for both 35 and 55 micron diameter nanovials was low when using the baseline Accudrop calibrated value (Figure 4-5C). In previous work manual adjustment of the drop delay parameter was shown to improve results for double emulsion sorting.[27] Sweeping drop delay measurements manually in 0.25 increments we found that a delay value of -1.75 offset from the Accudrop value led to the best recovery efficiency for both nanovial sizes tested with the 130 µm nozzle, improving recovery 4-8 fold over baseline for 55 and 35 µm nanovials. Similarly, we found manual adjustment improved recovery with 35 µm nanovials sorted with a 100 µm nozzle (Figure 4-6). We hypothesize that this deviation is due to a change in velocity of the nanovials in the nozzle. Nanovials cover a larger fraction of the cross section of the flow compared to a cell which could lead to variation in velocity for a non-uniform flow cross-section. For best practice it is recommended to perform manual drop delay adjustment before each sort or at least perform a test for different instruments or nozzles.

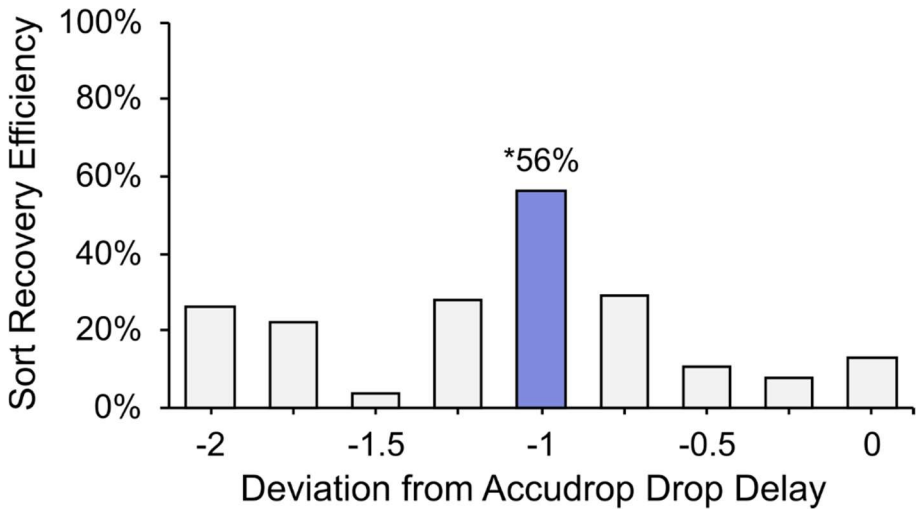

Figure 4-6 Recovery results for 35 µm nanovials sorted with a 100 µm nozzle on the FACSAria™ II
It was found that manually adjusting the drop delay from the system calibrated baseline resulted in improved sort recovery efficiency. For each condition 100 events were sorted into different wells of a 96-well plate and performance was quantified by counting recovered events. A 4-fold improvement in recovery was achieved by adjusting the delay settings.

Sorting masks can be adjusted to maximize purity or sort recovery efficiency. The Aria system defines its masks in reference to the interrogated droplet (the droplet where the target is predicted to be), the leading droplet (the droplet in front of the target), and the trailing droplet (that follows the target droplet) (Figure 4-5A). Each droplet is broken up into 32 fractions that define the relative coverage of each mask. The purity mask defines the fraction of the leading and trailing droplet in which the presence of another event will abort the sort. The phase mask defines which region of the interrogated droplet the target should be in to proceed with a sort. To prevent sample loss from targets partitioning into the incorrect droplets, phase masks will only trigger sorts when events are "centered" within a droplet, rather than localized to the droplets leading or trailing edges. Higher phase values define the center region of each droplet more stringently than lower values. Using a similar strategy as with the drop delay, we swept these conditions and quantified the sort purity, sort recovery efficiency, and the abort rate for each (Figure 4-5D). As expected, the best purity performance was found for the most restrictive purity masks. We further found that more restrictive phase masks improved the sort recovery from 29% to 55%. We hypothesize that since the particles are larger than normally sorted objects, target events near the edge of each drop may disrupt the stability of the aerosolizing stream, leading to over or under-deflection during sorting and a missed collection in the target container.

Sony SH800

To test the sorting performance of the Sony SH800 a population of fluorescently-labeled nanovials were spiked into a population of nanovials with a second label at a ratio of 1:5 and sorted into a 96-well plate using its index sorting feature (Figure 4-7). We found that both 35 and 55 μm nanovials were compatible with the larger 130 μm microfluidic chip available for the system and focused optimization for this setup.

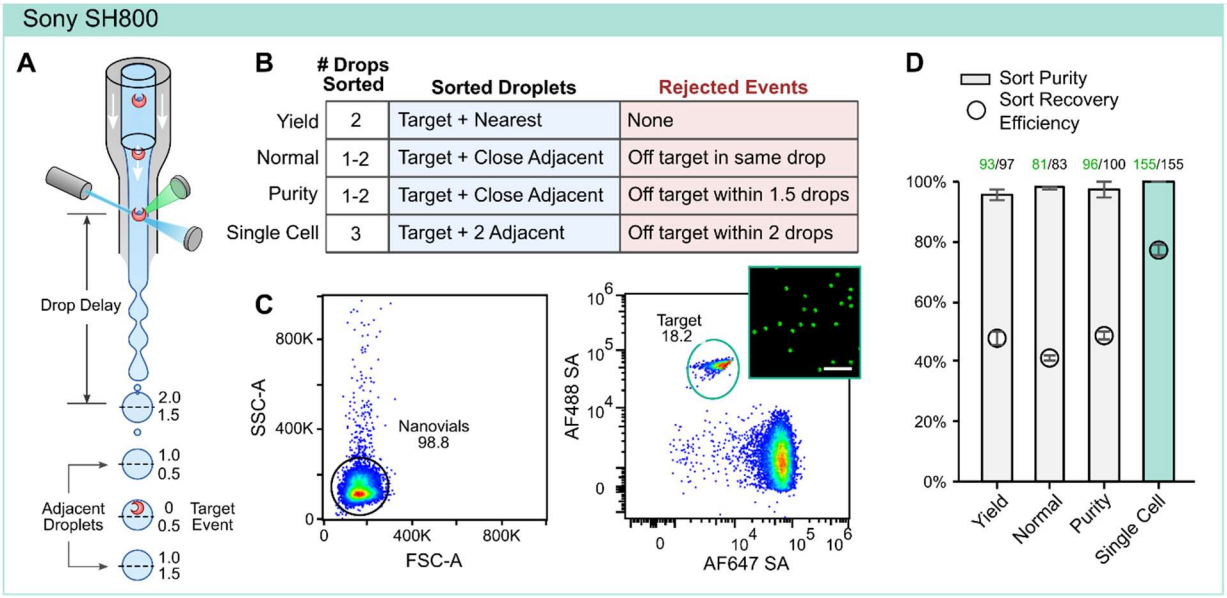

Figure 4-7 Optimized Nanovial sorting parameters on the Sony SH800.

(A) An overview schematic of the Sony SH800 system and sorting definitions. Sorting decisions are typically made in reference to the relative position of the target event and the distance between target and off target events. **(B)** Overview of four common sorting modes on the SH800 and the sort decision logic for the sort mode. **(C)** Scatter and fluorescence plots of Alexa Fluor™ 488 streptavidin labeled nanovials (35 µm) spiked into Alexa Fluor™ 647 streptavidin labeled nanovials (1:5 ratio). Inset image shows post sort example. Scale: 200 µm. **(D)** The different sort modes were tested and evaluated based on both purity of the sort and the sort recovery efficiency. Fluorescently-labeled nanovials were spiked into a non-labeled population at a ratio of 1:5, sorted and then characterized using fluorescence microscopy. At each condition 200 target events were sorted in triplicate. The numbers above each bar report the average number of target events recovered (green) over the average total number of recovered events over the three sorts. The optimal settings for purity and sort recovery efficiency are highlighted.

For the SH800 sort masking takes into account the target event droplet, adjacent droplets and the relative position of the target event to off target events (Figure 4-7A). We chose the four following sorting modes to evaluate in this study: yield, normal, purity, and single cell. Descriptions and sorting criteria are shown in Figure 4-7B. To characterize each sorting mode, AlexaFluor^{TM} 488 labeled nanovials were spiked into a population of AlexaFluor^{TM} 647 labeled nanovials at a 1:5 ratio. Single nanovial events were gated using forward scatter area and side scatter area, and target events were sorted based on high AF488 fluorescence and low AF647 fluorescence (Figure 4-7C). For each condition 200 nanovials were sorted into separate wells of a 96-well plate and sort purity and sort recovery efficiency was quantified using fluorescence microscopy. As expected, the lowest purity resulted from yield mode, as this mode does not reject a sort in the presence of adjacent off-target events. Despite this, purity was quite high (96%) and increased incrementally with the more restricted sorting modes, with the highest being for Single Cell recovery mode which had 100% purity across 3 separate sorts. Interestingly, the Single Cell mode had significantly higher sort recovery efficiency compared to any of the other modes. This was attributed to the fact that single cell mode will sort the target event droplet and both of the adjacent droplets. As described above, the larger size of the nanovials can potentially cause more inconsistency in sort timing as well as affect droplet deflection accuracy. Thereby including 3 droplets in the sort is expected to have better recovery compared to the other modes which only sort 1-2 of the droplets depending on the event conditions. One downside to this is that the Single Cell mode will only sort if there are no overlapping events in the adjacent droplets leading to a higher frequency of aborted target events during analysis of more concentrated nanovial samples (Figure 4-8).

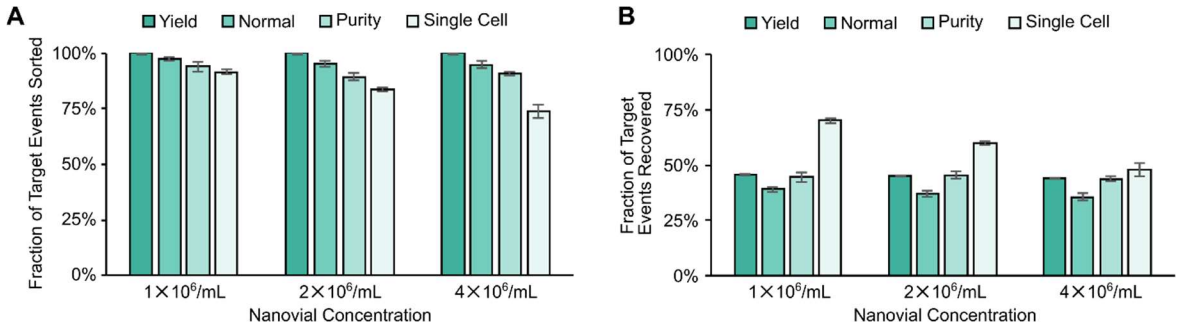

Figure 4-8 Fraction of target events sorted and recovered with the Sony SH800 using different sort modes and nanovial concentrations.

(A) At higher nanovial concentrations and stricter sort modes the abort rate increases reducing the fraction of target events that are sorted. **(B)** Expected recovery when taking into account abort rate and sort recovery using different modes. Despite the higher fraction of aborted events, single cell mode has the highest final target recovery.

However, we note that even at the highest nanovial concentration tested in this work, the single-cell mode abort rate of ~26% was sufficiently counteracted by the increased recovery efficiency and sort purity to obtain higher total target yields than could be achieved using any alternative sort mask at any sample concentration.

On-Chip Sort

The On-chip Sort system is unique compared to the other two systems in that it is aerosol free and has a larger range of particle size compatibilities. Like with the studies using the SH800 and FACSAria™ a fluorescently labeled subpopulation of nanovials was spiked into a larger population of unlabeled nanovials at a 1:10 ratio and sorted to characterize purity and recovery efficiency. Forward scatter height, side scatter height and fluorescence were used to gate single target nanovial events for sorting (Figure 4-9A). We found that we could easily sort nanovials up to 85 microns in diameter with the larger 150 micron chip available for the instrument achieving ~10 fold enrichment (Figure 4-9B). The instrument does not have a sample mixer and it was noted that nanovials settled and tended to aggregate at the sample inlet (Figure 4-9C). This often resulted in an initial moderate event rate followed by little to no events and eventually to a large spike in events as the last of the sample fluid was pushed through the channel. To address this, we tested Ficoll and Optiprep, two well-known density-modulating agents used for cell separation processes to tune the density of the sample solution such that the nanovials are nearly

neutrally buoyant. We also tested the On-chip sample buffer which increases settling time through increased viscosity. Each of these experiments was conducted with 55-micron nanovials as these samples gave us the most inconsistent event rate in PBS leading to lower purities.

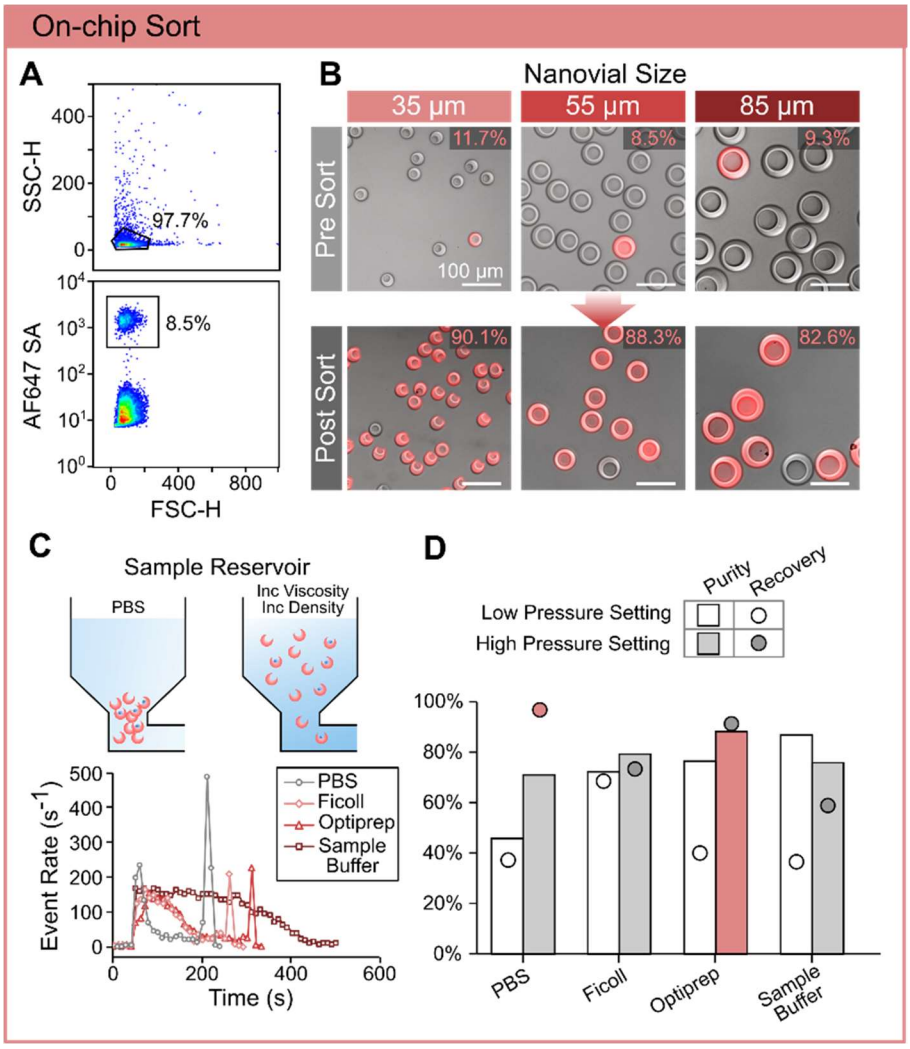

Figure 4-9 Optimized Nanovial sorting parameters on the On-chip Sort.

(A) Example scatter plot of 55 µm nanovials and fluorescence gating of Alexa Fluor™ 647 labeled nanovial sub-populations. **(B)** Pre and post sort images of 35, 55, and 85 µm nanovials. Fluorescence and brightfield channels are overlaid to aid in visualization. **(C)** Density matching to increase uniformity of sort event rates and improve performance. Event rate over time shown for 55 µm nanovials suspended in different buffers. (**D**) Purity and recovery efficiency of 55 µm nanovials for different buffers and pressure settings.

In addition to the different solutions the On-chip instrument has two standard pressure modes, low-pressure mode, optimized for lower viscosity solutions such as PBS and high-pressure mode used for sorting in more viscous solutions. We found that in general using the higher-pressure mode as well as using the buoyancy matched and higher viscosity solutions led to much more consistent event rates and improved the purity and recovery rates. Optiprep resulted in the highest purity of the solutions, however, it tended to cause large variation in scatter signal which may be non-optimal depending on application requirements (Figure 4-10). For further studies we utilized the Ficoll sample solution as it had the best balance of sorting results and optical properties. Although purity was lower for the On-chip Sort, the sort recovery efficiency was high. Since no aerosols are generated the device is more forgiving with compatible nanovial sizes and there is no risk of sorted droplets missing the recovery container. During default operation, the On-chip Sort targets maximizing yield. However, because sample loading, sorting, and collection all occurs within the same self-contained chip interface, higher purities can be achieved by collecting and re-sorting previously sorted samples.

4.3.3. Scatter based enrichment of cell-containing subpopulations

Unique scatter signatures can be used to identify populations of cell-containing nanovials among a background of free cells and nanovial-containing cells. Scatter based gating is powerful for both cleaning up data by removing debris or unwanted populations of cells and identifying sub-populations of interest. This can be advantageous for getting more accurate results, purer samples, and can free up fluorescence channels for additional stains. In previous nanovial workflows, cell-containing nanovial populations were either not discriminated from other populations or were identified using fluorescent staining.

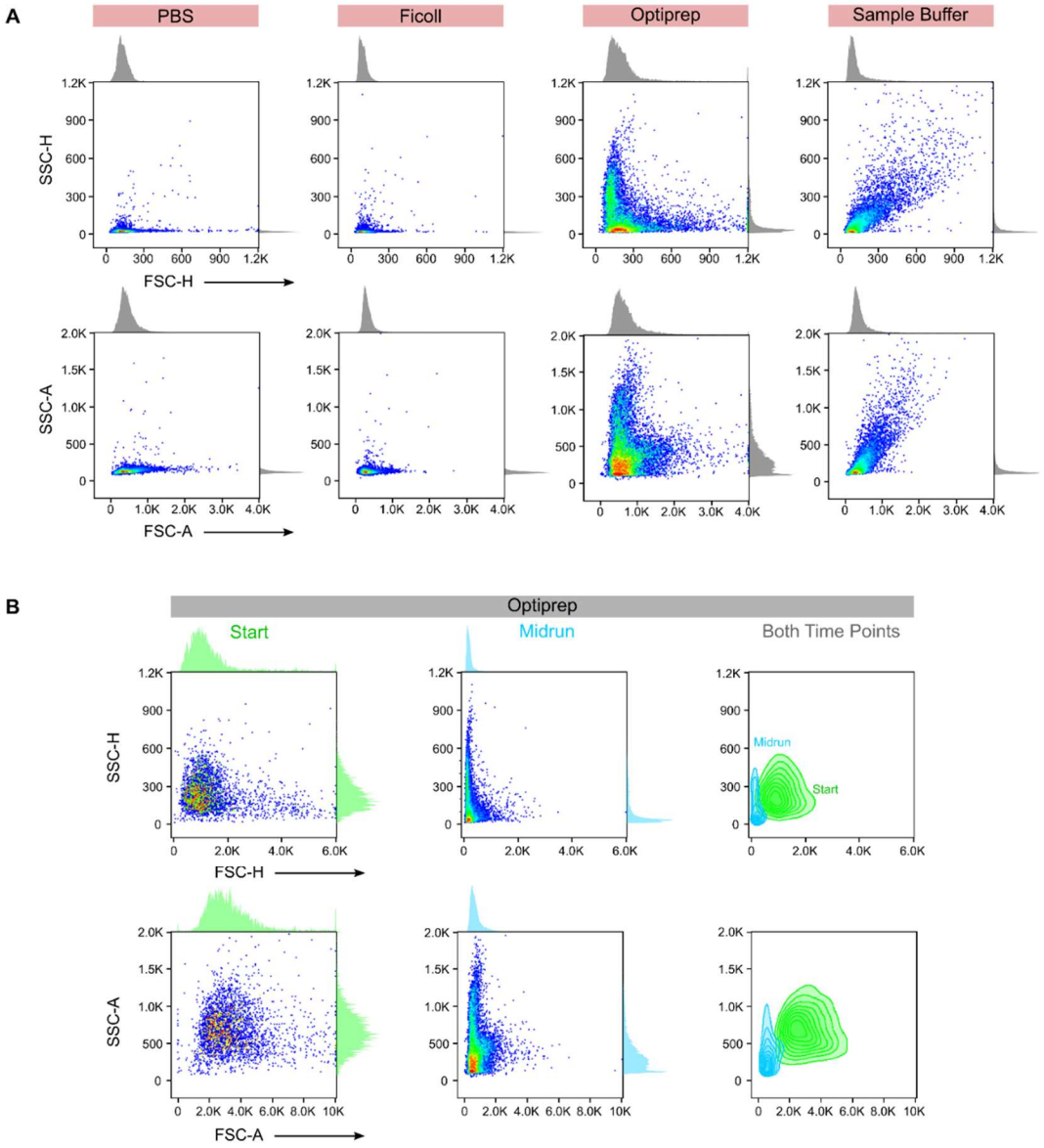

Figure 4-10 Scatter profiles of 55 µm Nanovials measured with the On-chip sort in various buffers. **(A)** Both forward and side scatter were comparable for nanovials in PBS and Ficoll solution. Noticeably more scatter was noted for both Optiprep and On-chip Sample buffers solutions. **(B)** It was noted that the scatter profile of the nanovials would drift significantly when using optiprep in the sample solution. This was attributed to sheath fluid mixing with the sample solution when the instrument was paused intermediately in the run due to hydrostatic pressure between the solution reservoirs on the larger 150 µm chip. Contour lines represent 10% of the corresponding population per level.

To improve the purity of the sample and free up fluorescence channels we systematically identify unique scatter signatures associated with nanovials containing cells using fluorescent stains as a ground truth. B lymphocytes stained with Deep Red CellTracker™ were bound to Alexa Fluor™ 488 labeled nanovials. A mixture of the cell-containing nanovials, empty nanovials, and free cells were analyzed using the Sony SH800 (Figure 4-11). Using the unique fluorescent signatures of each population we were able to back gate each target population to their associated scatter signals. In general cells were observed to have lower side scatter and higher forward scatter, while nanovials had higher side scatter and lower forward scatter. It was noted that both scatter height or area could be used to identify the subpopulation of interest (Figure 4-12). Cell-containing nanovials were enriched by gating off of high forward and side scatter (Figure 4-11C). As a control, cell-containing nanovials were also sorted based off of a fluorescence gate (Figure 4-11B). Samples were then imaged using fluorescence microscopy and analyzed to compare enrichment based on a fluorescence signature and scatter signature (Figure 4-11D). Nanovials containing cells were successfully enriched over 10-fold using both the scatter and fluorescence gating with no significant difference in purity (90%, and 88% respectively).

4.4. Discussion

In this work we systematically characterized the analysis and sorting of hydrogel nanovials with commercial FACS instruments (Table 4-2). By employing the high signal to noise of FACS readouts we are able to detect protein bound to nanovial surfaces with higher fluorescence intensity and dynamic range than high end fluorescence microscopy readouts, improving performance in terms of LOD and dynamic range by at least an order of magnitude.

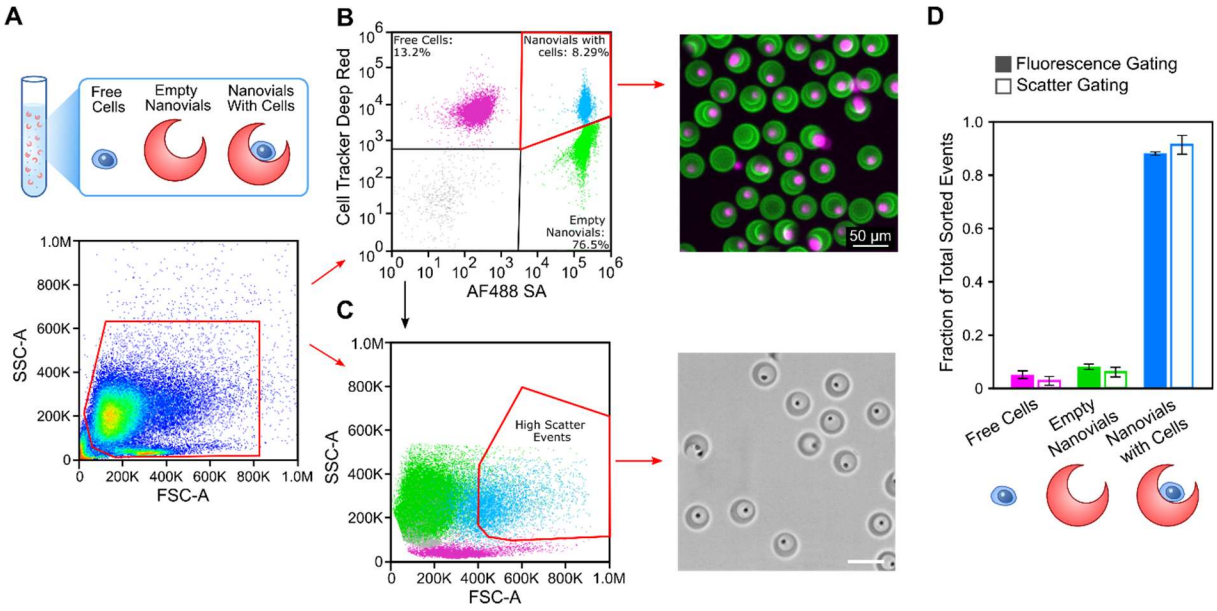

Figure 4-11 Nanovial scatter characterization and scatter-based enrichment of cell-containing nanovials.

(A) A mixture of free cells, nanovials, and cell-containing nanovials were analyzed to identify unique scatter signatures for each population and then sorted to enrich cell-containing nanovials. **(B)** The nanovials and cells were stained with unique fluorescent labels in order to accurately discriminate each population. **(C)** The fluorescent signatures were then correlated back to the scatter plots to identify each population based on scatter signature. **(D)** Samples were sorted based on fluorescent gating alone and scatter gating alone and imaged to compare enrichment of the cell-containing nanovials.

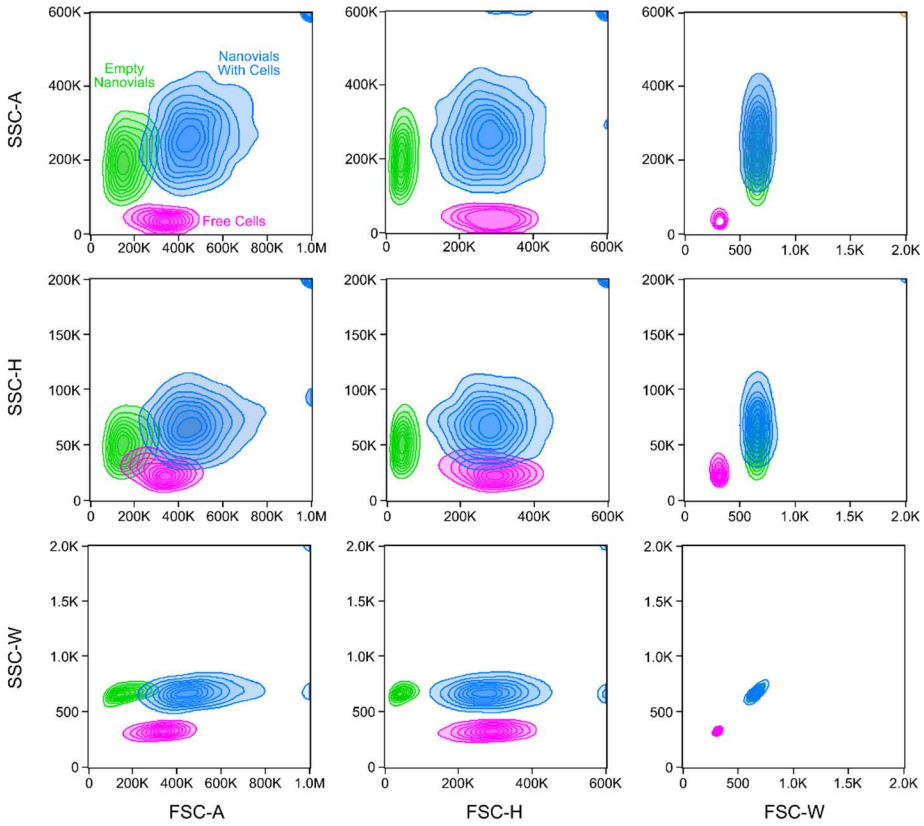

Figure 4-12 Contour plots for additional combinations of side scatter and forward scatter components for free cells, empty nanovials and cell loaded nanovials (Figure 4-9).

Contour lines represent 10% of the corresponding population per level. Cell loaded nanovials show the most separation from other populations using SSC-A vs FSC-H and SSC-W vs FSC-H. Cell loaded nanovials are also distinguishable for SSC-A vs FSC-A, SSC-H vs FSC-A, SSC-H vs FSC-H, and SSC-W vs FSC-A.

Table 4-2 Summary of Nanovial analysis and sorting capabilities across different flow sorters.

Instrument	Nanovial Diameter(μm)	Working Conc. (nanovials $\times 10^6$/mL)	Event rate (s^{-1})	Purity	Recovery Efficiency	LOD (# mol)	Max Dynamic Range
FACSAria II	35	1 – 4	200-800	95-99%	~40-60%	~10^4	3 Log
	55	0.25 – 1	50 - 200	95-99%	~40-60%		
	85	NA	NA	NA	NA		
Sony SH800	35	1 – 4	200-800	95-99%	70-80%	~10^4	3 Log
	55	0.25 – 1	50 - 200	NA*	NA*		
	85	NA	NA	NA	NA		
On-chip Sort	35	0.5 – 2	100 - 300	80 – 90%	70 - 95%	~10^5	2 Log
	55	0.25 – 0.5	20 - 50	80 – 90%	70 - 95%		
	85	0.1 – 1	20 - 100	80 – 90%	70 - 95%		

** Able to perform analysis, but had low sorting recovery.*

We characterized sorting performance on the different FACS instruments and identified optimal parameters that improved purity to up to 93% and sample recovery up to 8-fold over baseline settings. Using more widely available FACS instruments such as the FACSAria™ and Sony SH800 we were able to easily sort 35 μm nanovials, and larger 55 μm nanovials were successfully sorted with the FACSAria. Using the microfluidic chip based On-chip Sort system we were able to sort nanovials up to 85 microns in diameter which could further open up possibilities for performing assays with larger cells,multiple cells, or cell colonies. Further, this instrument is capable of sorting water-in-oil emulsions, enabling analysis and sorting of emulsified nanovials which may open up other homogenous assays such as substrate-based FRET or nucleic acid assays.

Beyond the nanovials we use here, our results may provide a guide for other large particle sorting using FACS, such as for sorting of beads,[10, 11] hollow shell (e.g. PicoShell) particles,[18] plant cells, cell clusters, and oocytes. In addition our results can inform sorting of double emulsions (e.g. water-in-oil-in-water), which have been applied to microfluidic droplet assays.[15]

Given the wide compatibility and analysis and sorting performance, we anticipate that nanovial-based approaches can transform almost any bulk assay currently performed in a well plate and analyzed with a well-plate reader into a single-cell assay performed on a nanovial and analyzed with a flow cytometer.

The presence of a cell on the solid phase of the nanovial unlocks the capability to perform sequential assays on the same single cell where information from the assay is stored on the nanovial for downstream sensitive analysis, e.g. by flow cytometry. Unlike traditional well plate assays, the ability to easily sort the cell associated with a reaction in a nanovial opens up new

opportunities for screening at throughputs unmatched by liquid handling and microfluidic techniques. Imaging of nanovials using next-generation imaging flow cytometry and image-activated cell sorters,[28-30] may further expand the capabilities, leading to high-content single-cell assays at extreme throughputs that can drive the next decades of discovery.

4.5. References

[1] D. Di Carlo, L.P. Lee, Dynamic single-cell analysis for quantitative biology, Anal Chem, 78 (2006) 7918-7925.

[2] D. Di Carlo, H.T.K. Tse, D.R. Gossett, Introduction: Why Analyze Single Cells?, in: S. Lindström, H. Andersson-Svahn (Eds.) Single-Cell Analysis: Methods and Protocols, Humana Press, Totowa, NJ, 2012, pp. 1-10.

[3] Z. Chen, J.J. Chen, R. Fan, Single-Cell Protein Secretion Detection and Profiling, Annu Rev Anal Chem, 12 (2019) 431-449.

[4] Y. Lu, Q. Xue, M.R. Eisele, E.S. Sulistijo, K. Brower, L. Han, E.A.D. Amir, D. Pe'er, K. Miller-Jensen, R. Fan, Highly multiplexed profiling of single-cell effector functions reveals deep functional heterogeneity in response to pathogenic ligands, P Natl Acad Sci USA, 112 (2015) E607-E615.

[5] A. Jin, T. Ozawa, K. Tajiri, T. Obata, S. Kondo, K. Kinoshita, S. Kadowaki, K. Takahashi, T. Sugiyama, H. Kishi, A. Muraguchi, A rapid and efficient single-cell manipulation method for screening antigen-specific antibody-secreting cells from human peripheral blood, Nat Med, 15 (2009) 1088-U1146.

[6] B.E. Jones, P.L. Brown-Augsburger, K.S. Corbett, K. Westendorf, J. Davies, T.P. Cujec, C.M. Wiethoff, J.L. Blackbourne, B.A. Heinz, D. Foster, R.E. Higgs, D. Balasubramaniam, L.S. Wang, Y. Zhang, E.S. Yang, R. Bidshahri, L. Kraft, Y. Hwang, S. Zentelis, K.R. Jepson, R. Goya, M.A. Smith, D.W. Collins, S.J. Hinshaw, S.A. Tycho, D. Pellacani, P. Xiang, K. Muthuraman, S. Sobhanifar, M.H. Piper, F.J. Triana, J. Hendle, A. Pustilnik, A.C. Adams, S.J. Berens, R.S. Baric, D.R. Martinez, R.W. Cross, T.W. Geisbert, V. Borisevich, O. Abiona, H.M. Belli, M. de Vries, A. Mohamed, M. Dittmann, M.I. Samanovic, M.J. Mulligan, J.A. Goldsmith, C.L. Hsieh, N.V. Johnson, D. Wrapp, J.S. McLellan, B.C. Barnhart, B.S. Graham, J.R. Mascola, C.L. Hansen, E. Falconer, The neutralizing antibody, LY-CoV555, protects against SARS-CoV-2 infection in nonhuman primates, Sci Transl Med, 13 (2021).

[7] A. Winters, K. McFadden, J. Bergen, J. Landas, K.A. Berry, A. Gonzalez, H. Salimi-Moosavi, C.M. Murawsky, P. Tagari, C.T. King, Rapid single B cell antibody discovery using nanopens and structured light, mAbs, 11 (2019) 1025-1035.

[8] K. Le, C. Tan, S. Gupta, T. Guhan, H. Barkhordarian, J. Lull, J. Stevens, T. Munro, A novel mammalian cell line development platform utilizing nanofluidics and optoelectro positioning technology, Biotechnology Progress, 34 (2018) 1438-1446.

[9] D. Josephides, S. Davoli, W. Whitley, R. Ruis, R. Salter, S. Gokkaya, M. Vallet, D. Matthews, G. Benazzi, E. Shvets, F. Gesellchen, D. Geere, X. Liu, X. Li, B. Mackworth, W. Young, Z. Owen, C. Smith, D. Starkie, J. White, B. Sweeney, M. Hinchliffe, S. Tickle, D.J. Lightwood, M. Rehak, F.F. Craig, D. Holmes, Cyto-Mine: An Integrated, Picodroplet System for High-Throughput Single-Cell Analysis, Sorting, Dispensing, and Monoclonality Assurance, Slas Technol, 25 (2020) 177-189.

[10] V. Chokkalingam, J. Tel, F. Wimmers, X. Liu, S. Semenov, J. Thiele, C.G. Figdor, W.T.S. Huck, Probing cellular heterogeneity in cytokine-secreting immune cells using droplet-based microfluidics, Lab on a Chip, 13 (2013) 4740-4740.

[11] M. Li, M. van Zee, C.T. Riche, B. Tofig, S.D. Gallaher, S.S. Merchant, R. Damoiseaux, K. Goda, D. Di Carlo, A Gelatin Microdroplet Platform for High-Throughput Sorting of Hyperproducing Single-Cell-Derived Microalgal Clones, Small, 14 (2018).

[12] D. Yanakieva, A. Elter, J. Bratsch, K. Friedrich, S. Becker, H. Kolmar, FACS-Based Functional Protein Screening via Microfluidic Co-encapsulation of Yeast Secretor and Mammalian Reporter Cells, Sci Rep-Uk, 10 (2020).

[13] Y.L. Fang, T.H. Chu, M.E. Ackerman, K.E. Griswold, Going native: Direct high throughput screening of secreted full-length IgG antibodies against cell membrane proteins, Mabs, 9 (2017) 1253-1261.

[14] Y.J. Eun, A.S. Utada, M.F. Copeland, S. Takeuchi, D.B. Weibel, Encapsulating Bacteria in Agarose Microparticles Using Microfluidics for High-Throughput Cell Analysis and Isolation, Acs Chem Biol, 6 (2011) 260-266.

[15] K.K. Brower, M. Khariton, P.H. Suzuki, C. Still, G. Kim, S.G.K. Calhoun, L.S. Qi, B. Wang, P.M. Fordyce, Double Emulsion Picoreactors for High-Throughput Single-Cell Encapsulation and Phenotyping via FACS, Anal Chem, 92 (2020) 13262-13270.

[16] A. Zinchenko, S.R.A. Devenish, B. Kintses, P.Y. Colin, M. Fischlechner, F. Hollfelder, One in a Million: Flow Cytometric Sorting of Single Cell-Lysate Assays in Monodisperse Picolitre Double Emulsion Droplets for Directed Evolution, Anal Chem, 86 (2014) 2526-2533.

[17] S.S. Terekhov, I.V. Smirnov, A.V. Stepanova, T.V. Bobik, Y.A. Mokrushina, N.A. Ponomarenko, A.A. Belogurov, M.P. Rubtsova, O.V. Kartseva, M.O. Gomzikova, A.A. Moskovtsev, A.S. Bukatin, M.V. Dubina, E.S. Kostryukova, V.V. Babenko, M.T. Vakhitova, A.I. Manolov, M.V. Malakhova, M.A. Kornienko, A.V. Tyakht, A.A. Vanyushkina, E.N. Ilina, P. Masson, A.G. Gabibov, S. Altman, Microfluidic droplet platform for ultrahigh-throughput single-cell screening of biodiversity, P Natl Acad Sci USA, 114 (2017) 2550-2555.

[18] M. van Zee, J. de Rutte, R. Rumyan, C. Williamson, T. Burnes, R. Radakovits, A.S. Eugenio, S. Badih, D.-H. Lee, M. Archang, D. Di Carlo, High-throughput selection of microalgae based on biomass accumulation rates in production environments using PicoShell Particles, bioRxiv, (2021) 2021.2002.2003.429271.

[19] C.Y. Wu, M.X. Ouyang, B. Wang, J. de Rutte, A. Joo, M. Jacobs, K. Ha, A.L. Bertozzi, D. Di Carlo, Monodisperse drops templated by 3D-structured microparticles, Sci Adv, 6 (2020).

[20] G. Destgeer, M.X. Ouyang, C.Y. Wu, D. Di Carlo, Fabrication of 3D concentric amphiphilic microparticles to form uniform nanoliter reaction volumes for amplified affinity assays, Lab on a Chip, 20 (2020) 3503-3514.

[21] J. de Rutte, R. Dimatteo, M. van Zee, R. Damoiseaux, D. Di Carlo, Massively parallel encapsulation of single cells with structured microparticles and secretion-based flow sorting, bioRxiv, (2020) 2020.2003.2009.984245.

[22] L.A. Sklar, M.B. Carter, B.S. Edwards, Flow cytometry for drug discovery, receptor pharmacology and high-throughput screening, Curr Opin Pharmacol, 7 (2007) 527-534.

[23] H. Zola, High-Sensitivity Immunofluorescence/Flow Cytometry: Detection of Cytokine Receptors and Other Low-Abundance Membrane Molecules, Current Protocols in Cytometry, 30 (2004) 6.3.1-6.3.13.

[24] Q. Han, E. Bradshaw, B. Nilsson, D. Hafler, J.C. Love, Multidimensional analysis of the frequencies, dynamics, and rates of cytokine secretion from single cells by quantitative microengraving, Abstr Pap Am Chem S, 240 (2010).

[25] N. Chaffey, Alberts, B., Johnson, A., Lewis, J., Raff, M., Roberts, K. and Walter, P. Molecular biology of the cell. 4th edn, Ann Bot, 91 (2003) 401-401.

[26] Z. Maciorowski, P.K. Chattopadhyay, P. Jain, Basic Multicolor Flow Cytometry, Current Protocols in Immunology, 117 (2017) 5.4.1-5.4.38.

[27] K.K. Brower, C. Carswell-Crumpton, S. Klemm, B. Cruz, G. Kim, S.G.K. Calhoun, L. Nichols, P.M. Fordyce, Double emulsion flow cytometry with high-throughput single droplet isolation and nucleic acid recovery, Lab on a Chip, 20 (2020) 2062-2074.

[28] N. Nitta, T. Sugimura, A. Isozaki, H. Mikami, K. Hiraki, S. Sakuma, T. Iino, F. Arai, T. Endo, Y. Fujiwaki, H. Fukuzawa, M. Hase, T. Hayakawa, K. Hiramatsu, Y. Hoshino, M. Inaba, T. Ito, H. Karakawa, Y. Kasai, K. Koizumi, S. Lee, C. Lei, M. Li, T. Maeno, S. Matsusaka, D. Murakami, A. Nakagawa, Y. Oguchi, M. Oikawa, T. Ota, K. Shiba, H. Shintaku, Y. Shirasaki, K. Suga, Y. Suzuki, N. Suzuki, Y. Tanaka, H. Tezuka, C. Toyokawa, Y. Yalikun, M. Yamada, M. Yamagishi, T. Yamano, A. Yasumoto, Y. Yatomi, M. Yazawa, D. Carlo, Y. Hosokawa, S. Uemura, Y. Ozeki, K. Goda, Intelligent Image-Activated Cell Sorting, Cell, 175 (2018) 266-+.

[29] A. Isozaki, H. Mikami, H. Tezuka, H. Matsumura, K.R. Huang, M. Akamine, K. Hiramatsu, T. Iino, T. Ito, H. Karakawa, Y. Kasai, Y. Li, Y. Nakagawa, S. Ohnuki, T. Ota, Y. Qian, S. Sakuma, T. Sekiya, Y. Shirasaki, N. Suzuki, E. Tayyabi, T. Wakamiya, M.Z. Xu, M. Yamagishi, H.C. Yan, Q. Yu, S. Yan, D. Yuan, W. Zhang, Y.Q. Zhao, F. Arai, R.E. Campbell, C. Danelon, D. Di Carlo, K. Hiraki, Y. Hoshino, Y. Hosokawa, M. Inaba, A. Nakagawa, Y. Ohya, M. Oikawa, S. Uemura, Y. Ozeki, T. Sugimura, N. Nitta, K. Goda, Intelligent image-activated cell sorting 2.0, Lab on a Chip, 20 (2020) 2263-2273.

[30] N. Nitta, T. Iino, A. Isozaki, M. Yamagishi, Y. Kitahama, S. Sakuma, Y. Suzuki, H. Tezuka, M. Oikawa, F. Arai, T. Asai, D.H. Deng, H. Fukuzawa, M. Hase, T. Hasunuma, T. Hayakawa, K. Hiraki, K. Hiramatsu, Y. Hoshino, M. Inaba, Y. Inoue, T. Ito, M. Kajikawa, H. Karakawa, Y. Kasai, Y. Kato, H. Kobayashi, C. Lei, S. Matsusaka, H. Mikami, A. Nakagawa, K. Numata, T. Ota, T. Sekiya, K. Shiba, Y. Shirasaki, N. Suzuki, S. Tanaka, S. Ueno, H. Watarai, T. Yamano, M. Yazawa, Y. Yonamine, D. Di Carlo, Y. Hosokawa, S. Uemura, T. Sugimura, Y. Ozeki, K. Goda, Raman image-activated cell sorting, Nature Communications, 11 (2020).

Chapter 5. Future Perspectives: How Single Cell Functional Screening Can Aid the Design of Next Generation Cell Therapies

5.1. Introduction

One area in which the continued advancement of robust functional single cell screening technologies may be able to make a significant contribution is in the understanding of the correlation between phenotype and function for immune cells used in cell therapy applications. While it is true that cellular therapeutics have completely revolutionized the way modern medicine approaches the treatment of systemic and chronic illnesses, the field as a whole is still in its infancy. Immune cell therapies used to treat cancer work remarkably well for a small subset of tumor types but are still incapable of effectively attenuating the progressions of solid tumors[1]. Additionally, the personalized nature of modern cell therapies coupled with the difficult manufacturing protocols utilized to generate clinical grade products imparts an astronomically high price tag on the use of cell therapies[2], such that broad clinical use is currently unfeasible. In order to design improved cell therapies, it will be imperative to elucidate fundamental design rules that can be used to assess product quality. The single-cell functional screening technologies reported in this work offer an avenue to accomplish these goals, significantly augmenting the engineering toolkit for cell therapy design. However, significant advances still need to be made in order to render such tools compatible with the population size scales and levels of resolution needed to be useful in clinical manufacturing. Below we briefly discuss several unmet needs in the design of cellular therapeutics and give thoughts on how improvements in single-cell functional screening technologies may one day be able to help researchers and clinicians solve these issues.

5.2. Assessing Immune Cell Therapy Product Quality

In a typical T cell immunotherapy workflow, cells are withdrawn from a patient, genetically engineered to target tumor cells, expanded *ex vivo*, and finally reinjected into the patient to systemically search for and destroy malignancies. This personalized therapeutic strategy is fundamental to preventing immune rejection, as a patient's own immune system is being used to treat their disease. However, this also means that variations in the basal potency of a patient's immune cells may fundamentally affect the final efficacy of the drug product[3, 4]. In general, it is understood that the main correlates of successful treatments are high levels of *in vivo* expansion by therapeutic cells after infusion, long term persistence of infused cells within the body, and high levels of pro-inflammatory cytokine production after stimulation with cognate tumor antigen, however it is currently not easy to predict which cell populations will excel in each of these areas[5, 6]. Several reports have alluded to certain non-terminally differentiated T cell phenotypes, such as stem like memory T cells (Tscm) and central memory T cells (Tcm) as potential drivers of tumor immune response[7], but sufficient numbers of these cells are not always available in pre-infusion products to have appreciable effects. Additionally, factors such as the patient treatment history, and the in vivo disease microenvironment may predispose T cells to enter a low activity metabolically exhausted state, often resulting in poorly functional products for the patients most in need.

Single-cell functional screening technologies may be able to directly assist in the assessment of T cell product quality. In the nearest term, longitudinal studies evaluating T cell surface marker expression, cytokine production, and correlated to patient disease status would provide significant depth towards our understanding of functional markers of response. Enriched populations of functionally active cell subsets may be present at the time of treatment or may

expand selectively after delivery into the patient to drive responses, but may remain unnoticed without functional analysis. As cell therapy is still an early-stage intervention, with costly manufacturing and potential toxicity, improved a priori prediction of patient response would be incredibly beneficial in clinical decision making of who should or should not be treated. Additionally, recent reports have begun to describe that the process of terminal T cell differentiation and exhaustion may be reversible, for example through epigenetic remodeling induced by targeted gene disruption[8], enhanced production of pertinent transcription factors[9], or through small molecule interventions[10, 11]. Thus, it may one day be feasible to rescue dysfunctional cell populations to improve drug efficacy. Functional screens again may directly assess the efficacy of such treatments through evaluation and enrichment of cell subsets that respond most effectively, and identification of their transcriptional and epigenetic state. Based on the results of such studies it may be feasible to implement strategies to broadly recover functional activity of T cells directly during product manufacturing.

5.3. Screening CAR Libraries

A second application of functional screening in cell therapies stems from the use of synthetic, chimeric antigen receptors (CARs) to retarget immune cells for tumor targeting. Chimeric antigen receptors are designed by pairing target antigen specific single chain variable fragments (scFvs) with components of the native intracellular T cell receptor signaling apparatus. While simple in principle, the modular design of CARs can become quite complex, with factors such as the affinity of the scFv, the length of the extracellular hinge region, the structure of the transmembrane region and the identities of the intracellular costimulatory domains each having significant impact on the final CAR activity[12]. At present, it is not possible to reliably predict how a specific CAR design will function without laborious empirical testing[13], and while large

libraries (10^6 constructs) of CARs can be generated and transferred into immune cells simultaneously, only a small fraction of the total library can be analyzed[14, 15].

Certain functional screening technologies such as the dropicle assay described in chapters 3 and 4 of this work may be able to address the screening bottleneck of synthetic CAR molecules by translating functional CAR assessment into a continuous process that can analyze entire CAR libraries using standard flow cytometry. For example, target antigens could be functionalized onto the surface of nanovials used to screen CAR T cell libraries, and individual clones demonstrating enhanced cytokine production could be recovered and sequenced to identify constructs of interest. This type of assay may also prove useful for analysis of unwanted phenomena such as tonic (constitutively or chronic) signaling from CAR constructs in the absence of target antigen. Providing a route to select out CAR designs that will result in rapid cell exhaustion.

5.4. Bridging Functional Analyses with Genotypic Information

Finally, as a general comment the ability to pair datasets across hierarchical levels of cellular behavior will be a game changing feature of mature single cell analysis platforms. Historically, many functional screening techniques such as ELISPOT or intracellular cytokine staining have been utilized as endpoint assays, and cellular function could not be paired with gene expression or sequence information. However, this is not a necessary assay limitation, and modern single-cell functional analysis technologies are already starting to bridge this gap. Both of the secretion analysis techniques presented in the prior chapter of this work are able to assess cellular function without loss of viability and can enrich interesting target cells for subsequent analysis. As novel cell types including natural killer (NK) cells, γδ T cells, NK T cells, and induced pluripotent stem cells (IPSCs) are beginning to be explored for cell therapy

applications[5] interesting combinations of therapeutic cell populations may be formed to enhance therapeutic efficacy. A holistic understanding of cell behavior will have to be ascertained to maximize the potential of such therapies.

5.5. Closing Remarks: Advancing Dropicles Towards Future Applications

The dropicle platform highlighted in chapters 3 and 4 of this work is a truly unique technology that has the potential to transform the study of single cell secretions across numerous applications. In addition to the assessment of antibody production from producer cell lines, hybridomas, and primary plasma cells we have also been able to detect the presence of various cytokines using similar fluorescent-based ELISA approaches on the nanovial surface (Figure 5-1), with a limit of detection down to 1 ng/mL of protein, similar to other state of the art single cell cytokine detection platforms[16, 17]. Additionally, we have been able to detect the production of both interferon-γ (IFN-γ) and tumor necrosis factor-α (TNF-α) from single viable T cells, and sort highly secreting cell clones out of a background of non-producers (Figure 5-2). We have previously demonstrated that the dropicle platform allows the coupled evaluation of protein secretions and RNA expression data using hybridomas. Thus, it is not difficult to envision how one might be able to couple similar genetic expression data with cytokine production rates to evaluate T cell phenotypes (Figure 5-3).

In closing we note that the work presented herein only begins to highlight the broad toolkit of applications unlocked through our dropicle technology. While we only functionalized nanovials using antibodies and integrin binding peptides, in principle any protein can be biotinylated and bound to the nanovial surface, including commonly used synthetic constructs such as major histocompatibility complex (MHC) tetramers.

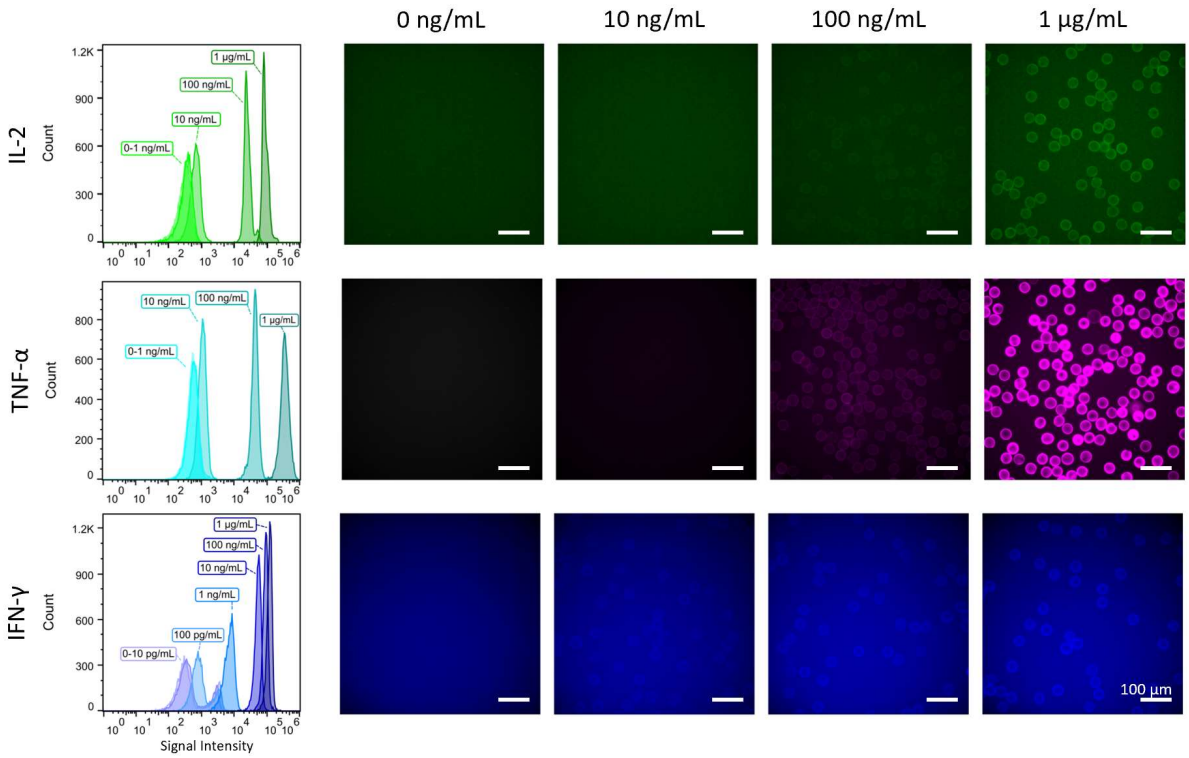

Figure 5-1 Recombinant Cytokine Detection on Nanovials.

Fluorescent sandwich immunoassays were successfully utilized to capture and detect cytokines on nanovial surfaces. Nanovials were functionalized with antibodies targeting either IL-2, TNF-α, or IFN-γ and incubated with varying concentrations of the appropriate cytokine. Samples were analyzed using both fluorescence microscopy and flow cytometry. Cytokines were detectable down to a concentration of 10-100 ng/mL using fluorescence microscopy, or 1-10 ng/mL using flow cytometry depending on the target cytokine.

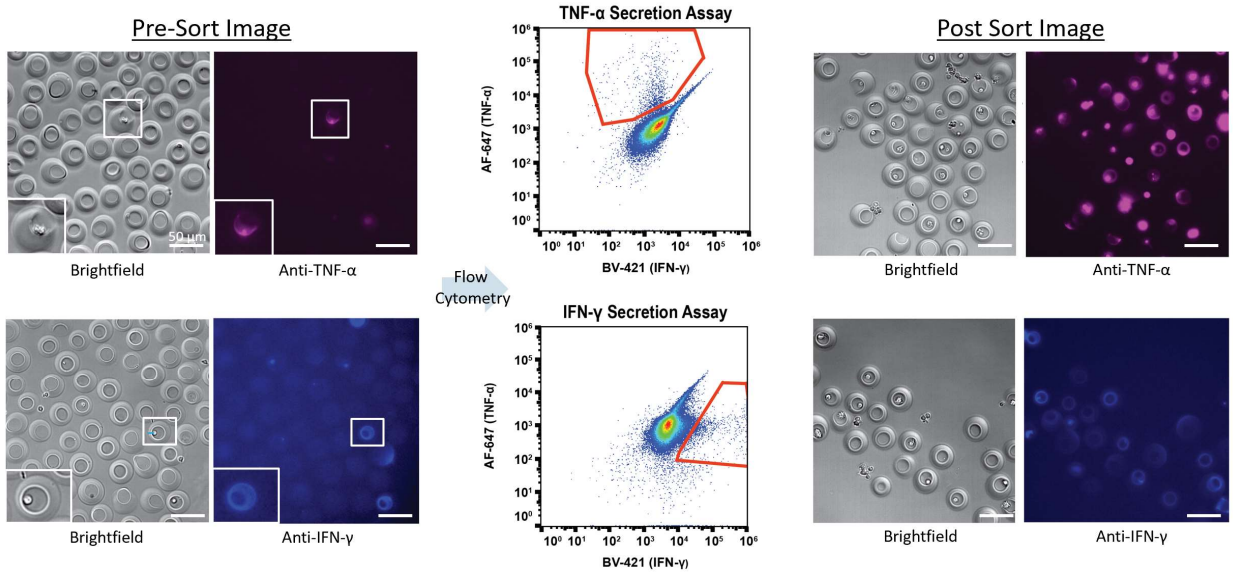

Figure 5-2 FACS enrichment of single T cells based on cytokine production

Individual T cells were bound to the inner surface of nanovials and secretion assays were performed to assess their production of either TNF-α (alexafluor 647) or IFN-γ (brilliant violet 421). T cells were activated using PMA/ionomycin and incubated in nanovials for a period of 3 hours to generate signal. After incubation and subsequent staining, bright fluorescent signals were visible along the edge of cell-filled nanovial cavities. Secreting cells were easily visualized using flow cytometry and could be enriched via standard FACS sorting.

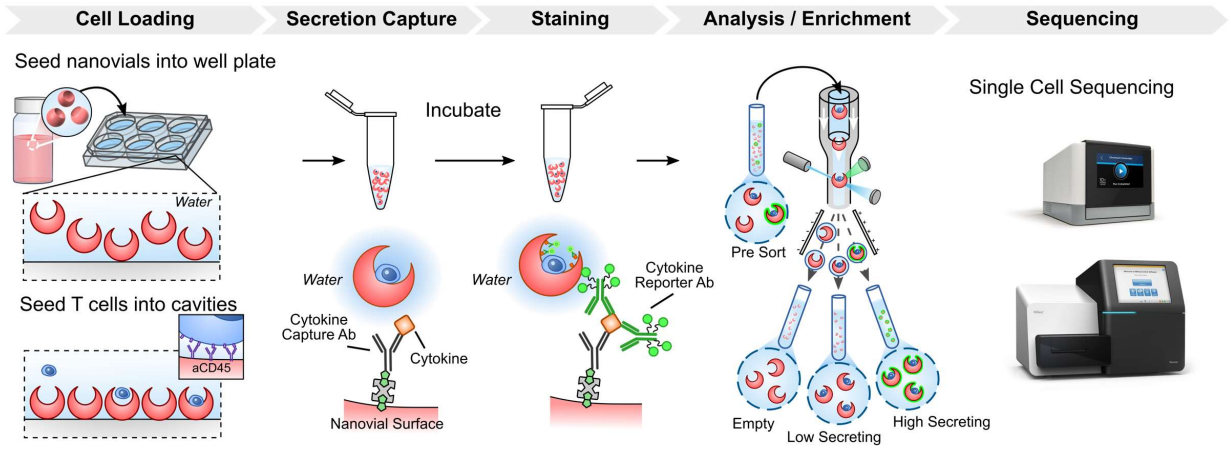

Figure 5-3 Proposed schematic to pair T cell sequence and function information using dropicles

T cells can be loaded into nanovials and bound via biotinylated antibodies targeting surface proteins such as CD45. After binding, non-adhered T cells can be strained out of the nanovial suspension and the cell loaded nanovials can be incubated to accumulate secreted cytokines. Because the rate of cytokine production from T cells is relatively low in comparison to secretions from producer cells or antibody secreting plasma cells encapsulation is not mandatory during this incubation step as appreciable signal will not accumulate on neighboring particles during short periods of incubation. Once sufficient signal has been bound to the nanovial surface, nanovials can be stained with secondary fluorescent reporter antibodies and sorted into individual wells using flow cytometry. Recovered cells in nanovials are viable and can be subsequently sequenced to assess the genetic, epigenetic, or transcriptional state of each cell.

Furthermore, the built-in solid surface within each droplet provides a matrix for cellular attachment and growth, enabling screening of adherent cell types which are difficult to probe in free floating droplets such as mesenchymal stem cells. Additionally, the size of each nanovial's cavity can be changed on demand and can even potentially be sized wide enough to accommodate two cells, such as a target tumor cell and an engineered T cell, to enhance the biologically relevancy of the cellular activation and subsequent cytokine production. Lastly, while the current cellular analysis throughput of dropicles (1000 events/second, 100 cells/second) is insufficient to support applications using large cell numbers (>10^7 cells), variations in the cell loading strategy to overcome poisson limitations, and pre-enrichment steps using magnetic isolation of cell loaded nanovials before flow cytometry are feasible and may alleviate some of these limitations. Dropicles should not be thought of as simple consumables that aid single applications, but part of a broader effort to democratize single cell screening for any researcher with basic experience and tools. While over the past several years microfluidic lab-on-a-chip technologies helped usher in an era of controllable and customizable microscale experimentation, lab-on-a-particles tools are poised to revolutionize the next generation of biotechnology.

5.6. References

[1] S. Ramakrishna, V. Barsan, C. Mackall, Prospects and challenges for use of CAR T cell therapies in solid tumors, Expert Opin Biol Th, 20 (2020) 503-516.

[2] S. Fiorenza, D.S. Ritchie, S.D. Ramsey, C.J. Turtle, J.A. Roth, Value and affordability of CAR T-cell therapy in the United States, Bone Marrow Transpl, 55 (2020) 1706-1715.

[3] R.G. Majzner, C.L. Mackall, Clinical lessons learned from the first leg of the CAR T cell journey, Nat Med, 25 (2019) 1341-1355.

[4] J.A. Fraietta, S.F. Lacey, E.J. Orlando, I. Pruteanu-Malinici, M. Gohil, S. Lundh, A.C. Boesteanu, Y. Wang, R.S. O'Connor, W.T. Hwang, E. Pequignot, D.E. Ambrose, C.F. Zhang, N. Wilcox, F. Bedoya, C. Dorfmeier, F. Chen, L.F. Tian, H. Parakandi, M. Gupta, R.M. Young, F.B. Johnson, I. Kulikovskaya, L. Liu, J. Xu, S.H. Kassim, M.M. Davis, B.L. Levine, N.V. Frey, D.L. Siegel, A.C. Huang, E.J. Wherry, H. Bitter, J.L. Brogdon, D.L. Porter, C.H. June, J.J. Melenhorst, Determinants of response and resistance to CD19 chimeric antigen receptor (CAR) T cell therapy of chronic lymphocytic leukemia, Nat Med, 24 (2018) 563-+.

[5] E.W. Weber, M.V. Maus, C.L. Mackall, The Emerging Landscape of Immune Cell Therapies, Cell, 181 (2020) 46-62.

[6] W.M. Kong, S.F. Lacey, J.J. Melenhorst, J.A. Fraietta, Biomarkers in chimeric antigen receptor T-cell therapy, Biomark Med, 12 (2018) 415-418.

[7] Q.J. Liu, Z.J. Sun, L.G. Chen, Memory T cells: strategies for optimizing tumor immunotherapy, Protein Cell, 11 (2020) 549-564.

[8] J.A. Fraietta, C.L. Nobles, M.A. Sammons, S. Lundh, S.A. Carty, T.J. Reich, A.P. Cogdill, J.J.D. Morrissette, J.E. DeNizio, S. Reddy, Y. Hwang, M. Gohil, I. Kulikovskaya, F. Nazimuddin, M. Gupta, F. Chen, J.K. Everett, K.A. Alexander, E. Lin-Shiao, M.H. Gee, X.J. Liu, R.M. Young, D. Ambrose, Y. Wang, J. Xu, M.S. Jordan, K.T. Marcucci, B.L. Levine, K.C. Garcia, Y.B. Zhao, M. Kalos, D.L. Porter, R.M. Kohli, S.F. Lacey, S.L. Berger, F.D. Bushman, C.H. June, J.J. Melenhorst, Disruption of TET2 promotes the therapeutic efficacy of CD19-targeted T cells, Nature, 558 (2018) 307-+.

[9] R.C. Lynn, E.W. Weber, E. Sotillo, D. Gennert, P. Xu, Z. Good, H. Anbunathan, J. Lattin, R. Jones, V. Tieu, S. Nagaraja, J. Granja, C.F.A. de Bourcy, R. Majzner, A.T. Satpathy, S.R. Quake, M. Monje, H.Y. Chang, C.L. Mackall, c-Jun overexpression in CAR T cells induces exhaustion resistance, Nature, 576 (2019) 293-+.

[10] E.W. Weber, K.R. Parker, E. Sotillo, R.C. Lynn, H. Anbunathan, J. Lattin, Z. Good, J.A. Belk, B. Daniel, D. Klysz, M. Malipatlolla, P. Xu, M. Bashti, S. Heitzeneder, L. Labanieh, P. Vandris, R.G. Majzner, Y. Qi, K. Sandor, L.-C. Chen, S. Prabhu, A.J. Gentles, T.J. Wandless, A.T. Satpathy, H.Y. Chang, C.L. Mackall, Transient rest restores functionality in exhausted CAR-T cells through epigenetic remodeling, Science, 372 (2021) eaba1786.

[11] J.A. Fraietta, K.A. Beckwith, P.R. Patel, M. Ruella, Z.H. Zheng, D.M. Barrett, S.F. Lacey, J.J. Melenhorst, S.E. McGettigan, D.R. Cook, C.F. Zhang, J. Xu, P. Do, J. Hulitt, S.B. Kudchodkar, A.P. Cogdill, S. Gill, D.L. Porter, J.A. Woyach, M.X. Long, A.J. Johnson, K. Maddocks, N. Muthusamy, B.L. Levine, C.H. June, J.C. Byrd, M.V. Maus, Ibrutinib enhances

chimeric antigen receptor T-cell engraftment and efficacy in leukemia, Blood, 127 (2016) 1117-1127.

[12] S. Guedan, H. Calderon, A.D. Posey, M.V. Maus, Engineering and Design of Chimeric Antigen Receptors, Mol Ther-Meth Clin D, 12 (2019) 145-156.

[13] J. Rydzek, T. Nerreter, H.Y. Peng, S. Jutz, J. Leitner, P. Steinberger, H. Einsele, C. Rader, M. Hudecek, Chimeric Antigen Receptor Library Screening Using a Novel NF-kappa B/NFAT Reporter Cell Platform, Mol Ther, 27 (2019) 287-299.

[14] D. Bloemberg, S. McComb, R. Weeratna, Building a better CAR: emerging high-throughput in vitro tools for CAR selection and optimization, Cell and Gene Therapy Insights, 5 (2019) 681-692.

[15] P.X. Ma, P. Ren, C.Y. Zhang, J.X. Tang, Z. Yu, X.K. Zhu, K. Fan, G.L. Li, W. Zhu, W. Sang, C.Y. Min, W.Z. Chen, X.X. Huang, G. Yang, R.A. Lerner, Avidity-Based Selection of Tissue-Specific CAR-T Cells from a Combinatorial Cellular Library of CARs, Adv Sci, 8 (2021).

[16] Y. Lu, Q. Xue, M.R. Eisele, E.S. Sulistijo, K. Brower, L. Han, E.A.D. Amir, D. Pe'er, K. Miller-Jensen, R. Fan, Highly multiplexed profiling of single-cell effector functions reveals deep functional heterogeneity in response to pathogenic ligands, P Natl Acad Sci USA, 112 (2015) E607-E615.

[17] Q. Han, E.M. Bradshaw, B. Nilsson, D.A. Hafler, J.C. Love, Multidimensional analysis of the frequencies and rates of cytokine secretion from single cells by quantitative microengraving, Lab on a Chip, 10 (2010) 1391-1400.